Silica gel/Water Based Adsorption Cooling System Employing Compact Fin-Tube Heat Exchanger

吳, 承澤

https://doi.org/10.15017/1398357

Silica gel/Water Based Adsorption Cooling System Employing Compact Fin-Tube Heat Exchanger

Ph.D. Thesis

Seung Taek Oh

Supervisor

Prof. Bidyut Baran Saha

Department of Mechanical Engineering

Graduate School of Engineering

Kyushu University

Japan

July 2013

Acknowledgments

First of all, I would like to express my gratitude to my supervisor, **Professor Bidyut Baran Saha**, for his invaluable guidance and inspiration to accomplish this thesis. I could learn a lot of things for not only research techniques but also human relationship from Professor.

I wish to express appreciation to reviewers, **Professor Bidyut Baran Saha**, **Professor Hideo Mori** and **Professor Shigeru Koyama** with their kind advices for manuscript of my thesis. Especially, I wish to appreciate to **Professor Hideo Mori** for providing me to study in Thermal Energy Conversion laboratory.

I have indebted to **Associate Professor Ibrahim I. El-Sharkawy** (Mansoura University, Egypt) that providing me some advices for my thesis and the opportunity to discuss technical results.

I wish to express my warm thanks to members of Thermal Energy Conversion laboratory. Especially, I really appreciate to Assistant Professor Keishi Kariya, Mr. Atsuroh Etoh and Mr. Takafumi Ouchi for assisting to set my experimental setup and supporting my Japan life.

My warm thanks are due to my friends in Kyushu University and special thanks to Jong Hyuk Park for teaching how to use the Fe-SEM.

I acknowledge with appreciation **Professor Jung In Yoon** in Pukyong National University in Korea for gave me foothold to study in Kyushu University in Japan.

At last, I wish to appreciate to my beloved father, mother, sister, brother-in-law and relatives for their moral supporting, boundless love and trust to me. I would like to attribute appreciation to my grandparents in heaven who wanted me to be a Doctor.

Contents

Summary…… v
List of Figures. …….. vii
List of Tables……..……..... x

Chapter 1. Introduction…....……..……. 1

1.1 Introduction……...…….……. 1
1.2 Literature review……...…….…..... 3
1.2.1 Adsorption cooling cycle……..…….…... 3
1.2.2 Advantages and disadvantages of adsorption cooling cycle..…... 5
1.2.2.1 Advantages……..…….……. 5
1.2.2.2 Disadvantages…….…….. 5
1.2.3 Adsorbents…….. 6
1.2.3.1 Physical adsorbents…….……. 6
1.2.3.2 Chemical adsorbents…….……... 9
1.2.3.3 Composite adsorbents…….……. 10
1.2.4 Adsorption working pairs…….…….. 11
1.2.4.1 Zeolite/water working pair……..……..... 11
1.2.4.2 Silica gel/water working pair…….…… 11
1.2.4.3 Activated carbon/ethanol working pair…..…….…… 12
1.2.5 Advanced adsorption systems…….... 13
1.2.5.1 Two-bed type adsorption refrigeration cycle…….……... 13
1.2.5.2 Two-stage adsorption chiller using re-heat…….. 15
1.2.5.3 Three-bed adsorption chiller…….…….. 16
1.2.6 Applications…….…… 18
1.2.6.1 Waste heat utilization…….……. 18
1.2.6.2 Solar energy utilization…….…….. 24
1.2.6.3 Fuel cell waste heat utilization.……...……..... 24
1.3 Objective and scopes……...…….……..... 25
1.4 Thesis outline……..…….…….….... 26
References……..……...…….…… 28

Chapter 2. Thermophysical Properties of Silica Gel RD 2060 and the Investigation of Adsorption Dynamics of Silica Gel/Water Pair … 36

2.1 Introduction …….. 36

2.2 Thermophysical properties of silica gel RD 2060 …….. 38

2.2.1 Experiment …… 38

2.2.2 Adsorption/desorption isotherms of N_2 …… 40

2.2.3 *BET* and micropore analysis …….. 43

2.2.4 Pore size distribution …….. 46

2.3 Simulation of adsorption dynamic of cylindrical silica gel particle ……..... 49

2.3.1 Model description …… 49

2.3.2 Governing equations …… 50

2.3.3 The numerical method …….. 55

2.3.4 Initial and boundary conditions …….. 55

2.4 Simulation results …… 56

2.5 Conclusions …… 61

Nomenclature …….. 62

References ……... 63

Chapter 3. Equilibrium Adsorption Isotherm Characteristics of Water onto Silica Gel RD using Compact Fin-Tube Heat Exchanger …… 66

3.1 Introduction …….. 66

3.1.1 Development/modification of adsorbent materials …… 67

3.1.2 Enhancement in heat transfer …….. 67

3.1.3 Development and/or modification of adsorption system …… 68

3.2 Experiment …… 69

3.3 Adsorption equilibrium uptake equation …….. 78

3.3.1 *Freundlich* equation …….. 78

3.3.2 *S-B-K* equation …… 78

3.4 Results and discussion ……... 80

3.4.1 Temperature profiles and uptake rate …….. 80

3.4.2 Equilibrium isotherms …….. 82

3.4.3 Ideal cycles on Dühring diagram……..……..……. 86
3.5 Conclusions…….…….. 88
Nomenclature…….……..……... 89
References……..…….…… 90

Chapter 4. Dynamic Behavior and Performance Evaluation of a Two-Bed Silica Gel/Water Based Adsorption Cooling System Employing Compact Fin-Tube Heat Exchanger……..…….…….. 93

4.1 Introduction……...……... 93
4.2 System description and working principle……...…..……. 95
4.3 Mathematical modeling……..…..……. 100
4.3.1 Adsorption isotherm.……..... 100
4.3.2 Adsorption kinetics……..……..…….. 100
4.3.3 Energy balance of adsorber/desorber heat exchanger……..…. 102
4.3.4 Condenser energy balance……..……..….. 107
4.3.5 Evaporator energy balance……..……..….. 108
4.3.6 Mass balance……..……..…… 110
4.3.7 System performances……..……..……... 110
4.4 Results and discussion…...……..……..……..……..…….. 111
4.4.1 Effects of cycle and switching times…..……...…….. 111
4.4.2 Effects of operating temperatures……...……..……..…….. 117
4.4.3 Effects of heat transfer fluids flow rate ….……. 120
4.5 Conclusions……...…….. 123
Nomenclature……..……..…….. 124
References……...…… 126

Chapter 5. Fuel Cell Waste Heat Powered Two-Bed Adsorption Cooling System……... 129

5.1 Introduction……..……..…….. 129
5.2 System description and working principle…….……...…. 131
5.3 Mathematical modeling……..……..…..……... 133
5.3.1 Adsorption isotherm.…….……...…….…….. 133

5.3.2 Adsorption kinetics…….……..…..……..…….. 133
5.4 Heat recovery from fuel cells…...……...……..……..……... 133
5.5 Results and discussion……. 134
5.5.1 Adsorption cooling system powered by PEFC waste heat…….…….... 134
5.5.2 Adsorption cooling system powered by SOFC waste heat ……..…… 139
5.5.3 Thermodynamic process on the Dühring diagram.…….……..…… 142
5.5.4 Comparison of performances with conventional adsorption cooling system..... 144
5.6 Conclusions……..……..….. 146
Nomenclature……..…….. 147
References……...…….. 148

Chapter 6. Overall Conclusions……..……..…….…… 151

6.1 Main application of adsorption refrigeration system…….……..... 151
6.2 Chapter summaries……..……..……..... 152
6.3 Overall conclusions…..……..……. 155
6.4 Future work…….……..... 156

Appendix A. Evaporator and Condenser Surface Area……..…… 157

Summary

A central challenge in cooling science today is the development of thermally powered miniaturized chillers employing environmentally benign adsorbent/refrigerant pairs. The general aim is to develop a device that is: (1) compact, (2) environmentally benign, (3) virtually free of moving parts or highly reliable, (4) capable of exploiting low-temperature waste heat, and (5) highly efficient in converting input to cooling power.

From the above perspective, this thesis presents the theoretical and experimental studies of adsorption cooling cycles which utilize low-temperature heat sources such as waste heat from fuel cells or solar thermal energy. Silica gel and water has been considered as the adsorbent/adsorbate pair as silica gel is abundantly available and water is a natural refrigerant with high latent heat of vaporization and the working pair is environmentally friendly.

In analyzing silica gel-water based adsorption cooling system, thermophysical properties and water vapor uptake performance of silica gels are important. In this study, thermophysical properties of three different sizes of RD 2060 type silica gels are determined using N_2 adsorption isotherm data by volumetric adsorption characteristic analyzer. Water vapor adsorption dynamic on to cylindrical silica gel has been analyzed using finite volume based ANSYS FLUENT environment.

The equilibrium isotherm characteristics of water onto granular RD type silica gel have been experimentally studied at three evaporation temperatures employing a compact fin-tube type adsorbent bed (heat exchanger). The adsorbents were packed between the fins of the compact heat exchanger. The experimental adsorption equilibrium isotherms data have been fitted with popular isotherm models and the modified Freundlich equation which is known as the S-B-K adsorption isotherm model fits satisfactorily the present experimental results.

The theoretical study modeled the mass and energy balances of the adsorption cooling cycle that operates in a batch manner, using the governing equations developed based on thermodynamic property fields of an adsorbent/adsorbate system. Dynamic behavior of silica gel-water based adsorption cooling system employing the compact fin-tube type heat exchanger has been determined in terms of cooling capacity and coefficient of performance

(COP) by varying heat transfer fluid (hot, cooling and chilled water) inlet temperatures, heat transfer fluid flow rates, adsorption/desorption cycle time and switching time.

Finally, the performance of silica gel-water based adsorption cooling systems powered by two different temperature levels of waste heat from polymer electrolyte fuel cell (PEFC) and solid oxide fuel cell (SOFC) has been determined. System performance in terms of specific cooling capacity (SCC) and COP are determined and compared and are found to be suitable for low-temperature waste heat utilization. In short, these cited advantages of low-temperature thermally powered adsorption cycle offers great potential for a large scale implementation for cooling applications.

List of Figures

Figure 1.1	Configuration of ideal thermodynamaic adsorption cycle
Figure 1.2	Clapeyron diagram for thermodynamic adsorption cycle
Figure 1.3	Array of SiO_4 in the silica gel
Figure 1.4	Structure of activated carbon
Figure 1.5	Structures of synthesized zeolites
Figure 1.6	Schematic diagram of two-bed type adsorption chiller
Figure 1.7	Schematic diagram of two-stage adsorption chiller
Figure 1.8(a)	Single-stage three-bed adsorption cycle in parallel heat transfer fluid flow configuration
Figure 1.8(b)	Single-stage three-bed adsorption cycle in series heat transfer fluid flow configuration
Figure 1.9(a)	Schematic diagram of adsorption ice maker system
Figure 1.9(b)	Pictorial view of adsorption ice maker prototype
Figure 1.10(a)	Schematic diagram of adsorption air conditioner
Figure 1.10(b)	Pictorial view of adsorption air conditioner
Figure 1.11	Structure of the adsorber
Figure 1.12	Double tube pipe type adsorber
Figure 1.13	Schematic diagram adsorption cooling system for automobile
Figure 2.1	Pictures of three types of silica gel RD 2060
Figure 2.2	Schematic diagram of Belsorp Mini II machine
Figure 2.3	Adsorption isotherms of N_2 on silica gel RD 2060 samples
Figure 2.4	Brunauer classification of adsorption isotherms
Figure 2.5	The *BET plots* of present samples
Figure 2.6	The *t-plots* of present samples
Figure 2.7	Micropore size distribution by *MP* method
Figure 2.8	Pictures of surface of samples by Fe-SEM
Figure 2.9	Three different arrangements of silica gel particles
Figure 2.10	Temperature contours
Figure 2.11	Uptake contours on the surface and cross section
Figure 2.12	Variation of normalized average uptake as time

Figure 2.13(a)	Arrangement 1
Figure 2.13(b)	Arrangement 2
Figure 2.13(c)	Arrangement 3
Figure 3.1	Schematic diagram of the experimental apparatus
Figure 3.2	Pictorial view of the experimental setup
Figure 3.3	Side view of the adsorption chamber
Figure 3.4	Configuration of the fin-tube heat exchanger
Figure 3.5	Pictorial view of the compact fin-tube heat exchanger
Figure 3.6	Side view of the evaporator
Figure 3.7	Temperature profiles of adsorbents
Figure 3.8	Adsorption uptake rate
Figure 3.9	Comparison of equilibrium uptakes with Freundlich and S-B-K equations
Figure 3.10	Uptake balance between present experimental results and computed results
Figure 3.11	Isotherm data for water vapor adsorption onto silica gel
Figure 3.12	Variations of equilibrium uptakes for water vapor adsorption onto silica gel
Figure 3.13	Computed adsorption isotherms versus equilibrium pressure
Figure 3.14	Ideal cycles on Dühring diagram
Figure 4.1(a)	Operation mode A
Figure 4.1(b)	Operation mode B
Figure 4.1(c)	Operation mode C
Figure 4.1(d)	Operation mode D
Figure 4.2	Configuration of incremental thermal analysis
Figure 4.3	Cycle time effect on cooling capacity and COP
Figure 4.4	Switching time effect on cooling capacity and COP
Figure 4.5	Temperature profiles of each component for optimized cycle time
Figure 4.6	Outlet water temperature profiles of heat transfer fluids for optimized cycle time
Figure 4.7	Comparison of optimized cycle with ideal cycle on Dühring diagram
Figure 4.8	Hot water temperature effect on cooling capacity and COP

Figure 4.9	Cooling water temperature effect on cooling capacity and COP
Figure 4.10	Chilled water temperature effect on cooling capacity and COP
Figure 4.11	Hot water flow rate effect on cooling capacity and COP
Figure 4.12	Cooling water flow rate effect on cooling capacity and COP
Figure 4.13	Chilled water flow rate effect on cooling capacity and COP
Figure 5.1	Silica gel/water based adsorption cooling system powered by fuel cell waste heat
Figure 5.2	Cycle time effect on performances of cycle powered by PEFC waste heat
Figure 5.3	Switching time effect on performances of cycle powered by PEFC waste heat.
Figure 5.4	Temperature profiles of each component for cycle powered by PEFC
Figure 5.5	Outlet temperature profiles of heat transfer fluids for cycle powered by PEFC
Figure 5.6	Cycle time effect on performances of cycle powered by SOFC waste heat
Figure 5.7	Switching time effect on performances of cycle powered by SOFC waste heat
Figure 5.8	Temperature profiles of each component for cycle powered by SOFC
Figure 5.9	Outlet temperature profiles of heat transfer fluids for cycle powered by SOFC
Figure 5.10	Comparison of thermodynamic processes between PEFC and SOFC systems
Figure 5.11	Comparison of SCC and COP with conventional adsorption cooling system
Figure 5.12	Comparison of thermodynamic process with conventional adsorption cooling system
Figure A.1	Shell and tube type heat exchanger

List of tables

Table 2.1	Thermophysical properties by *BET* analysis
Table 2.2	Micropore properties by *t-plot* method
Table 2.3	The values of properties for simulation
Table 3.1	Specifications of measuring devices
Table 3.2	Values of parameters used in Eqs. (3.5) and (3.6)
Table 4.1	Operation schedules of refrigerant valves and sorption elements
Table 4.2	Values of physical parameters
Table 4.3	Related temperature conditions of heat transfer fluids
Table 4.4	Related flow rates of heat transfer fluids
Table 5.1	Specifications of fuel cells
Table 5.2	Values of physical parameters

Chapter 1

Chapter 1

Introduction

1.1. Introduction

The use of refrigeration and air-conditioning system has increased rapidly due to acceleration of global temperature rise. The International Institute of Refrigeration in Paris has estimated that approximately 15 % of all the electricity produced in the whole world is employed to refrigeration and air-conditioning processes and the energy consumption for air-conditioning systems has been estimated to be 45 % of the whole households and commercial buildings [1 - 3]. For such a reason, adsorption cooling technology has been gained attention as a novel technology to alternate vapor compression cooling system with the conservation of energy and environmental friendliness. Combined heating and power (CHP) system was proven and reliable technology in utilizing waste heat for decades [4]. However, the conventional way to provide electricity and heat is to purchase electricity from the local grid and generate heat by burning fuel in the boiler [5]. Accordingly, at present, CHP system which can be free in using of other energy sources has been studied actively as well as combined cooling, heating and power (CCHP) system.

From the above perspective, integrated heat driven adsorption cooling/refrigeration system and CHP system such as solar heat and fuel cell waste heat driven adsorption cooling systems seem to be promising technologies to achieve, effectively both energy

conservation and environmental protection.

This chapter presents a comprehensive review of various adsorption cooling systems. Extensive studies are conducted to investigate the performance of adsorption cooling systems using various adsorbent/refrigerant pairs and to enhance the performance of adsorption cooling system by the development and/or improvement of new and/or parent adsorbent materials. Advanced cooling systems have been proposed either to improve the performance of conventional systems or to utilize relatively lower temperature heat sources which otherwise should be purged to the ambient. Scopes and objectives of the present thesis are also discussed in this chapter.

1.2 Literature review

1.2.1 Adsorption cooling cycle

An adsorption cooling cycle comprises a pair of sorption elements (adsorber/desorber heat exchangers), a condenser, an evaporator and an expansion device [6 - 7]. The sorption element which plays the role of thermal compressor is replaced to the mechanical compressor in the vapor compression heat pump cycle. Figure 1.1 and Fig. 1.2 [6] show configuration of ideal adsorption thermodynamic cycle and Clapeyron diagram for adsorption thermodynamic cycle, respectively. As can be seen from these figures, adsorption cooling cycle is divided into two cycles; refrigeration cycle (adsorption + evaporation) and heat engine cycle (desorption + condensation). In the refrigeration cycle, the working fluid is vaporized in the evaporator by taking the heat (Q_{eva}) from low temperature of heat source then released heat (Q_{ads}) to ambient temperature by secondary fluid in the adsorber. This cycle represents adsorption phase. In the heat engine cycle, adsorbed working fluid is desorbed by taking heat (Q_{des}) from high temperature of heat source then released heat (Q_{cond}) to ambient temperature by secondary fluid in the condenser. This cycle represents desorption phase.

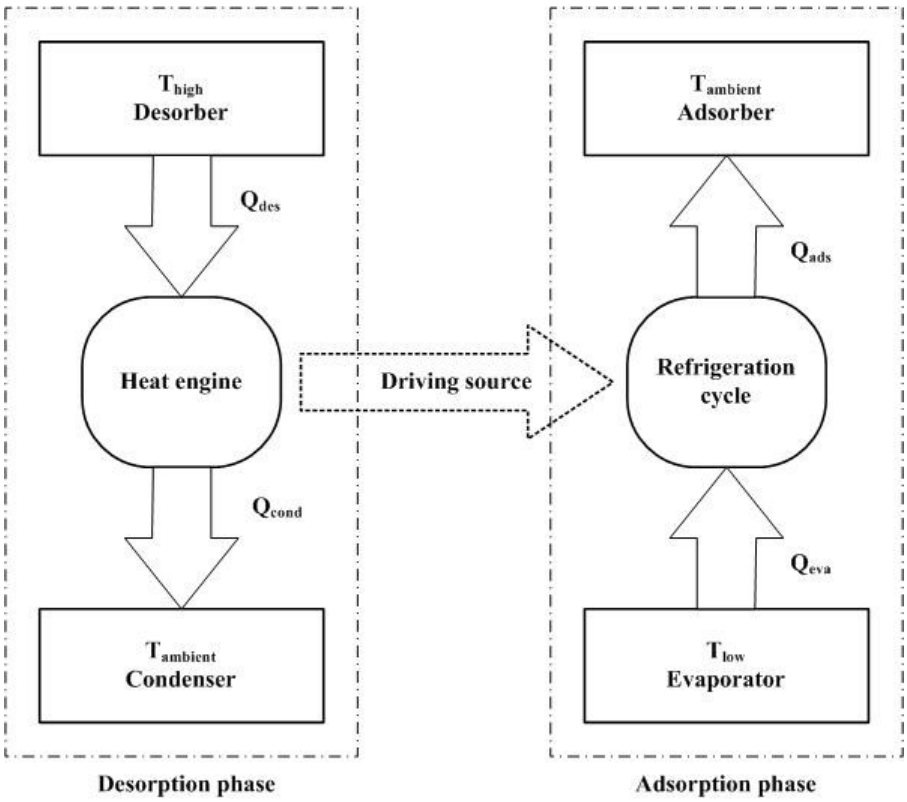

Fig. 1.1 Configuration of ideal thermodynamic adsorption cycle. [6]

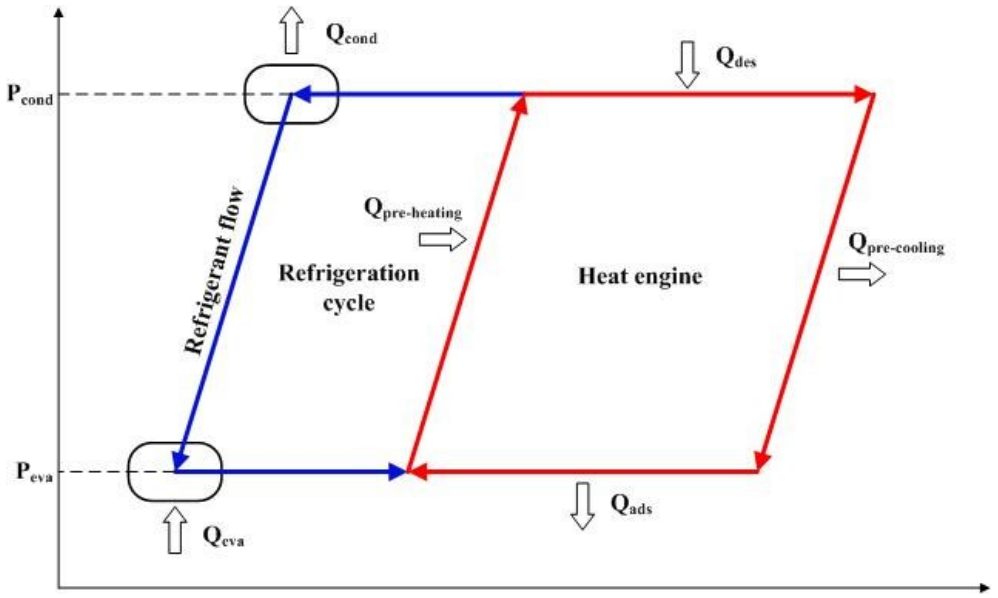

Fig. 1.2 Clapeyron diagram for thermodynamic adsorption cycle. [6]

1.2.2 Advantages and disadvantages of adsorption cooling cycle

1.2.2.1 Advantages

Over the past decades, adsorption cooling system has been considered alternative system for mechanical compression cooling system with some advantages in the energy saving and environmental friendliness. The important advantages are summarized as follows [7 - 10];

- Employing environmental friendly working pair.
- Various thermal energy sources such as waste heat, solar energy and geothermal energy can be used as driving source.
- Lower temperature level of driving heat source as 50˚C.
- No noise and vibration during the operation where there are few moving parts.
- Suitable in the condition with serious vibration, such as fishing boats and locomotive on the contrary to absorption system.
- Simple working principle
- Relatively longer lifetime.

1.2.2.2 Disadvantages

Adsorption cooling system has many advantages as mentioned above to alternate mechanical compression cooling system, while it has relatively critical disadvantages. The disadvantages are summarized as follows [9 - 11];

- Relatively lower COP.
- Larger foot print compare with mechanical compression system.

- Intermittent output.

1.2.3. Adsorbents

Adsorbents can be classified into three categories, such as (i) physical adsorbent [12 - 14], (ii) chemical adsorbent [15 - 17] and (iii) composite adsorbent [18 - 20]. In the following subsections, characteristics of each type of adsorbents are briefly presented.

1.2.3.1. Physical adsorbents

Physical adsorption is occurred by an intermolecular force, namely van der Waals force between surface of adsorbent and adsorbate [21]. The physical adsorbent preserves its true characteristics even though repetitive adsorption and desorption processes are occurred. The physical adsorbents which are commonly used in the adsorption cooling system are silica gel, activated carbon and zeolite.

Silica gel

The silica gel is a type of amorphous synthetic silica which consists of rigid and continuous net of colloidal silica connected to very small grains of hydrated SiO4 as shown in Fig. 1.3 [22]. Silica gel maintains chemically bonded traces of water about 2 - 3 % and it loses adsorptivity by overheating temperature above 120˚C, thereby it is generally used in temperature system as low as 200˚C. Silica gel is divided into type A (2 to 3 nm of pore diameter) and B (about 0.7 nm of pore diameter) which are commonly used in the commercial application and they have 100 - 1000 m2/g of specific surface area and about 2800 kJ/kg of adsorption heat [21, 23, 24, 25]. Type A can be used for general desiccant systems, however type B can be used in the higher

relative humidity condition than 50 %.

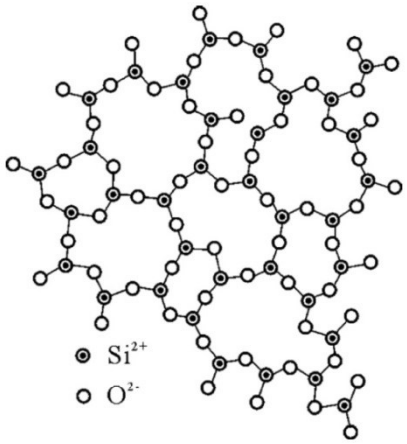

Fig. 1.3 Array of SiO_4 in the silica gel [22].

Activated carbon

Activated carbon is prepared from various carbonaceous precursors containing coal, lignite, fossil fuel, char, peat, coconut shell, nut stone and bone which are carbonized, either by oxidization with CO_2 of stream, or by treatment with acids [26]. Activated carbon can be made in many forms; powder, grain, molecular sieve and fiber, and used in liquid adsorption, air and water purification, gas separation and adsorption cooling system, and it has more than 1500 m^2/g of surface area [15, 27]. Structure of activated carbon is shown in Fig. 1.4 [28]. The microcrystal for activated carbon produced hexagonal carboatomic ring, and adsorption performance is influenced by the functional groups which connected to the carboatomic ring [29]. The activated carbon fiber has better performance in terms of mass and heat transfer with larger surface area and more uniformed pore size [30], where as it has anisotropic thermal conductivity and higher thermal resistance between the fiber and surface of heat exchanger compared with

activated carbon.

Fig. 1.4 Structure of activated carbon [28].

Zeolite

Zeolite is crystalline alumina silicate composed of alkali/alkali soil, namely molecular sieve, and alumina silicate skeletal has 0.2 - 0.5 cm^3/g of porosity. The adsorption capability of zeolite is related to the proportion between aluminum and silicon and it is higher in smaller proportion between aluminum and silicon. In the zeolite, there are 40 types of natural zeolite and 150 types of artificial zeolite regarding to synthesis method [29]. The synthesized zeolites have higher bulk specific weight and better heat transfer performance. Figure 1.5 shows structures of synthesized zeolites [31]. The zeolite has cage structure which is connected by six casement section thereby it can adsorbs a large amount of extra molecules [22]. Most zeolites maintain their adsorption and regeneration properties up to 500˚C of regeneration temperature, whilst synthesized zeolite can withstand up to 800˚C. Zeolites has 3300 - 4200 kJ/ kg of adsorption heat and they are usually employed in adsorption air cooling system which

requires regenerating temperature heat source as high as 200 - 300˚C.

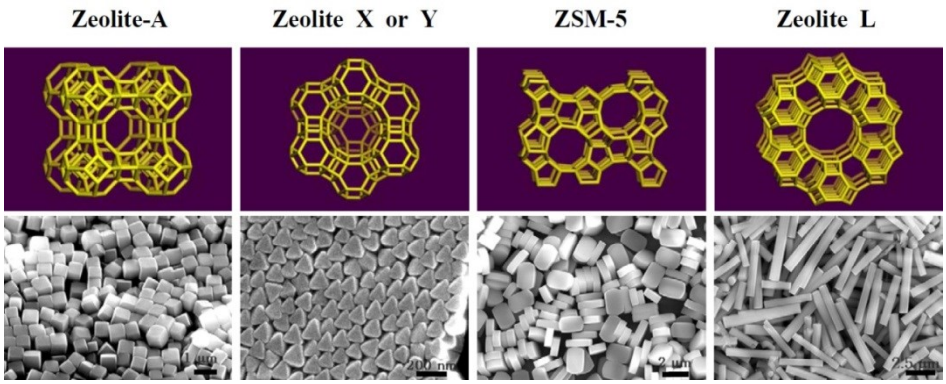

Fig 1.5 Structures of synthesized zeolites [31].

1.2.3.2. Chemical adsorbents

Chemical adsorption is occurred by Valence force which is reaction between adsorbate and surface molecules of chemical adsorbent. Chemical adsorbents mainly divided into metal chlorides, metal hydrides and metal oxides. Chemical adsorbent has better adsorption performance while it has lower stability that cannot keep the original properties [32].

Metal chlorides

Calcium chloride, strontium chloride, magnesium chloride and barium chloride are mainly used in the metal chloride adsorbents for adsorption cooling system [33]. Metal chloride performs high adsorption capacity up to 1 kg_{ref}/kg_{ads} whereas it influences negatively to heat and mass transfer with swelling and agglomeration during the adsorption. Methanol and ethanol are mainly employed as adsorbate for calcium chloride and ammonia is used as adsorbate for metal chloride [15].

Salt and metal hydrides

Lithium hydrides, calcium hydrides and covalent high polymerized hydrides are promisingly used in the salt and metal hydrides for adsorption cooling system using hydrogen refrigerant.

Metal oxides

The metal oxides are usually used in catalyst for oxidation and deoxidation reactions, thus they are employed as adsorbent for adsorption heat pump using oxygen as refrigerant [34, 35]. Metal oxide/oxygen pair is suitable for cryogenic heat pump application of temperature below 120 K with large enthalpy of reaction between oxides and oxygen [15].

1.2.3.3 Composite adsorbents

Physical adsorbent has higher thermal conductivity due to its uniform skeletal structure, while it has lower adsorption capacity than chemical adsorbent. On the other hand, chemical adsorbent has higher adsorption capacity, whilst it has poor heat and mass transfer caused by its swelling and agglomeration phenomena [36]. The composite adsorbent is made from the combination of chemical sorbents and porous media to enhance adsorption performance of physical adsorbents and supplement drawback (poor thermal conductivity caused by swelling and agglomeration) of chemical adsorbents [37, 38]. Typical composite adsorbents are metal chlorides and activated carbon/activated carbon fiber, or expanded graphite, silica gel or zeolite.

1.2.4. Adsorption working pairs

D. I. Tchernev [39] mentioned that a naturally created mineral, namely zeolite adsorbs or desorbs large amounts of water vapor while it is being cooled or heated, thus providing a unique opportunity for its utilization in refrigeration applications. A demonstration unit of a refrigerator was first commercialized by Tchernev using zeolite-water as the working pair [1].

1.2.4.1. Zeolite/water working pair

The zeolite/water pair can be utilized in dehumidification cooling system and adsorption cooling system. This pair has high adsorption heat about 3300 - 4200 kJ/kg and can be regenerated at high temperature over 200˚C. Tather et al. [40] evaluated performances of zeolite 13X and 4A flake under different thickness. Zhu et al. [41] developed medium size prototype of zeolite/water adsorption chiller using waste heat from diesel engine. Wang et al. [42] investigated design and performance prediction of novel zeolite/water based two-bed type adsorption air conditioner.

1.2.4.2. Silica gel/water working pair

Silica gel/water based adsorption system can be driven at heat source temperature as low as 50˚C and silica gel/water pair has about 2500 kJ/kg of adsorption heat [22]. Silica gel/water based adsorption cooling system is better to be applied to air-conditioning system where requires relatively higher evaporating temperature. Yeh et al. [43] evaluated effects of regeneration temperatures and times on adsorption isotherm for water vapor onto silica gel. Ng et al. [44], Chua et al. [45] and X. Wang et al. [46] studied adsorption characteristics and thermo physical properties of various kinds of

silica gel/water working pairs. Miyazaki et al. [47] found 6 % cooling capacity improvement with a new cycle time allocation in both silica gel/water and $CaCl_2$-in-silica gel/water based two-bed type adsorption chillers. Chua et al. [48] presented transient modeling of two-bed silica gel/water adsorption chiller. Khan et al. [49] investigate silica gel/water based two-stage adsorption chiller using waste heat between 50 and 70˚C numerically. Saha et al. [50] investigated silica gel/water based three-stage adsorption chiller using 50˚C of waste heat and determined effect of thermal conductance of sorption bed on the performance. Saha et al. [13] proposed a three-bed non-regenerative silica gel-water adsorption chiller design. Alam et al. [51] investigated heat exchanger design effect on the performance of two-bed adsorption cooling system with silica gel/water. Li et al. [52] developed a fin-type silica gel tube (FST) module, and analyzed numerically the heat and mass transfer characteristics.

1.2.4.3. Activated carbon/ethanol working pair

Activated carbon (AC)/ethanol based adsorption system have been studied since 1980s in Europe. AC/ethanol pair has relatively low adsorption heat about 1200 - 1400 kJ/kg and AC/ethanol system requires relatively higher heat source temperature than that of silica gel/water system [53]. El-Sharkawy et al. [54] investigated adsorption characteristics of activated carbon fibers (ACFs; A-15 and A-20)/ethanol pairs. Saha et al. [55] determined thermophysical properties of ACF (A-20), ACF (A-15) and ACF (A-10) by N_2 isotherms and adsorption characteristics of ethanol onto ACF (A-20) using plate fin heat exchanger is also investigated. Modeling of activated carbon/ethanol based adsorption chiller was proposed by Saha et al. [56] and the performance of the cycle was evaluated by the same author [30].

1.2.5. Advanced adsorption systems

1.2.5.1. Two-bed type adsorption refrigeration cycle

Two-bed type adsorption refrigeration system was developed to enhance heat and mass transfer with continuous cycle operation. This system consists of two sorption elements (SEs), a condenser and an evaporator. The cycle has four modes, Mode A, B, C and D. In Mode A, the evaporator and the SE 1 is in adsorption process and the condenser and the SE 2 is in desorption process. When the refrigerant concentrations in the adsorber and the desorber are at or near their equilibrium levels, the cycle is continued by changing into a short duration (30 s) named pre-heating or pre-cooling mode (Mode B). In Mode B, heat transfer fluids (hot and cooling water) flows are redirected to ensure pre-heating and pre-cooling process of SE 1 and SE 2, respectively. When the pressures of desorber and adsorber are nearly equal to the pressures of condenser and evaporator, respectively, the cycle continued to Mode C. In Mode C, the condenser and the SE 1 is in desorption process and the evaporator and the SE 2 is in adsorption process. After the completion of Mode C, pre-heating of SE 2 or pre-cooling of SE 1 occurred, which is opposite of Mode B and known as Mode D. After Mode D, the adsorption cooling system returns to Mode A.

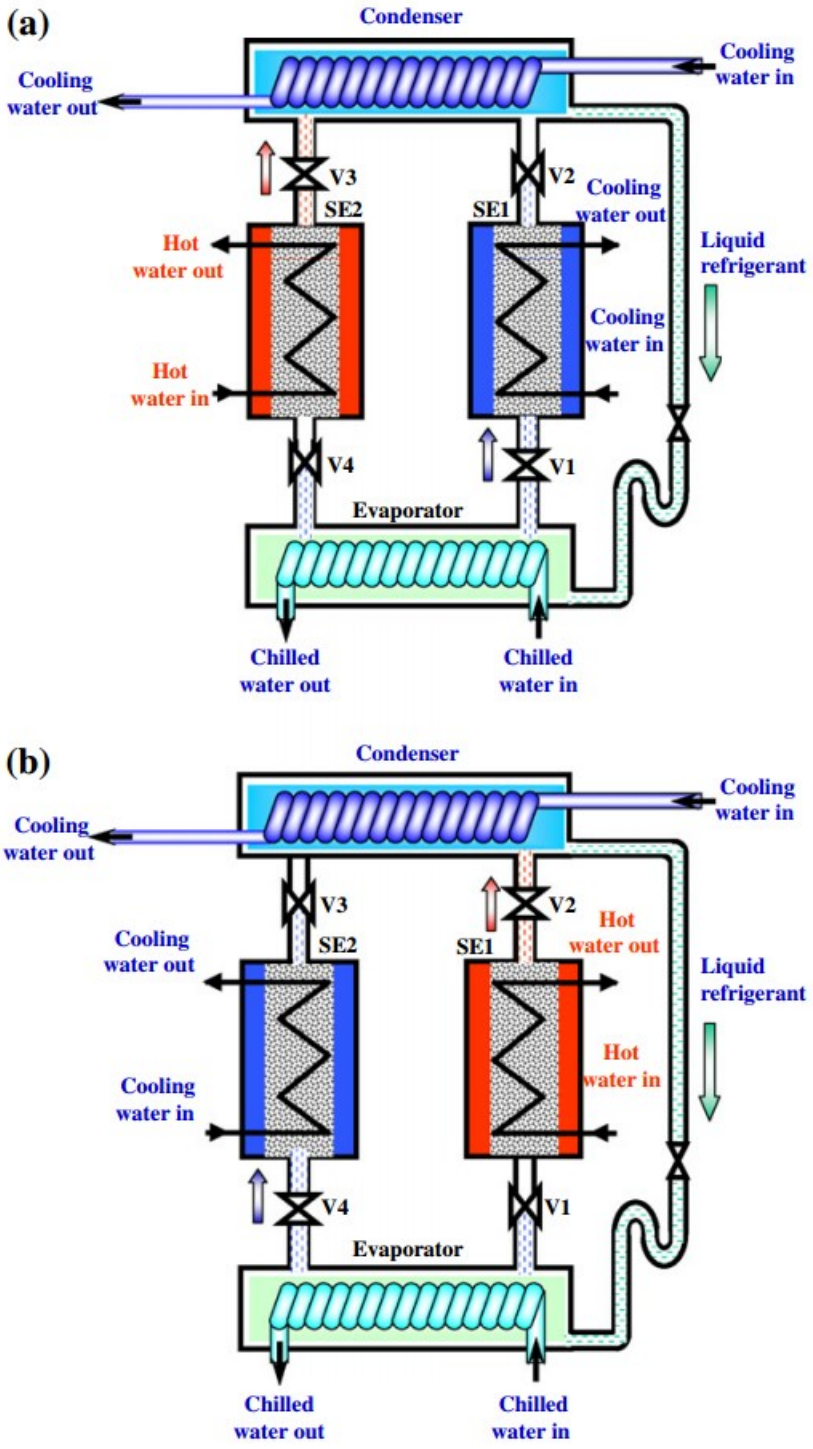

(a) Mode A (b) Mode C

Fig. 1.6 Schematic diagram of two-bed type adsorption chiller [30, 47, 56].

1.2.5.2. Two-stage adsorption chiller using re-heat

The two-stage adsorption chiller was investigated to use lower heat source temperature by division of the evaporating pressure lift into two consecutive pressures. Operational strategy of the chiller, however, is completely different from the operational strategy of a conventional two-stage chiller. This system comprises with four adsorbent beds, a condenser and an evaporator as similar as convectional two-stage adsorption chiller as shown in Fig. 1.7. In a conventional two-stage chiller, lower two beds never interact with the condenser and upper two beds never interact with the evaporator. However, in the two-stage adsorption chiller using re-heat, all beds undergo through all processes and interact with the condenser and evaporator. The chiller can be operated in different strategies.

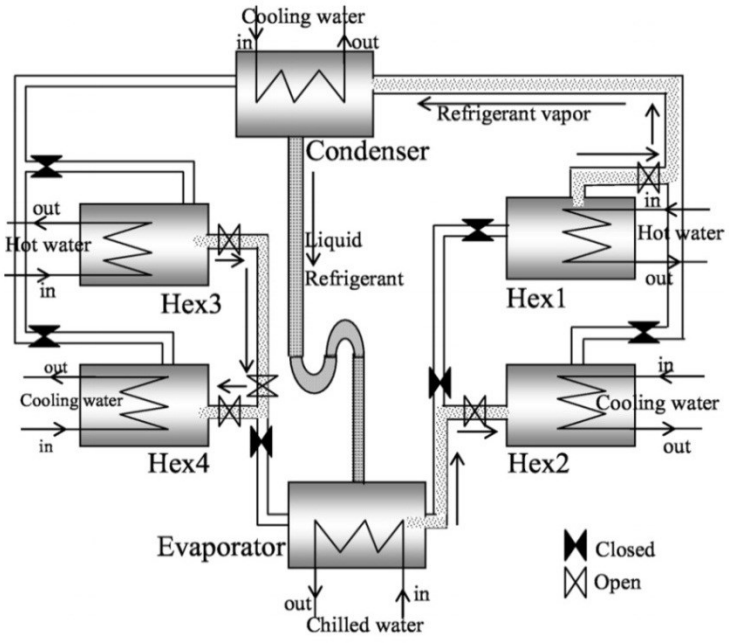

Fig. 1.7 Schematic diagram of two-stage adsorption chiller [49].

1.2.5.3. Three-bed adsorption chiller

The three-bed adsorption chiller strategy was developed to reduce the peak temperatures in both the evaporator and condenser from the conventional (two-bed) operation by dislocated cycle time for each three beds. The three-bed cycle comprises with an evaporator, a condenser and three sorption elements (adsorber/desorber heat exchangers) as shown in Fig. 1.8(a). The same chiller in series flow configuration is shown in Fig. 1.8(b). In this mode, by capitalizing the phase difference between the three sorption elements, the heat source from the lead desorber can be used to regenerate another cooler desorber that will act as the lack desorber. The outlet hot water from the lack desorber will be discharged to ambient. Similarly, the coolant from the sorption element(s) in adsorption mode can be used in cascaded manner (cooling water outlet from the low-temperature adsorber to lack adsorber before being sent back to the cooling tower).

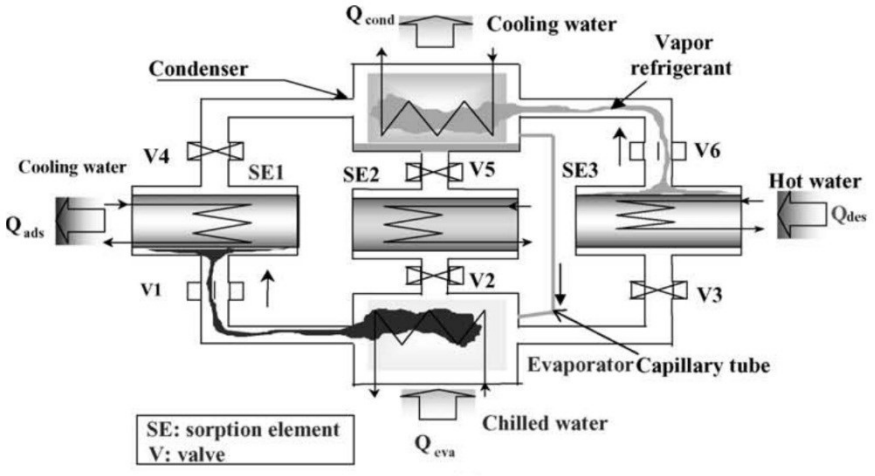

(a) Single-stage three-bed adsorption cycle in parallel heat transfer fluid flow configuration.

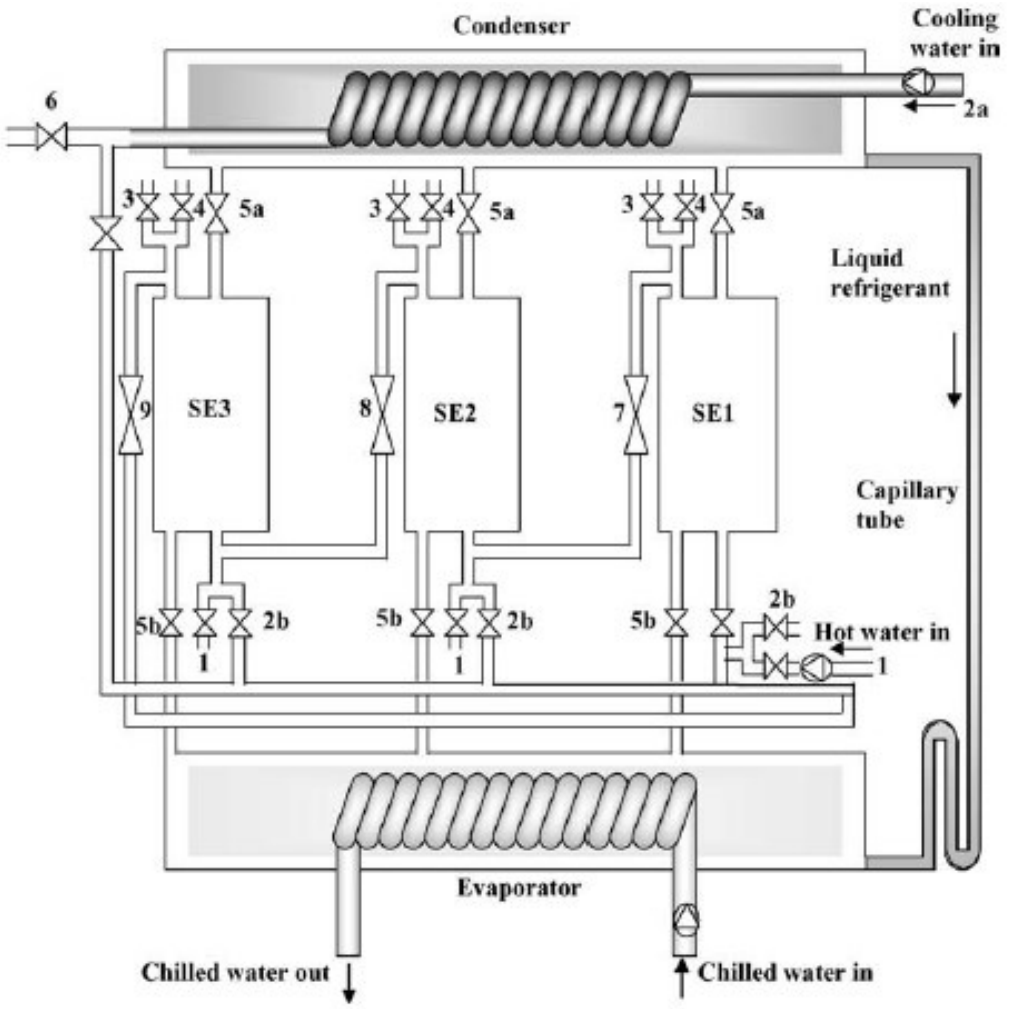

(b) Single-stage three-bed adsorption cycle in series heat transfer fluid flow configuration.

Fig. 1.8 Schematic diagram of three bed adsorption chiller [13].

1.2.6. Applications

1.2.6.1. Waste heat utilization

Waste heat, low grade waste heat, can be used for driving source of adsorption cooling system. A large amount of waste heat is yielded from the processes in field of chemical plant, steel plant, power plant, engine of automobiles and ships and so on. Adsorption system is better to be applied using the waste heat from any process than absorption system. Because adsorption system has several advantages such as low grade of waste heat required, less influence of vibration, compact and simple structure, simple control and so on. Wang et al. [18] designed and develop prototype adsorption ice maker system for fishing boat using three different adsorbent/refrigerant pairs; activated carbon/methanol, $CaCl_2/NH_3$ and activated carbon + $CaCl_2$/ NH_3 pairs. This system employs two sorption elements to improve heat and mass recovery as shown in Fig. 1.9. Cooling water is supplied directly from the sea to cool adsorber. The heat source for desorption is taken by hot water which exchanged heat with the exhausted gas from the diesel engine in the exhausted gas-water heat exchanger. In order to accumulate the heat from exhausted gas, hot water storage vessel is used. In case of activated carbon/methanol pair, it produced 1.99 kW of cooling power and about 15 kg of ice per 1 hour while cycle time is 76 min. $CaCl_2/NH_3$ and activated carbon + $CaCl_2/NH_3$ pairs performed much higher than activated carbon/methanol pair with 14.75 and 20.32 kW of cooling power while cycle time is 60 min.

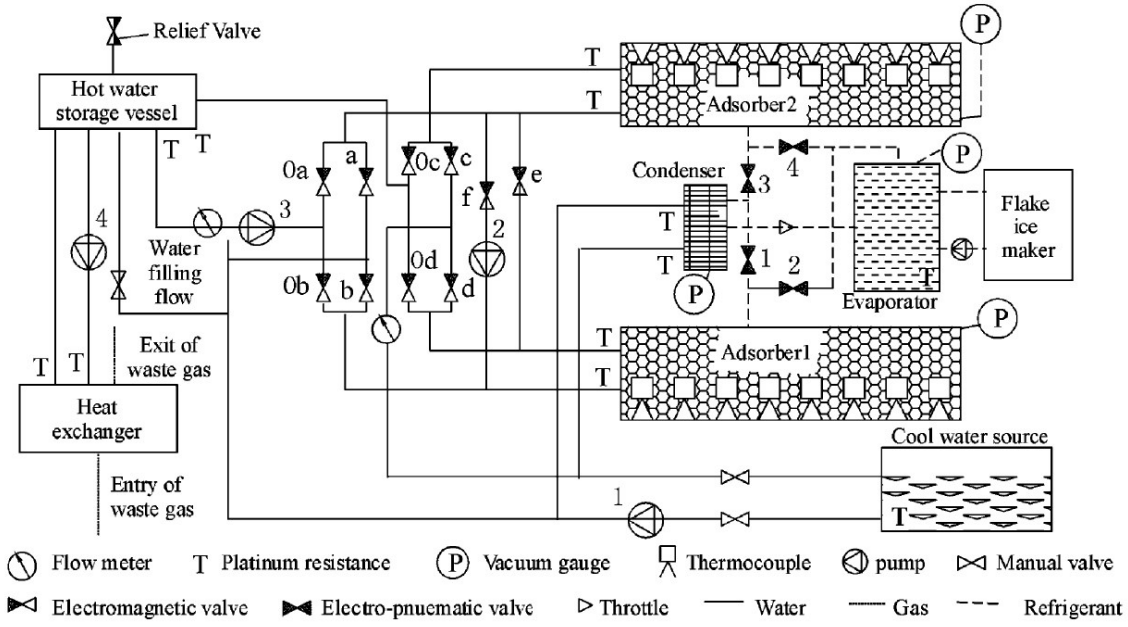

(a) Schematic diagram of adsorption ice maker system

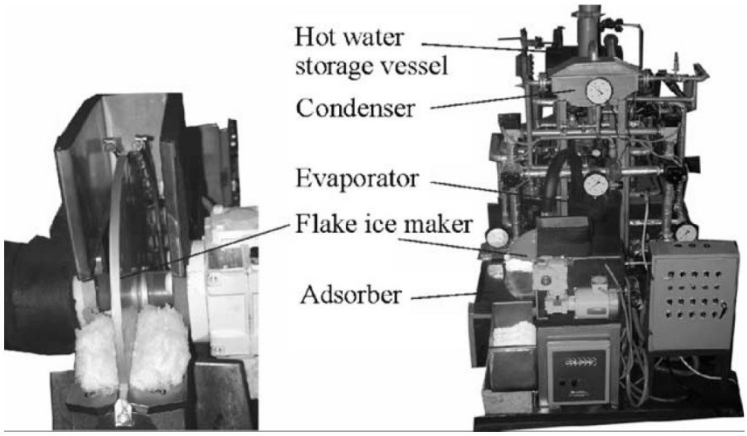

(b) Pictorial view of adsorption ice maker prototype.

Fig. 1.9 Adsorption ice maker system for fishing boat [18].

Wang et al. [42] designed zeolite 13X/water based adsorption air conditioner for locomotive and performances are investigated experimentally. This system consists of two independent adsorption system including one ads/des element, one condenser and one evaporator as shown in Fig. 1.10. The ambient air is employed to cooling source and exhausted gas from diesel engine of locomotive is employed to heat source. In this article, the heat transfer area is increased in order to enhance the heat transfer performance of the adsorber caused by poor conductivity of zeolite 13X. In the adsorbent side, the mass transfer channels are designed and leaved space from the adsorbent layer, and there are 2 mm diameter holes on the fins in the adsorbent side as work as mass transfer channel as shown in Fig. 1.11. Plate fin heat exchangers are employed to evaporator and condenser.

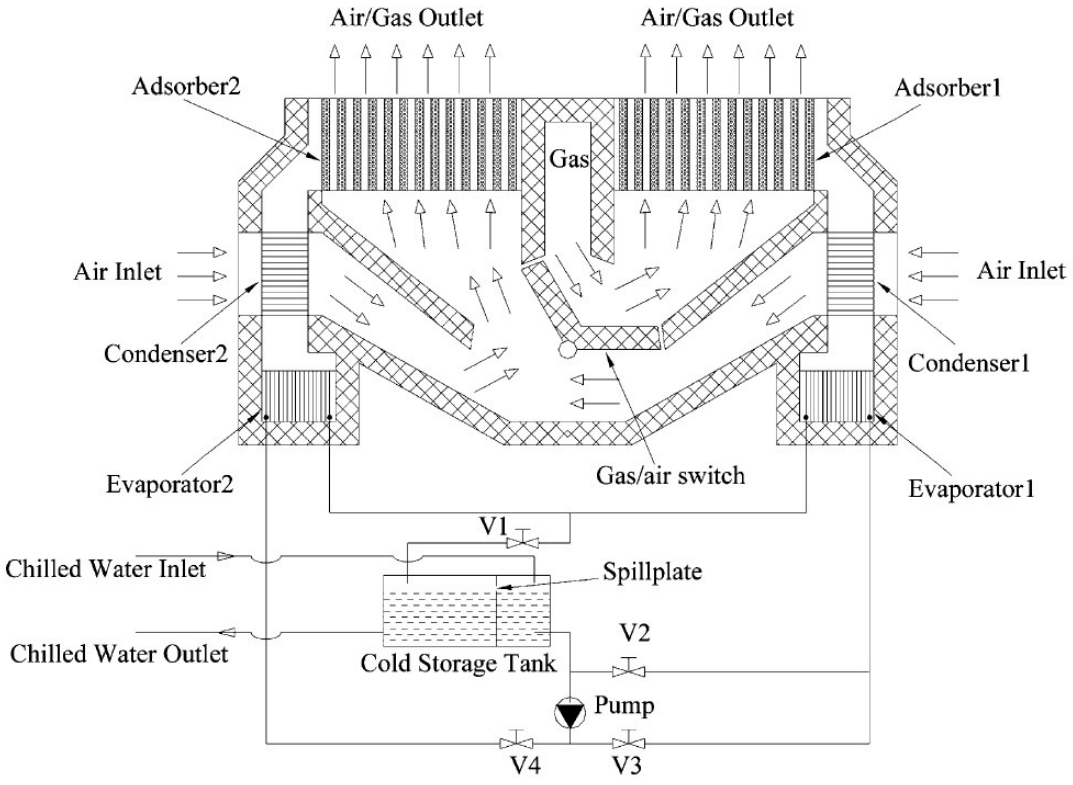

(a) Schematic diagram of adsorption air conditioner.

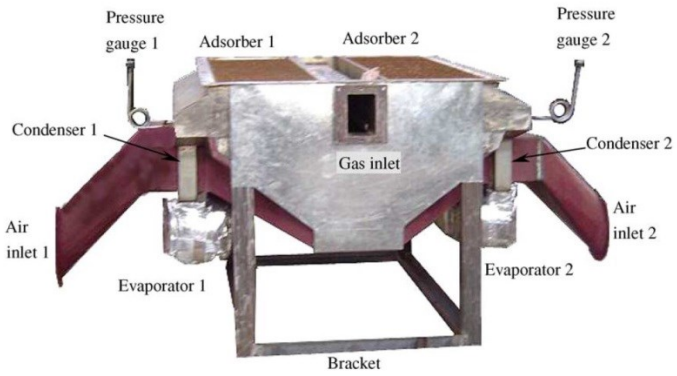

(b) Pictorial view of adsorption air conditioner.

Fig. 1.10 Adsorption air conditioner for locomotive [42].

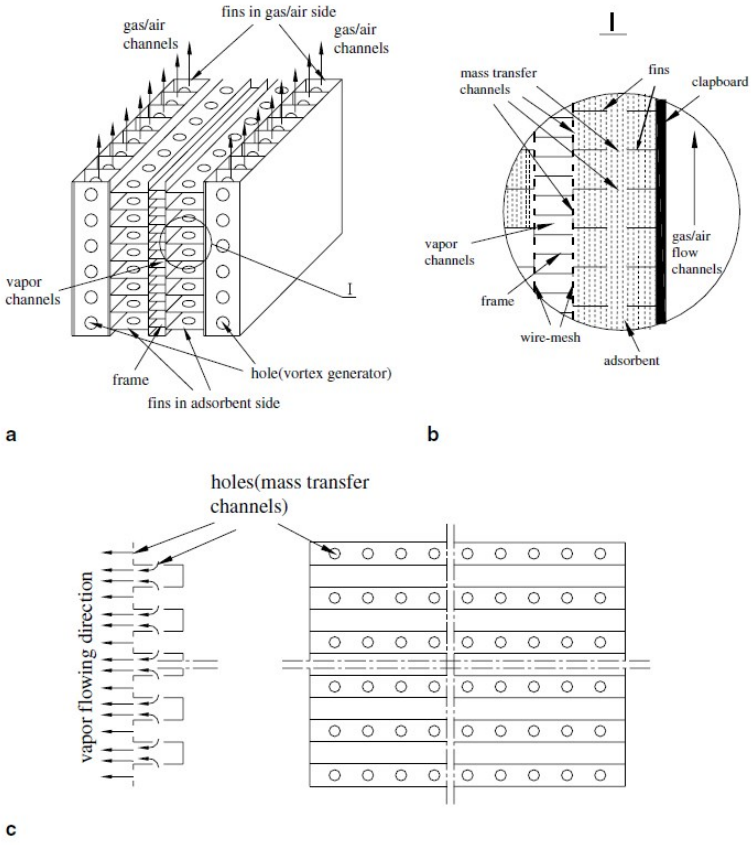

(a) Full view (b) Partial enlarged detail (c) Perforated fin arrangement in the adsorbent side

Fig. 1.11 Structure of the adsorber [42].

L. Z. Zhang [57] developed zeolite 13X/water based adsorption cooling system powered by waste heat from diesel engine in the automobile and performances are also evaluated. In this system, double-tube pipe is employed as sorption bed and zeolite 13X pallets are packed between inner and outer tubes as shown in Fig. 1.12. The cooling and heating sources flow through the inner tube to supply or extract heat from the adsorbent. Exhausted gas from engine and ambient air are used as heating and cooling sources and flow to the inside of inner tube directly. The schematic diagram of test section is shows in Fig. 1.13. SCP and COP are found to be 25.7 W/kg and 0.38 in this system.

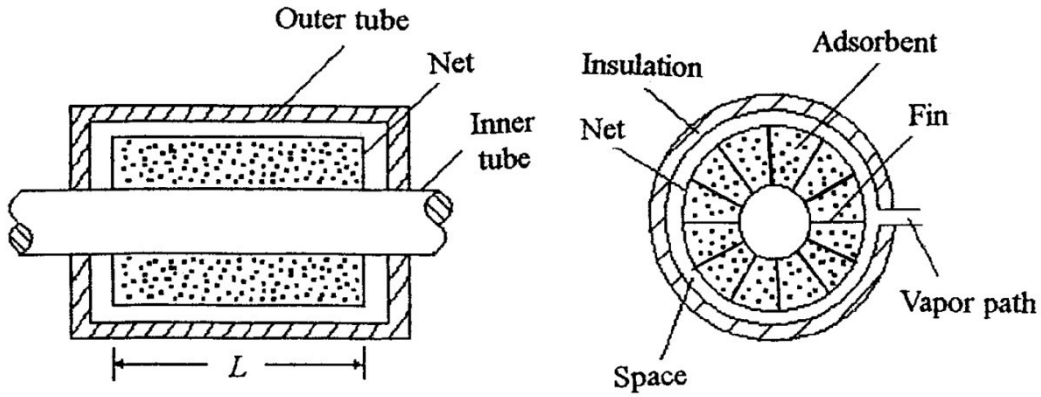

Fig. 1.12 Double tube pipe type adsorber [57].

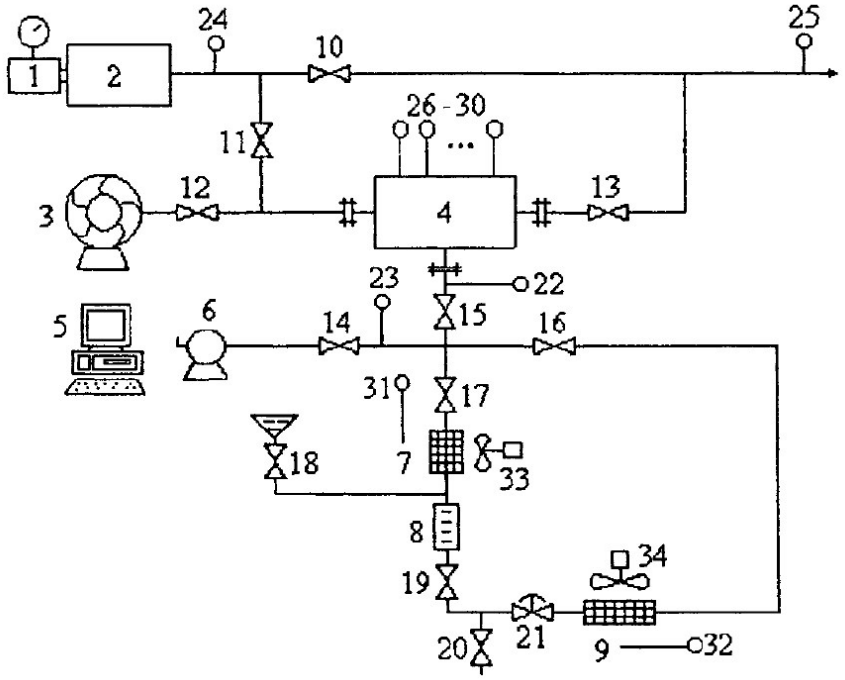

Fig. 1.13 Schematic diagram adsorption cooling system for automobile [57].

(1) Power gauge, (2) Engine, (3) Blower, (4) Adsorber, (5) Computer, (6) Vacuum pump, (7) Condenser, (8) Graduated bottle, (9) Evaporator, (10 - 13) Valves, (14 - 21) Vacuum valves, (22 - 23) Pressure gauges, (24 - 32) Thermocouples, (33, 34) Fans.

1.2.6.2. Solar energy utilization

Recent, solar energy is getting attention as useful clean energy in various fields such as house heating and electricity production. Solar energy can be also applied to the driving source of adsorption cooling system. Fadar et al. [58] proposed numerical modeling of continuous two-bed type adsorption refrigeration system powered by parabolic trough solar collector using activated/carbon pair and determined the performances. Alghoul et al. [59] proposed a dual purpose continuous solar adsorption system employing activated carbon/methanol pair and estimated the performance theoretically. Mahesh et al. [60] reviewed various types of adsorption cooling systems powered by solar energy and compared the performances of those systems. Hassan et al. [61] reviewed previous studies on solar driven closed type physisorption refrigeration systems and discussed various refrigeration technologies and advancements to improve the performance of adsorption systems.

1.2.6.3. Fuel cell waste heat utilization

At present, many researches are involved in conducting research, development and demonstration (RD&D) activities on the fuel cell co-generation system as an energy saving technology for industry and building applications. However, application to the adsorption refrigeration system has not been actively studied. Clausse et al. [62] compared the performances of adsorption air conditioning systems powered by PEMFC waste heat for activated carbon/methanol, silica gel/water and zeolite/water pairs.

1.3. Objective and scopes

The Main objective of this work is to develop fuel cell waste heat powered adsorption cooling system using compact fin-tube adsorber/desorber heat exchanger which employs silica gel RD (2060)/water as adsorbent/refrigerant pair. This work contributes in reducing the footprint of the adsorption cooling system and to improve the system performance. The scopes of the present work are:

I. To determine the thermophysical properties of the three different sizes of silica gel RD 2060 (fine powder; 75 - 150 μm, roughed powder; 250 μm - 1 mm, grain; 1 - 1.81 mm) by measurement of N_2 adsorption isotherms using BELSORP Mini II.
II. To measure adsorption isotherms of water vapor onto granular silica gel of type RD (2060) employing the compact fin-tube heat exchanger and to fit the adsorption isotherm data with popular isotherm models.
III. To study the transient behavior of two-bed adsorption cooling system using compact fin-tube heat exchanger employing silica gel RD (2060)/water pair and to investigate the effect of operating parameter in terms of heat transfer fluid inlet temperatures, flow rates and operation cycle time and switching time allocation on the system performance.
IV. To study the dynamic behavior of fuel cell waste heat powered adsorption cooling system using compact fin-tube adsorber/desorber heat exchanger.

1.4. Thesis outline

This thesis consists of seven chapters followings are brief description of the contents of each chapter.

Chapter 1 introduces the research objective and thesis outline and presents a comprehensive review of various adsorption cooling systems. The operation method of basic adsorption cooling cycle is also discussed. In this chapter, various adsorbents, commonly used adsorbent/refrigerant pairs, advanced technologies of adsorption cooling systems and applications of adsorption cooling systems are reviewed.

In chapter 2, thermophysical properties of three different sizes of silica gel RD 2060 are determined using volumetric N_2 adsorption isotherms such as pore size, pore volume, surface area and pore size distribution to select most suitable adsorbent among three different sizes of silica gels prior to conduct experiment using the compact fin-tube heat exchanger. Furthermore, adsorption dynamics of water onto cylindrical shape silica gel particles are determined numerically in three different arrangements by coupled heat and mass transfer equations using finite volume based ANSYS FLUENT environment.

Adsorption isotherm experiment of silica gel RD/water pair employing a compact fin-tube heat exchanger has been conducted in chapter 3. The temperature profiles of the adsorbent inside the compact fin-tube heat exchanger, adsorption uptake rate and adsorption isotherms are also presented.

Chapter 4 provides dynamic behavior of silica gel/water based adsorption cooling system employing a compact heat exchanger. Overall heat transfer coefficient of the

compact heat exchanger is experimentally evaluated and the numerical value is employed in the mathematical model. Parametric study is also conducted to estimate effects of heat transfer fluid (hot, cooling and chilled water) inlet temperatures, heat transfer fluid flow rates, adsorption/desorption cycle time and switching time on the system performance in terms of cooling capacity and COP.

Chapter 5 presents numerical analysis of adsorption cooling system powered by waste heat extracted from two types of fuel cells employing a compact fin-tube heat exchanger. A heat source temperature of 61.2˚C that extracted from PEFC and 90˚C that provided by SOFC are used in mathematical modeling. The Effects of cycle time allocation, heat transfer fluid temperatures and flow rate are also investigated and presented.

The overall conclusion of this thesis has been presented in Chapter. 6. The present work may lead to reduce the adsorption system footprint due to employing the compact fin-tube adsorber/desorber heat exchanger. Furthermore, the integrated adsorption cooling and fuel cell system will be promising technology for both power generation and cooling application.

References

[1] B. Choudhury, B. B. Saha, P. K. Chatterjee and J. P. Sarkar, An overview of developments in adsorption refrigeration systems towards a sustainable way of cooling, Applied Energy 104, (2013) 554 - 567.

[2] B.B. Saha, K. Thu, A. Chakraborty and K.C. Ng, Most energy efficient approach of desalination and cooling, Cooling India 5 (2), (2009) 70 - 76.

[3] A. A. Askalany, B. B. Saha, K. Kariya, I. M. Ismail, M. Salem, A. H. H. Ali and M. G. Morsy, Hybrid adsorption cooling systems-An overview, Renewable and Sustainable Energy Reviews 16, (2012) 5787 - 5801.

[4] The European educational tool on co generation 2nd Edition, COGEN Europe (The European Association for the Promotion of Cogeneration), (2001).

[5] D. W. Wu and R. Z. Wang, Combined cooling, heating and power; A review, Progress in Energy and Combustion Science 32, (2006) 459 - 495.

[6] A. S. Ülkü, Adsorption heat pumps, Journal of Heat Recovery System 6 (4), (1986) 227-284.

[7] F. Meunier, Adsorptive cooling: a clean technology, Clean Products and Processes 3 (2001) 8-20.

[8] H. T. Chua, K. C. Ng, A. Malek, T. Kashiwagi, A. Akisawa and B. B. Saha, Multi-bed regenerative adsorption chiller-improving the utilization of waste heat and reducing the chilled water outlet temperature fluctuation, International Journal of Refrigeration 24, (2001) 124-136.

[9] M. Ron, A hydrogen heat pump as a bus air conditioner, Journal of the Less Common Metals 104 (2), (1984) 259-278.

[10] B. Q. Han, R. Q. Zhu and J. Y. Wu, A study on zeolite molecular sieve adsorption refrigeration using exhaust heat from diesel engine, Proceeding of the international conference on energy saving in refrigeration, (1986) 104-109.

[11] A. S. Ülkü and M. Mobedi, Adsorption in energy storage, Energy Storage systems NATO ASI series 167, (1989) 487-507.

[12] R. E. Critoph and S. J. Metcalf, Specific cooling power intensification limits in ammonia-carbon adsorption refrigeration systems, Applied thermal Engineering 24, (2004) 661-678.

[13] B. B. Saha, S. Koyama, J. B. Lee, K. Kuwahara, K. C. A. Alam, Y. Hamamoto, A. Akisawa and T. Kashiwagi, Performance evaluation of a low-temperature waste heat driven multi-bed adsorption chiller, International Journal of Multi Phase Flow 29 (8), (2003) 1249-1263.

[14] H. T. Chua, K. C. Ng, A. Malek, T. Kashiwagi, A. Akisawa and B. B. Saha, Modeling the performance of two-bed, silica gel-water adsorption chillers, International journal of Refrigeration 22 (3), (1999) 194-204.

[15] N. C. Srivastava and I. W. Eames, A review of adsorbents and adsorbates in solid-vapor adsorption heat pump systems, Applied Thermal Engineering 18, (1998) 707-714.

[16] O. C. Iloeje, A. N. Ndili and S. O. Enibe, Computer simulation of a $CaCl_2$ solid adsorption solar refrigerator, Energy 20 (11), (1995) 1141-1151.

[17] Y. Kato, M. Yamada, T. Kanie and Y. Yoshizawa, Calcium oxide/carbon dioxide reactivity in a packed bed reactor of a chemical heat pump for high-temperature gas reactors, Nuclear Engineering and Design 210, (2001) 1-8.

[18] L. W. Wang, R. Z. Wang, J. Y. Wu, K. Wang and S. G. Wang, Adsorption ice maker for fishing boats driven by exhaust heat from diesel engine: choice of adsorption pair, Energy Conversion and Management 45, (2004) 2043-2057.

[19] L. W. Wang, R. Z. Wang, J. Y. Wu and K. Wang, Compound adsorbent for adsorption ice maker on fishing boats, International Journal of Refrigeration 27, (2006) 401-408.

[20] M. Groll, Reaction beds for dry sorption machines, Heat Recovery Systems and CHP 13, (1993) 341-346.

[21] V. Ponec, Z. Knor and S. Cerny, Adsorption on solids, Butterworths, 1974.

[22] R. T. Yang, Gas separation by adsorption methods, Publishing House of Chemical Industry, 1991.

[23] J. Oscik, Adsorption, Ellis Horwood Ltd./John Wiley and Sons, 1982.

[24] D. M. Ruthven, Principles of adsorption and adsorption process, John Wiley and Sons, 1984.

[25] M. Suzuki, Adsorption Engineering, Elsevier Science Publishers, 1990.

[26] H. Marsh and F. Rodríguez-Reinoso, Activated carbon, Oxford: Elsevier.

[27] L. W. Wang, S. J. Metcalf, R. E. Critoph, R. Thorpe and Z. Tamainot-Telto, Development of thermal conductive consolidated activated carbon for adsorption refrigeration, Carbon 50 (3), (2012) 977-986.

[28] P. J. F. Harris, Z. Liu and K. Suenaga, Imaging the atomic structure of activated carbon, Journal of Physics: Condensed Matter 20, (2008) 1-5.

[29] Y. H. Zhang, Adsorption function, Publishing House of Scientific and Technological Literature, (1989).

[30] B. B. Saha, I. I. El-Sharkawy, A. Chakraborty and S. Koyama, Study on an activated carbon fiber-ethanol adsorption chiller: Part Ⅱ - Performance evaluation, International Journal of Refrigeration 30 (1), (2007) 96-102.

[31] K. B. Yoon, Nanoporous Material, Physical and High technology 13, 2004, 2-11.

[32] S. L. Li, J. Y. Wu, Z. Z. Xia and R. Z. Wang, Study on adsorption performance of adsorbent of $CaCl_2$ and expanded graphite with ammonia as adsorbate, Energy Conversion and Management 50 (4), (2009) 1011-1017.

[33] Y. Zhong, R. E. Critoph, R. N. Thorpe, Z. Tamainot-Telto, Yu. I. Aristov, Isothermal sorption characteristics of the BaCl2-NH3 pair in vermiculite host matrix, Applied Thermal Engineering 27, (2007) 2455-2462.

[34] Y. Kato, F. Takahashi, A. Watanabe and Y. Yoshizawa, Thermal analysis of a magnesium oxide/water chemical heat pump for cogeneration system, Applied Thermal Engineering 21, (2001) 1067-1081.

[35] Y. Kato, Y. Sasaki and Y. Yoshizawa, Magnesium oxide/water chemical heat pump to enhance energy utilization of a cogeneration system, Energy 30 (11-12), (2005) 2144-2155.

[36] T. X. Li, R. Z. Wang, R. G. Oliveira, J. K. Kiplagat and L. W. Wang, A combined double-way chemisorption refrigeration cycle based on adsorption and resorption processes, International Journal of Refrigeration 32 (1), (2009) 47-57.

[37] V. Valkov, R. Cpte, G. Perron and G. B. B. La, Experimentation of a new thermochemical material based on carbon fiber, Proceeding of the International Sorption Heat Pump Conference, (1999) 239-245.

[38] C. H. Lee, S. H. Park, S. H. Choi, Y. S. Kim and S. H. Kim, characteristics of non-uniform reaction blocks for chemical heat pump, Chemical Engineering Science 60, (2005) 1401-1409.

[39] D. I. Tchernev, Solar Refrigeration utilizing zeolites, Intersociety Energy Conversion Engineering Conference 2, (1980) 2070-2073.

[40] M. Tather, A. Erdem-Senatalar, When do thin zeolite layers and large void volume in the adsorber limit the performance of adsorption heat pump?, Microporous and Mesoporous Material 54 (1-2), (2002) 89-96.

[41] R. Q. Zhu, B. Q. Han, M. Z. Lin and Y. Z. Yu, Experimental investigation on an adsorption system for producing chiller water, International Journal of Refrigeration 15 (1), (1992) 31-34.

[42] D. C. Wang, Z. Z. Xia and J. Y. Wu, Design and performance prediction of a novel zeolite-water adsorption air conditioner, Energy Conversion and Management 47, (2006) 590-610.

[43] R. L. Yeh, T. K. Ghosh and A. L. Hines, Effects of regeneration condition on the characteristics of water vapor adsorption on silica gel, Journal of Chemical Engineering 37, (1997) 259-261.

[44] K. C. Ng, H. T. Chua, C. Y. Chung, C. H. Loke, T. Kashiwagi, A. Akisawa and B. B. Saha, Experimental investigation of the silica gel-water adsorption isotherm characteristics, Applied Thermal Engineering 21, (2001) 1631-1642.

[45] H. T. Chua, K. C. Ng, A. Chakraborty, N. M. Oo and M. A. Othman, Adsorption characteristics of silica gel + water systems, Journal of Chemical Engineering 47, (2002) 1177-1181.

[46] X. Wang, W. Zimmermann, K. C. Ng, A. Chakraborty and J. U. Keller, Investigation of the isotherm of silica gel + water systems : TG and volumetric methods, Journal of Thermal Analysis and Calorimetry 76, (2004) 659-669.

[47] T. Miyazaki, A. Akisawa, B. B. Saha, I. I. El-Sharkawy and A. Chakraborty, A new cycle time allocation for enhancing the performance of two-bed adsorption chiller, International Journal of Refrigeration 32, (2009) 846-853.

[48] H. T. Chua, K. C. Ng, W. Wang, C. Yap and X. L. Wang, Transient modeling of a two-bed silica gel-water adsorption chiller, International Journal of Heat and Mass Transfer 47, (2004) 659-669.

[49] M. Z. I. Khan, K. C. A. Alam, B. B. Saha, Y. Hamamoto, A. Akisawa and T. Kashiwagi, Parametric study of a two-stage adsorption chiller using re-heat-The effect of overall thermal conductance and adsorbent mass on system performance, International Journal of Thermal Sciences 45, (2006) 511-519.

[50] B. B. Saha, A. Akisawa and T. Kashiwagi, Silica gel water advanced adsorption refrigeration cycle, Energy 22-4, (1997) 437-447.

[51] K. C. Alam, B. B. Saha, Y. T. Kang, A. Akisawa and T. Kashiwagi, Heat exchanger design effect on the system performance of silica gel adsorption refrigeration systems, International Journal of Heat and Mass Transfer 43, (2000) 4419-4431.

[52] J. Li, M. Kubota, F. Watanabe, N. Kobayashi and M. Hasatani, Optimal design of a fin-type silica gel tube module in the silica gel/water adsorption heat pump, Journal of Chemical Engineering of Japan 37 (4), (2004) 551-557.

[53] G. Maggio, L. G. Gordeeva, A. Freni, Yu. I. Aristov, G. Santori, F. Polonara and G. Restuccia, Somulation of a solid sorption ice-maker based on the novel composite

sorbent “lithium chloride in silica gel pores”, Applied Thermal Engineering 29 (8-9), (2009) 1714-1720.

[54] I. I. El-Sharkawy, K. Kuwahara, B. B. Saha, S. Koyama and K. C. Ng, Experimental investigation of activated carbon fibers/ethanol pairs for adsorption cooling system application, Applied Thermal Engineering 26, (2006) 859-865.

[55] B. B. Saha, S. Koyama, I. I. El-Sharkawy, K. Kuwahara, K. Kariya and K. C. Ng, Experiments for measuring adsorption characteristics of an activated carbon fiber/ethanol pair using plate-fin heat exchanger, Heating Ventilating and Air Conditioning Research Special Issue 12 (3b), (2006) 767-782.

[56] B. B. Saha, I. I. El-Sharkawy, A. Chakraborty and S. Koyama, Study on activated carbon fiber-ethanol adsorption chiller: Part Ⅰ - system description and modeling, International Journal of Refrigeration 30 (1), (2007) 86-95.

[57] L. Z. Zhang, Design and testing of an automobile waste heat adsorption cooling system, Applied Thermal Engineering 20, (2000) 103-114.

[58] A. El Fadar, A, Mimet and M. Pérez-García, Modeling and performance study of a continuous adsorption refrigeration system driven by parabolic trough solar collector, Solar Energy 83 (2009) 850-861.

[59] M. A. Alghoul, M. Y. Sulaiman, K. sopian and B. Z. Azmi, Performance of dual purpose solar continuous adsorption system, Renewable Energy 34 (2009) 920-927.

[60] A. Mahesh and S. C. Kaushik, Solar adsorption cooling system: An overview, Journal of Renewable and Sustainable Energy 4 (2012) 022701.

[61] H. Z. Hassan and A. A. Mohamad, A review on solar powered closed physisorption cooling systems, Renewable and Sustainable Energy Reviews 16 (2012) 2516-2538.

[62] M. Clausse, F. Meunier, J. Coulie and E. Herail, Comparison of adsorption system using natural gas fired fuel cell as heat source, for residential air conditioning, International Journal of Refrigeration 32 (2009) 712-719.

Chapter 2

Chapter 2

Thermophysical Properties of Silica Gel RD 2060 and the Investigation of Adsorption Dynamics of Silica Gel/Water Pair

2.1. Introduction

In the past decades, adsorption thermodynamic processes are widely used in the industries such as gas separation, purification, adsorption cooling, gas storage, dehydration and desalination applications with their environmentally friendliness and high utilization of low grade of waste heat [1]. Whereas, adsorption processes still contains lower adsorption performance and heat transfer. Demir et al. [2] and Wang et al. [3] reported comprehensive review of adsorption technologies and deteriorations, and their solutions were also proposed. The adsorption performance is influenced by working conditions such as temperature of adsorption, desorption and evaporation as well as thermophysical properties such as surface area, pore diameter, pore volume. Thermophysical properties and adsorption isotherm characteristics for adsorbent/adsorbate pair are reported by various authors.

Yeh et al. [4] evaluated effects of regeneration temperatures and times on adsorption isotherm for water vapor onto silica gel and the role of surface heterogeneity on the adsorption process were determined using adsorption isotherm data. Ng et al. [5] conducted adsorption equilibrium uptake of water on type A, 3A and RD silica gels using control volume variable pressure (CVVP) apparatus and isothermal characteristics of these three types of adsorbents are presented by Henry-type isotherm model. Chua et al. [6] and X. Wang et al. [7] investigated equilibrium uptake of water on type A and type RD silica gels using the same apparatus of CVVP. They also determined the thermophysical properties of the studied adsorbents. Thu et al. [8] evaluated thermophysical properties and surface characteristics of three different types of silica gels, namely, Type RD 2560, Type A5BW and Type A^{++} using N_2 adsorption isotherm data and water uptake on these three different types of silica gels are also investigated. Saha et al. [9] investigated adsorption isotherm of N_2 on Cu-sputtered type

RD silica gel using Autosorb 1-MP machine and compared with isotherms of 3A, A++, parent RD silica gels. Thermophysical properties are also determined and compared with that of parent RD type silica gel. Glaznev et al. [10] determined thermophysical properties of SBA-15 + $CaCl_2$ composited adsorbent and compared with those of parent SBA-15 and SWS-1L by N_2 adsorption using a Micromeritics ASAP 2040 analyzer. Water adsorption isotherm on synthesized SBA-15 was also measured and compared with those of type RD silica gel, SWS-1L and FAM-Z02. Same author [11] investigated grain size effects of silica gel RD on the water adsorption isotherm at various cycle boundary conditions. Gong et al. [12] measured equilibrium uptake of water on composited adsorbent (silica gel + lithium chloride) by the sorption isosteric method and thermophysical properties are also determined, thereby, compared the results with those of parent silica gel.

Moreover, how to improve efficiency of adsorptive heat transfer (AHT), is also being issued in that field. Various authors presented several methods to enhance the heat transfer in the adsorption system.

Freni et al. [13] conducted to experiment of water adsorption employing finned tubes heat exchanger coated with SWS-1L compact layer and compared performances with those of typical SWS-1L pelletized bed. Simulation of water adsorption heat transfer on the grain of silica gel Type RD was conducted by Freni et al. [14]. In this simulation, adsorption heat transfer characteristics in the variation of layers were estimated on the three types of grain size and compared with those of experiment. Chang et al. [15] have studied heat transfer performance between adsorbent and metal substrate in the silica gel-coated adsorber. Furthermore, effect of the thickness of silica gel layer and the particle size on the heat transfer was investigated. Li et al. [16] developed the fin-type silica gel tube (FST) module and heat and mass transfer characteristics in using FST module were analyzed numerically.

This study aims to determine thermophysical properties of three different sizes of silica gel RD 2060 using volumetric N_2 adsorption isotherms such as pore size, surface area and pore size distribution to choose most suitable adsorbent among three different sizes of silica gels prior to conduct experiment using compact fin-tube heat exchanger. Furthermore, arrangement and fin effects on the adsorption characteristic of water onto cylindrical silica gel particle are evaluated numerically.

2.2. Thermophysical properties of silica gel RD 2060

2.2.1 Experiment

Three different sizes of silica gel RD 2060, namely powder 1 (fine powder; 75 - 250 μm), powder 2 (roughed powder; 250 μm - 1 mm) and grain (1 - 1.81 mm) types are selected for adsorption isotherm and adsorption characteristic measurements as shown in Fig. 2.1. The porosity, average pore diameter and surface area of the samples were measured by the adsorption isotherm of N_2 at 77.4 K by Belsorp Mini II machine and the analysis was performed using system's built-in data reduction software, BELMASTER. Sample cell was first filled with about 0.1g of samples and treated for possible degassing at a temperature of 473.15K for 6h during evacuation with pressure as 10^{-4} Pa to eliminate residual water vapor from the samples using BELPREP-vac II. Figure 2.2 shows schematic diagram of Belsorp Mini II machine. As shown in Fig. 2. 2, this machine comprises measuring parts; two sample cells, one dead volume cell and P_0 tube, and measuring device parts; five pressure sensors, one pirani vacuum gauge and one temperature sensor, and valves including two needle valves, namely, V5 and V6 which control flow rate of N_2, and 2L of the Dewar vessel. It operates by measuring the quantity of adsorbate (gas phase) adsorbed onto or desorbed from a surface of adsorbent (solid phase) at an equilibrium vapor pressure by volumetric method which is useful to measure N_2 isotherm [17]. The dead volume is also measured using advanced free space measurement (AFSM) method to calculate uptake amount with high precision and reproducibility while measuring the adsorption isotherm. The data are obtained by admitting or removing a known quantity of adsorbate gas into or out of a sample cell containing the solid adsorbent which is maintained at a constant temperature below the critical temperature of the adsorbate. As adsorption or desorption occurs, the pressure in the sample cell changes until equilibrium is established. The quantity of adsorbate gas adsorbed or desorbed at the equilibrium pressure is expressed by the difference between the amount of adsorbate gas admitted or removed and amount required to fill the space around the void space of the assorted adsorbent.

a) powder1 b) powder2 C) grain

Fig. 2.1 Pictures of three types of silica gel RD 2060.

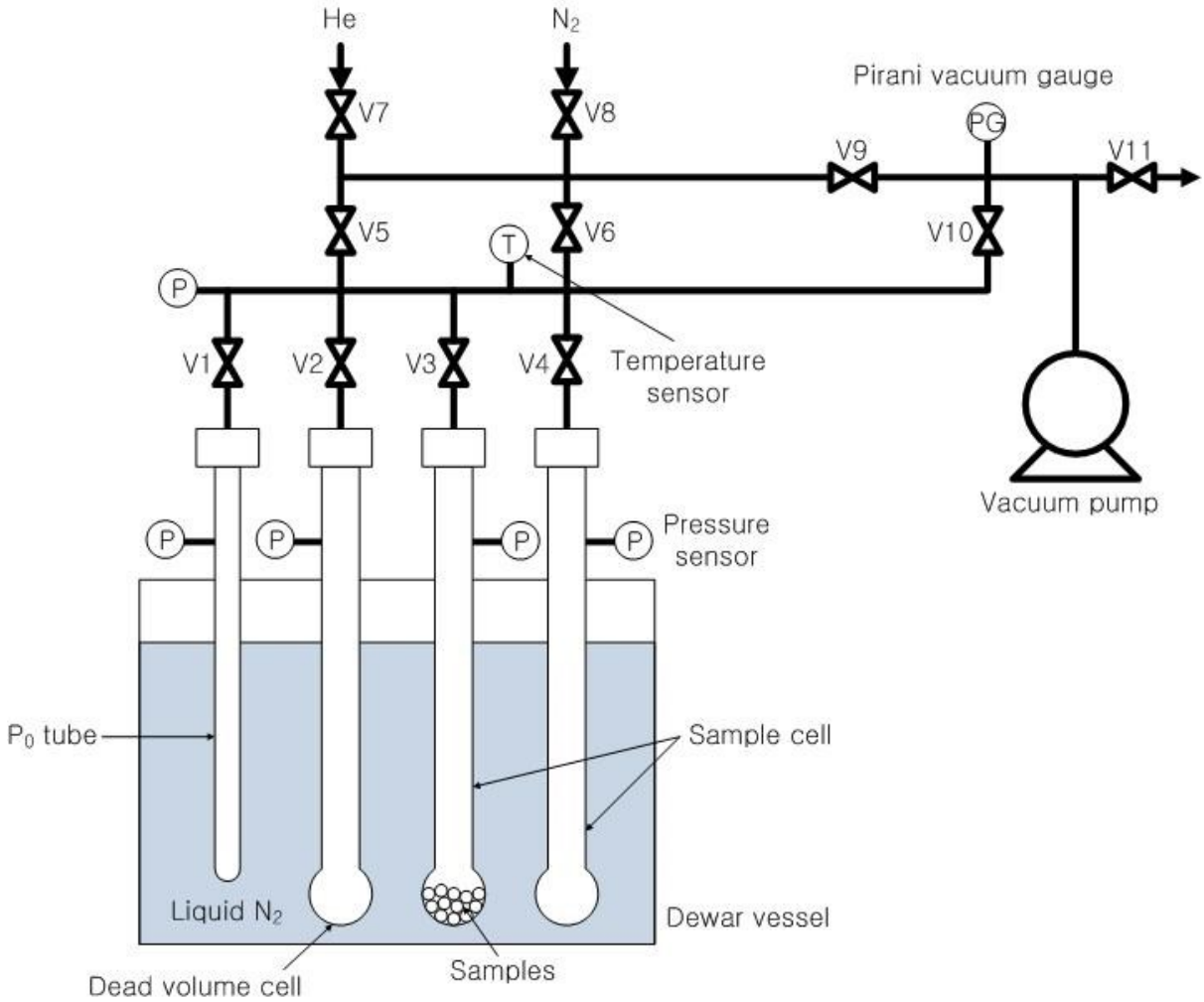

Fig. 2.2 Schematic diagram of Belsorp Mini II machine.

2.2.2. Adsorption/desorption isotherms of N_2

Silica gel RD 2060 powder1, mass 0.0944 g; and powder2, mass 0.1120 g; grain, mass 0.1056 g; are prepared as adsorbents to measure adsorption/desorption isotherm. Figure 2.3 shows the adsorption isotherms of N_2 on three kinds of sample at 77 K of adsorption temperature. The N_2 isotherms of these samples can be classified as type I adsorption isotherm of Brunauer classification [18] which is shown in Fig. 2.4. According to Brunauer classification, adsorption isotherms can be classified into five types. Isotherms of type I are generally true for microporous adsorbents. Adsorption of ethanol on activated carbon fiber is an example of this type of isotherms [19]. Type II is observed in adsorbents having a wide range of pore sizes, with ether mono or multi-molecular adsorption layers. Adsorption of benzene vapor on graphitized carbon represents an example of this type of isotherms. Type III is uncommon and they include capillary condensation in addition to the multi-molecular adsorption layer. Adsorption of bromine on silica gel is an example of this type of isotherms. Isotherms of type IV involve formation of two surface layers on the adsorbents having pore size much larger than the molecule diameter of the adsorbate. Isotherms of type V are observed on the adsorbents involving large forces produced by intermolecular attraction such as adsorption of phosphorus on NaX.

These samples have relatively stronger interaction between surface of adsorbent and adsorbate. The maximum uptake of grain was found to be 0.2845 g/g, that of powder2 was found to be 0.235 g/g and that of powder 1 was found to be 0.22 g/g at 0.99 of relative pressure. Grain type of silica gel exhibits a small hysteresis at the relative pressures from 0.45 to 0.47. We have supposed that smaller particle size of adsorbent has larger uptake amount. However, these isotherms show increasing tendency in bigger particle size.

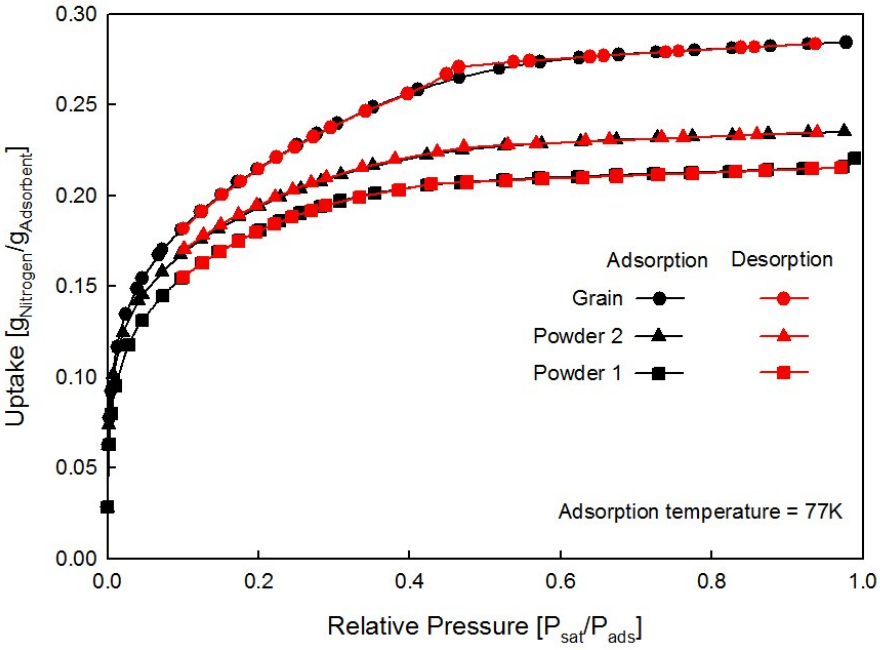

Fig. 2.3 Adsorption isotherms of N_2 on silica gel RD 2060 samples.

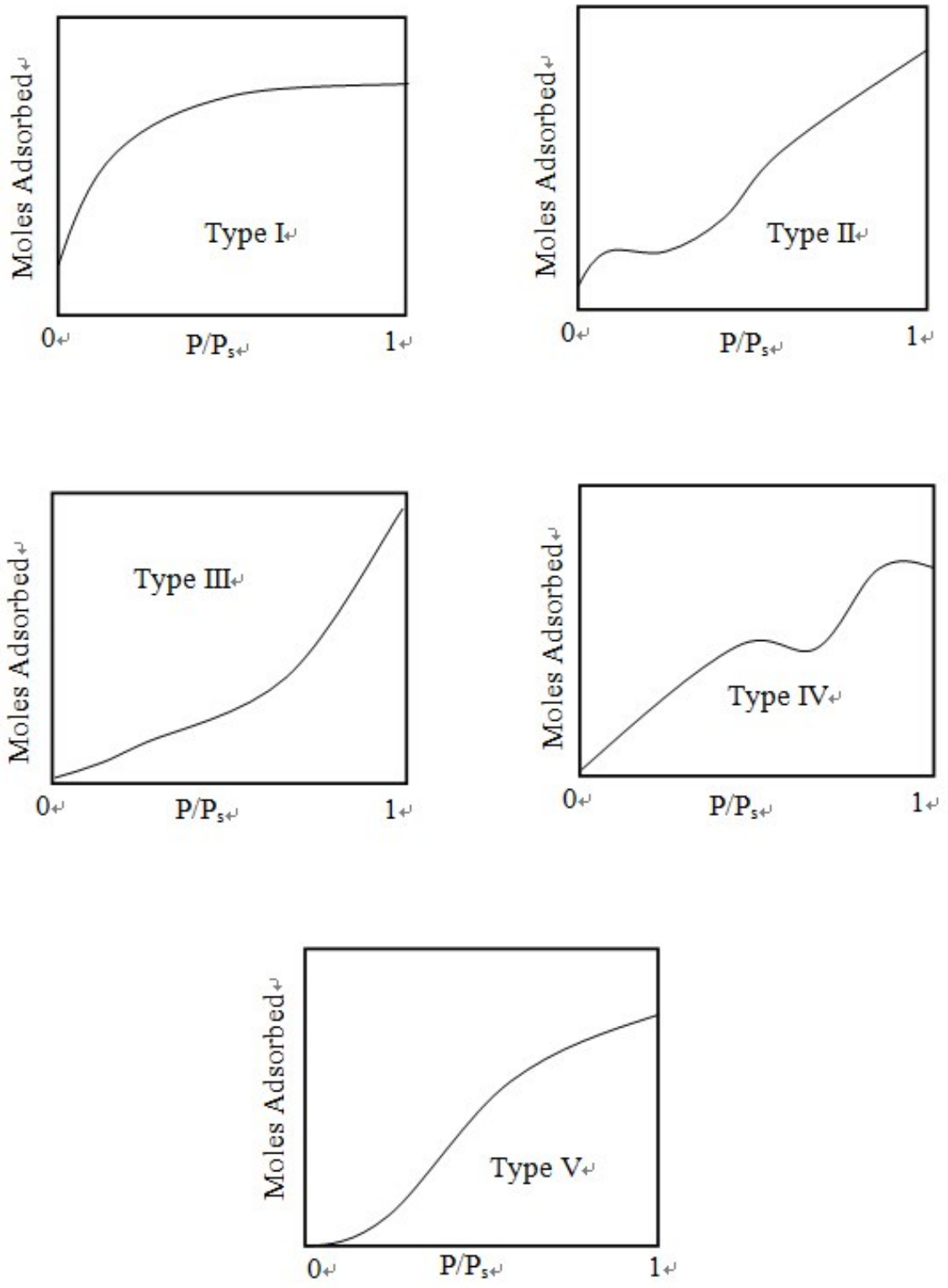

Fig. 2.4 Brunauer classification of adsorption isotherms.

2.2.3. BET and micropore analysis

Thermophysical properties are analyzed with *Brunauer-Emmett-Teller* (*BET*) and *t-plot* method to support isotherm results. In the *BET* analysis, two analysis points were selected between 0.05 and 0.35 and Energy constant C is set to 120 to adjust best leaner fit between N_2 adsorption plots and standard *BET* plots of silica gel. *BET* equation is given as

$$\frac{P_{sat}}{V\left(P_{ads}-P_{sat}\right)}=\frac{1}{V_m c}+\frac{C-1}{V_m c}\left(\frac{P_{sat}}{P_{ads}}\right) \tag{2-1}$$

where, V is the volume of adsorbed N_2, P_{sat} is the saturation pressure at saturation temperature of the adsorbate (N_2) and P_{ads} is the saturation pressure, corresponding to the adsorbent temperature, V_m is volume of adosorbate at monolayer coverage, and C is *BET* constant. *BET plots* are shown in Fig. 2.5 and thermophysical properties by the *BET* analysis are summarized in Table 2.1. These results shows that the granular silica gel possesses larger surface area of 618.36 m^2/g compared with those of powdered silica gels.

Table 2.1 Thermophysical properties by *BET* analysis.

Properties	Units	Values		
		Powder 1	Powder 2	Grain
BET constant	[-]	120	120	122
Correlation coefficient	[-]	0.99	1	0.99
BET surface area	[m^2/g]	523.02	567.3	618.36
Mean pore diameter	[nm]	2.09	2.05	2.28

The *t-plot* method which was investigated by Boer et al. [20], [22] is employed to analyze micropore surface area and micro pore volume for present samples. The *t-plots* indicates volume of adsorbed N_2 versus the statistical thickness of adsorbed film on the adsorbent, t. Figure 2.6 gives *t-plots* of studied samples and micropore properties are furnished in table 2.2. As shown in Fig. 2.6, it can be observed that slopes of curves increase drastically and those become then gradual. That is why pores are filled with adsorbate, thereby adsorbed amount increases drastically in the earlier stage of adsorption, then adsorption occurs only on the

surface of adsorbent after complete adsorption into pores. In these results, both micropore surface area and external surface of granular silica gel are larger than those of powdered silica gels with values of 597.97 m^2/g and 11.3 m^2/g. Values of surface area from the *t-plot* method are found to be agreement compared with those of surface area from *BET* analysis.

Table 2.2 Micropore properties by *t-plot* method.

Properties		Units	Values		
			Powder 1	Powder 2	Grain
Micropore	surface area	[m^2/g]	508.84	559.13	597.97
	volume	[cm^3/g]	0.26	0.28	0.34
External surface		[m^2/g]	6.9	8.3	11.3

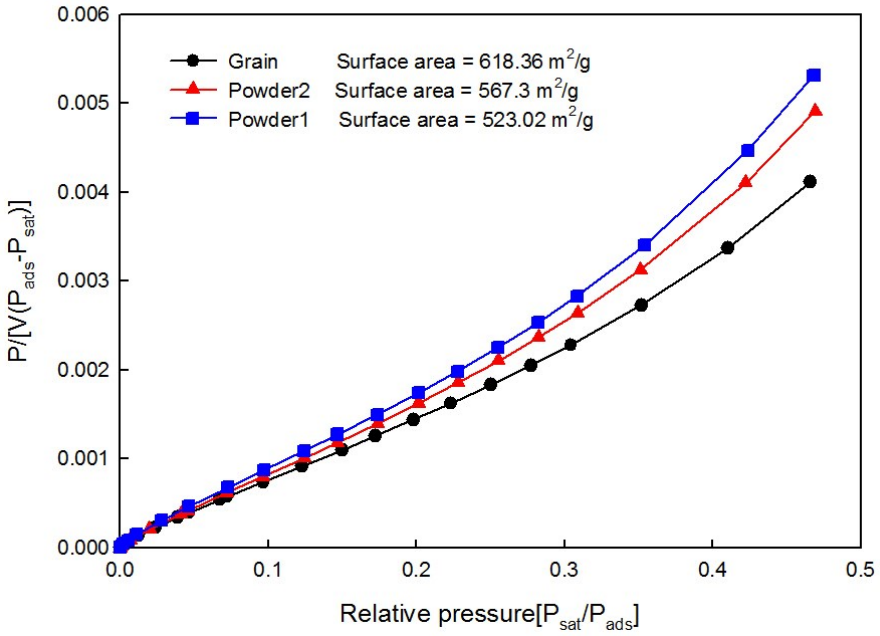

Fig. 2.5 The *BET plots* of present samples.

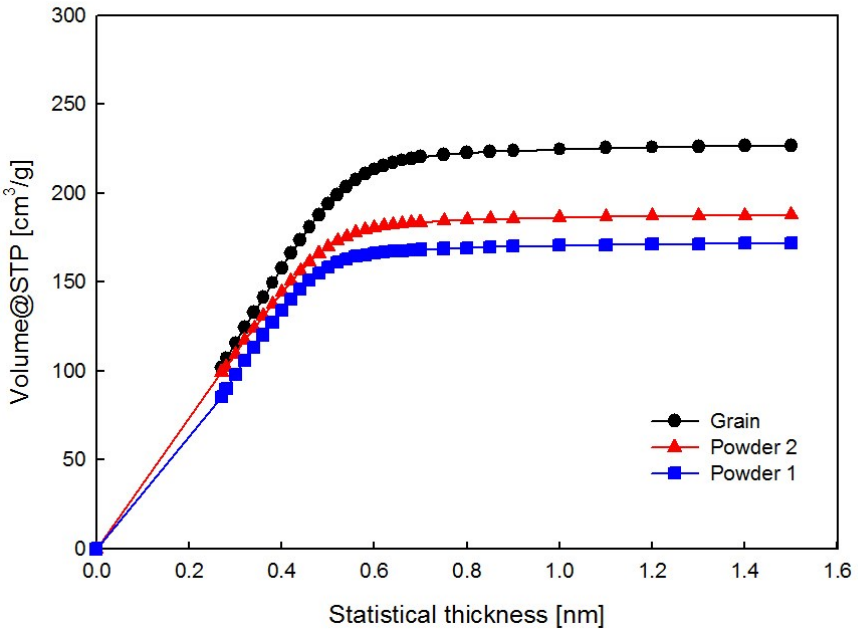

Fig. 2.6 The *t-plots* of present samples.

2.2.4. Pore size distribution

The *MP* method related strongly with *t-plot* method which was investigated by Mikhail et al. [21], [22] was employed to determine pore size distribution (PSD). Figure 2.7 shows PSD of studied samples and all three sizes of silica gel showed similar PSD curves. Pore size of grain type silica gel is distributed at 1.1 nm of pore diameter and those of two different sizes of powder type silica gels are distributed at 1 nm of pore diameter, respectively. In the grain type silica gel, small hysteresis was observed between 0.7 - 0.8 nm of pore diameter. It is found to be that pores of studied three sizes of silica gels distributed in the range of micropores between 0.5 and 2 nm of pore diameter.

From these results, it is found that the sample having bigger particle size shows better performance in terms of uptake and thermophysical properties than samples having smaller particle size. Furthermore, mean pore diameters of three sizes are slightly larger than 2 nm which is known as range of mesopore from the *BET* analysis, whereas micropores are distributed mostly on the surface of these studied samples from the *t-plot* and *MP* analyses. Therefore, it can be concluded that these silica gel RD 2060 samples possess the almost of micropores and some of mesopores.

Additionally, pictures of studied silica gels surface were taken by Fe-SEM (ULTRA 55) at same magnification of 70,000 times. In the surface of silica gel grain, many pores which can be supposed as macro-pore and mesopore are found and surface seems to be very rough as shown in Fig. 2.8(a). On the other hand, lesser pores are observed on the surface of powdered silica gel, powder2, than that of granular silica gel. Some protrusions are observed on the surface like as silica gel grain, however it has smoother surface than silica gel grain as shown in Fig. 2.8(b). In Fig. 2.8(c), surface of the silica gel powder1 is found to be too smooth surface and few pores are detected. These can be inferred that pores on surface of particle were filled with ground particle and blocked when granular silica gel was ground to the powder. These can support above results that the sample having bigger particle size shows better adsorption performance.

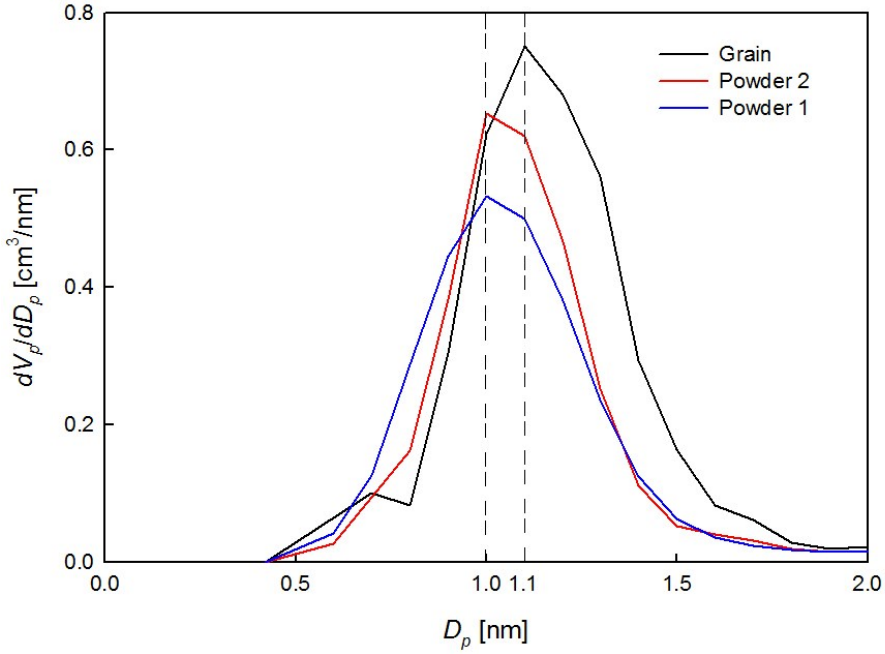

Fig. 2.7 Micropore size distribution by *MP* method.

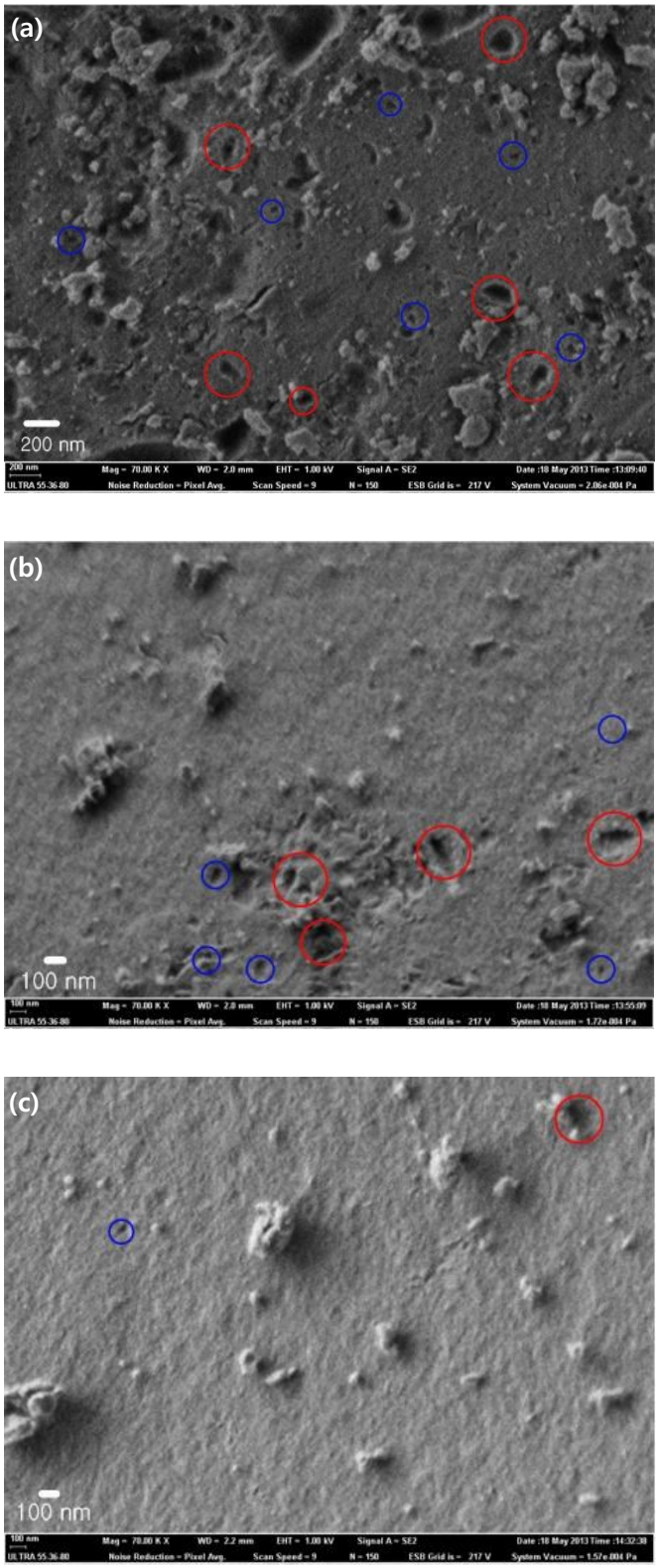

(a) Grain (b) Powder 2 (c) Powder 1

Fig. 2.8 Pictures of surface of samples by Fe-SEM.

(Red circle = Macropore, Blue circle = Mesopore)

2.3. Simulation of adsorption dynamic of cylindrical silica gel particle

The following subscriptions presents a simulation study of loose cylindrical shaped particles packed within copper plate and aluminum fins. The model presented solves coupled heat and mass transfer equations using finite volume based ANSYS FLUENT environment.

2.3.1. Model description

The simulated configuration consists of three cylindrical particles in contact with each other and surrounded by vapor at constant pressure. The diameter of particle d_p is 1.6 mm and the length l_p is 2 mm. The particles are kept on a copper plate of 1 mm thick (t_{cu}) which is assumed to be in direct thermal contact with coolant. The particles are surrounded from two sides by aluminum fin of 0.2 mm thickness (t_{al}). Three possible configurations of cylindrical particle arrangement are considered for analysis as shown in Fig. 2.9(a) - (c). The various assumptions employed in the current model are as follows:

a) The adsorbent grains are identical in shape and size and all its properties are isotropic.
b) The vapor surrounding the grains is stagnant.
c) The vapor phase behaves as ideal gas.
d) Radiation heat transfer is neglected.
e) Tóth's [7] isotherm equation is used to calculate the equilibrium uptake.
f) The adsorbent grain surface is always in equilibrium with the surrounding vapor.
g) The coolant is not simulated and an appropriate convective heat transfer boundary condition is applied between the coolant and the bottom surface of the copper plate.

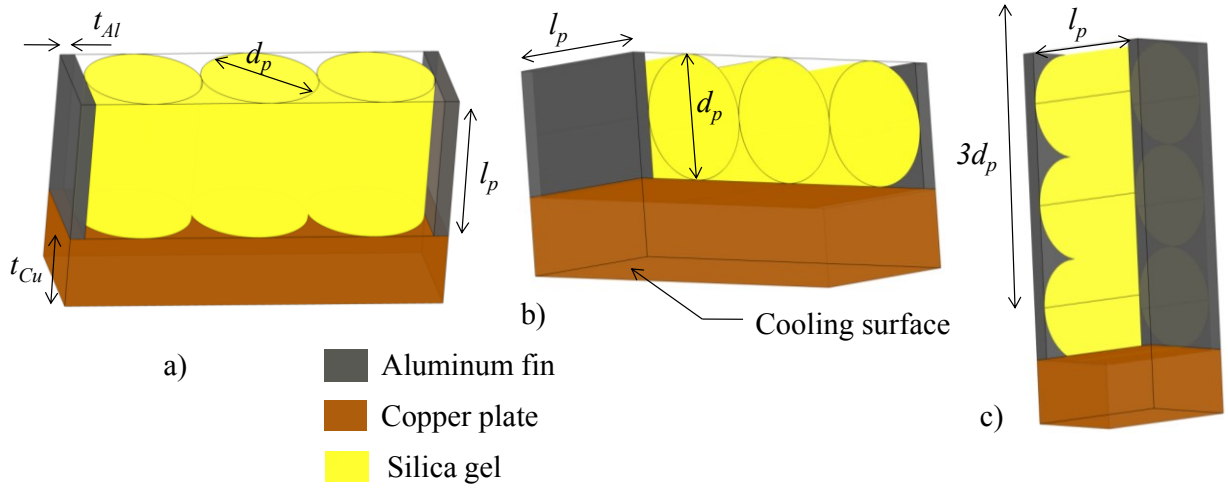

a) Arrangement 1 b) Arrangement 2 c) Arrangement 3.

Fig. 2.9 Three different arrangements of silica gel particles.

2.3.2. Governing equations

The most important feature of adsorbent materials is the large surface area arising from the presence of micro pores. Adsorption occurs in these pores thus requiring the adsorbate to diffuse into the interior of the adsorbent. The two major mechanisms through which the diffusion occurs are pore diffusion of gaseous phase and surface diffusion of the adsorbed phase [25]. The macroscopic mass transfer equation for the silica gel grains taking into account the combined effect of pore diffusion and surface diffusion is given by [25];

$$\varepsilon_p \frac{\partial c}{\partial t} + \rho_{grain} \frac{\partial \phi}{\partial t} = \nabla(D_p \nabla c) + \rho_{grain} \nabla(D_s \nabla \phi) \tag{2-2}$$

Since, the gaseous phase is assumed to behave ideally; the following relation can be used;

$$c = \frac{P}{R_m T} \tag{2-3}$$

The Eq. (2-2) has two unknowns; hence it is necessary to relate the water vapor concentration occupying the void space to that in the adsorbed phase. The uptake of silica gel grain can be expressed as a function of pressure and temperature;

$$\phi = F(P,T) \tag{2-4}$$

In the current study the function $F(P,T)$ used is the Tóth's isotherm equation for water silica gel and is given by [7];

$$F(P,T) = \frac{K_0 P \ \exp\left(\frac{\Delta H_{st}}{R_m T}\right)}{\left[1+\left\{(K_0/q_m)P \ \exp\left(\frac{\Delta H_{st}}{R_m T}\right)\right\}^x\right]^{1/x}} \tag{2-5}$$

The time derivative of uptake can be written using chain rule as follows;

$$\frac{\partial \phi}{\partial t} = \left(\frac{\partial F}{\partial c}\right)\left(\frac{\partial c}{\partial t}\right) = \left[\left(\frac{\partial F}{\partial T}\right)_P \left(\frac{\partial T}{\partial c}\right)_P + \left(\frac{\partial F}{\partial P}\right)_T \left(\frac{\partial P}{\partial c}\right)_T\right]\left(\frac{\partial c}{\partial t}\right) \tag{2-6}$$

Hence, the time derivative of the water vapor concentration in the void is given by;

$$\left(\frac{\partial c}{\partial t}\right) = \frac{\frac{\partial \phi}{\partial t}}{\left[\left(\frac{\partial F}{\partial T}\right)_P \left(\frac{\partial T}{\partial c}\right)_P + \left(\frac{\partial F}{\partial P}\right)_T \left(\frac{\partial P}{\partial c}\right)_T\right]} \tag{2-7}$$

Invoking ideal gas equation the above relation reduces to;

$$\left(\frac{\partial c}{\partial t}\right) = \frac{\frac{\partial \phi}{\partial t}}{\left[\left(\frac{\partial F}{\partial T}\right)_P \left(\frac{-R_m T^2}{P}\right) + \left(\frac{\partial F}{\partial P}\right)_T \left(R_m T\right)\right]} \tag{2-8}$$

$$\Rightarrow \left(\frac{\partial c}{\partial t}\right) = K\left(\frac{\partial \phi}{\partial t}\right) \tag{2-9}$$

$$\text{where,}\quad K=\left[\left(\frac{\partial F}{\partial T}\right)_P\left(\frac{-R_mT^2}{P}\right)+\left(\frac{\partial F}{\partial P}\right)_T\left(R_mT\right)\right]^{-1} \tag{2-10}$$

Similarly, it can be shown that;

$$\nabla c = K\nabla\phi \tag{2-11}$$

Substituting Eq. (2-9) and (2-11) in Eq. (2-2) the following can be obtained;

$$(\varepsilon_p K+\rho_{grain})\frac{\partial\phi}{\partial t}=\rho_{grain}\nabla\left[\left(D_s+KD_p\right)\nabla\phi\right] \tag{2-12}$$

The surface diffusion coefficient is determined as follows [23];

$$D_s = 5.71\times10^{-7}\exp[-0.947\times10^{-3}(\Delta H_{st}/T)] \tag{2-13}$$

The pore diffusion constant of water vapor in pores of radius a can be approximated by the Knudsen diffusion coefficient [23] given by;

$$D_P = 22.86\times a\sqrt{T} \tag{2-14}$$

The typical pore radius of RD type silica gel is 1 nm [24]. The numerical value for K obtained from Tóth's isotherm relation for RD silica gel in the temperature range of 303.15 K to 323.15 K at 900 Pa pressure is found to be 0.002 - 0.0065 kg/m^3. Hence, it may be observed that $KD_p << D_s$ and $\varepsilon_p K << \rho_{grain}$.

The energy equation for the silica gel particle is given by;

$$\rho_{eff}Cp_{eff}\frac{\partial T}{\partial t}=\lambda_{grain}\nabla^2T+\rho_{grain}\Delta H_{st}\left(\frac{\partial\phi}{\partial t}\right) \tag{2-15}$$

where, the effective specific heat capacity of silica gel is defined as;

$$Cp_{eff} = \frac{\rho_{grain}(Cp_{grain} + \phi Cp_a) + \varepsilon_p \rho_v Cp_v}{\rho_{eff}} \tag{2-16}$$

where, effective density of the silica gel particle is determined as;

$$\rho_{eff} = \rho_{grain}(1+\phi) + \varepsilon_p \rho_v \tag{2-17}$$

The last term in Eq. (2-15) is the energy source term due to the adsorption process. The energy diffusion equation for the water vapor and metal zones in the domain is given by;

$$\frac{\partial T}{\partial t} = \alpha_v \nabla^2 T \tag{2-18}$$

$$\frac{\partial T}{\partial t} = \alpha_{Cu} \nabla^2 T \tag{2-19}$$

$$\frac{\partial T}{\partial t} = \alpha_{Al} \nabla^2 T \tag{2-20}$$

The Eq. (2-12), (2-15) and (2-18) to (2-20) are solved simultaneously to determine the temperature and uptake contours. The property values used in the current model are tabulated in Table 2.3. The volume average uptake and temperature for silica gel grain at any given time is defined as;

$$\bar{\phi} = \frac{\int \phi \, dV}{\int dV} \tag{2-21}$$

$$\bar{T} = \frac{\int T \, dV}{\int dV} \tag{2-22}$$

The average uptake and temperature has been normalized with respect to their initial and final value as follows;

$$\bar{\phi}_{norm} = \frac{\bar{\phi} - \phi_o}{\phi_\infty - \phi_o} \tag{2-23}$$

$$\bar{T}_{norm} = \frac{\bar{T} - T_\infty}{T_o - T_\infty} \tag{2-24}$$

Table 2.3 The values of properties for simulation.

Properties		Value
$C_{p,grain}$	[J/kg·K]	920
Cp_a	[J/kg·K]	4180
K_0	[kg/kg·kPa]	7.3 x 10^{-10}
q_m	[kg/kg]	0.45
h_b	[W/m^2·K]	1400
X	[-]	12
ε_p	[-]	0.37
α_{Al}	[m^2/s]	8.4 x 10^{-5}
α_{Cu}	[m^2/s]	1.1 x 10^{-4}
α_v	[m^2/s]	1.7 x 10^{-3}
λ_p	[W/m·K]	1.2
ρ_{grain}	[kg/m^3]	1150
ΔH_{st}	[kJ/kg]	2700

2.3.3. The numerical method

The 3-dimensional finite volume method is adopted for solving the coupled energy and mass diffusion equations in the present analysis. The commercially available software ANSYS FLUENT is used wherein the necessary used defined functions were formulated for achieving the coupling between the thermal and mass diffusion equations. The entire domain of study has been divided into 36000 - 43000 grids. An implicit scheme with a time step of 0.1 seconds has been used for solving the equations in the current study.

2.3.4. Initial and boundary conditions

The adsorption pressure is assumed to be constant at P = 900 Pa, which typically corresponds to an evaporator temperature of about 278.15 K in adsorption chiller units. Initially, the whole domain is assumed to be at an equilibrium condition with a temperature of T_0 = 323.15 K and corresponding silica gel uptake obtained from Tóth's equation as ϕ_0 = 0.045 kg/kg. At t = 0, the temperature of the bottom surface of the copper plate is assumed to be exposed to the coolant. A suitable convective heat transfer coefficient is assumed between the copper surface and coolant. Hence, the boundary condition at the bottom surface is given by;

$$-\lambda_{cu}\nabla T\big|_b = h_c(T_b - T_c) \tag{2-25}$$

The entire numerical domain governed by the mass and thermal diffusion equations, responds to this cooling boundary condition. The top and side walls are provided with symmetry boundary conditions. Symmetry boundary condition is mathematically represented as;

$$\nabla T\big|_b = 0 \tag{2-26}$$

The boundary condition for mass diffusion is obtained by assuming equilibrium between the grain boundary and vapor surrounding it. Hence, the uptake at the boundary of the grain at any given instant is given by the equilibrium uptake ϕ_e at the grain boundary temperature and adsorption pressure.

2.4. Simulation results

The temperature contours for the domains after 30s are as shown in Fig. 2.10(a) - (c). It can be observed from the figures that the variation in temperature for all the arrangements is marginal. Thus it may be concluded that the heat transfer occurs rapidly through the domain and the effect of mono and tri layer arrangement is negligible. Figure 2.11(a) - (c) shows the variation of uptake on the outer surface of particles and also along the cross-section of the particles. It can be observed from the figure that the uptake contours on the outer surface of silica gel particles show negligible variance owing to an almost isothermal domain. However, it can be observed from that the uptake in the interior section of the silica gel particles is significantly less than that on the outer surface for all the arrangements. This indicates that the diffusion process is the rate limiting phenomenon for the current study. Further, no significant variation was observed in the uptake contours between all the three arrangements.

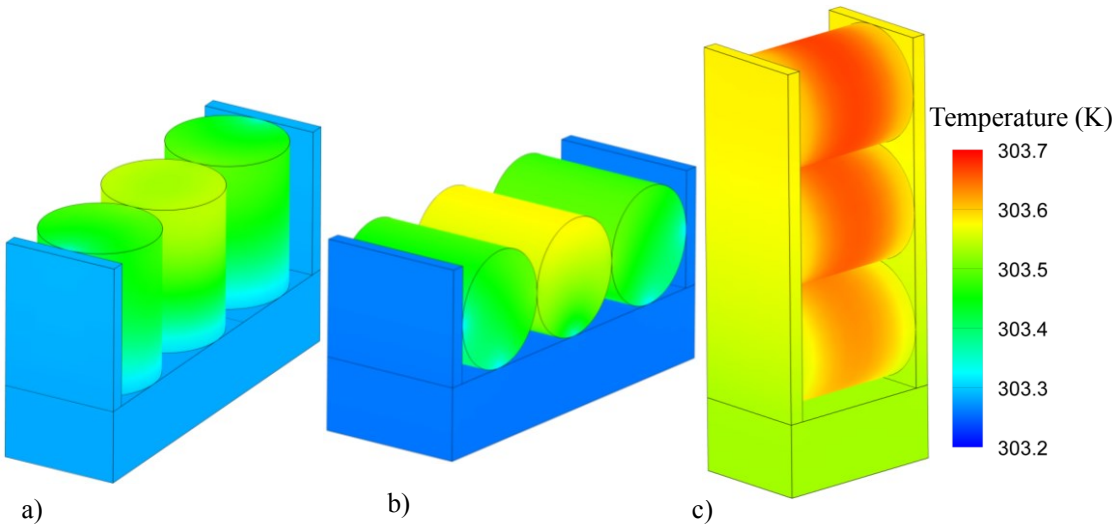

a) Arrangement 1 b) Arrangement 2 c) Arrangement 3

Fig. 2.10 Temperature contours

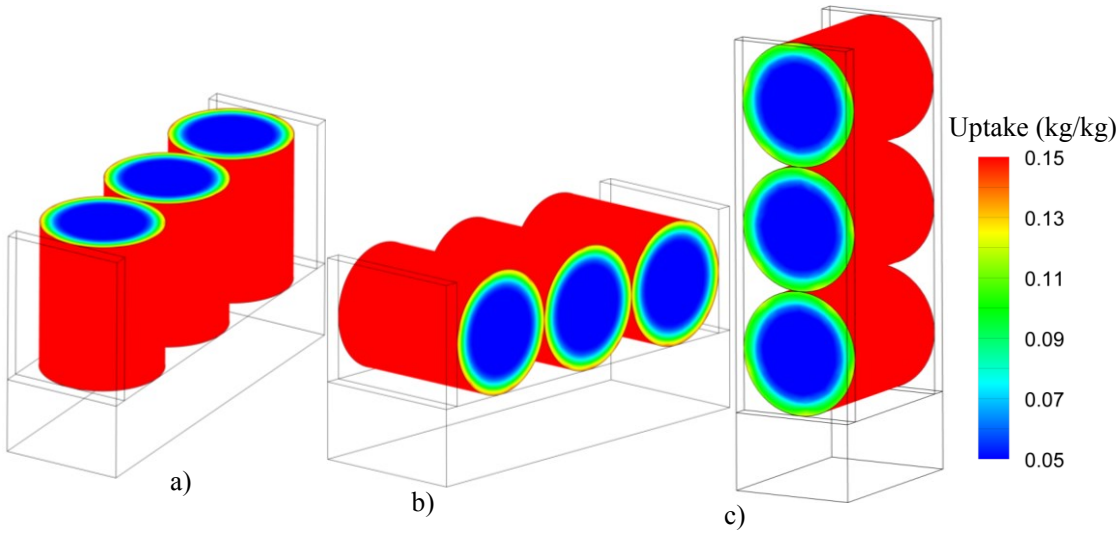

a) Arrangement 1 b) Arrangement 2 c) Arrangement 3

Fig. 2.11 Uptake contours on the surface and cross section.

A characteristic time constant $\tau_{0.63}$ may be defined as the time when normalized uptake reaches 0.63. It can be observed that there is no significant difference in time constant between the three arrangements. Further, the time constant obtained in the present study is similar to the time constant obtained for monolayer of 1.7 mm diameter spherical particles [14]. This can be attributed to the fact that the diffusion length scale is similar for cylindrical particles of diameter 1.6mm used in the current study and spherical particles studied in literature. However, the packing density of the system with cylindrical silica gel particles analyzed in the present study is found to be 920 kg/m^3; whereas it is 600 kg/m^3 for spherical particles with same diameter. Thus, an adsorber with cylindrical particles should be more compact than spherical particles for same cooling load.

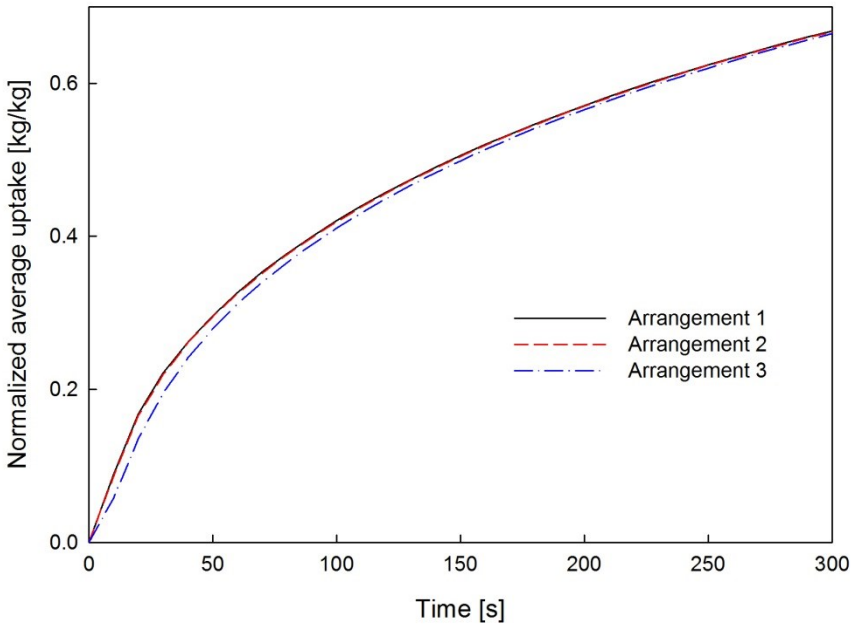

Fig. 2.12 Variation of normalized average uptake as time.

In the previous section it was observed that the spatial temperature variation is not significant for all arrangements especially for the third arrangement. Hence, the analysis is mainly focused on the uptake curves of all three studied arrangements. Figure 2.13(a) - (c) show uptake curves for all arrangements with and without the fins. It can be observed that the absence of fins have negligible effect on the first two arrangements whereas it is significant for the third arrangement. Thus, it can be concluded that the potential benefit of fins increases for multi-layer configurations.

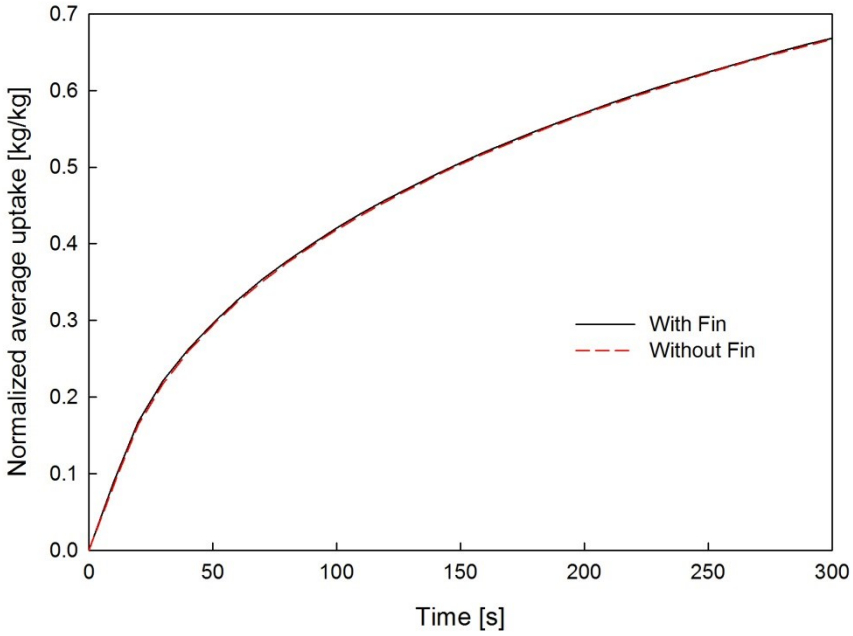

a) Arrangement 1.

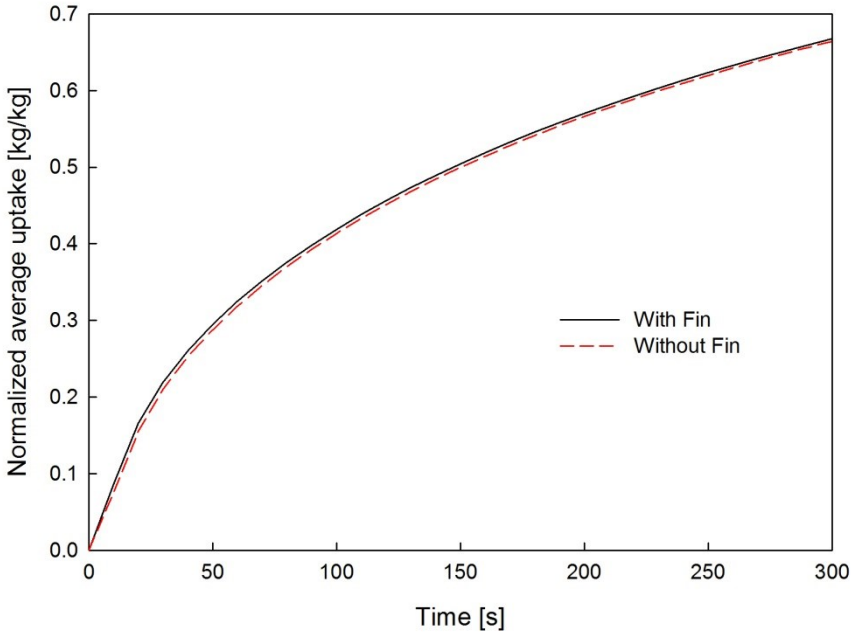

b) Arrangement 2.

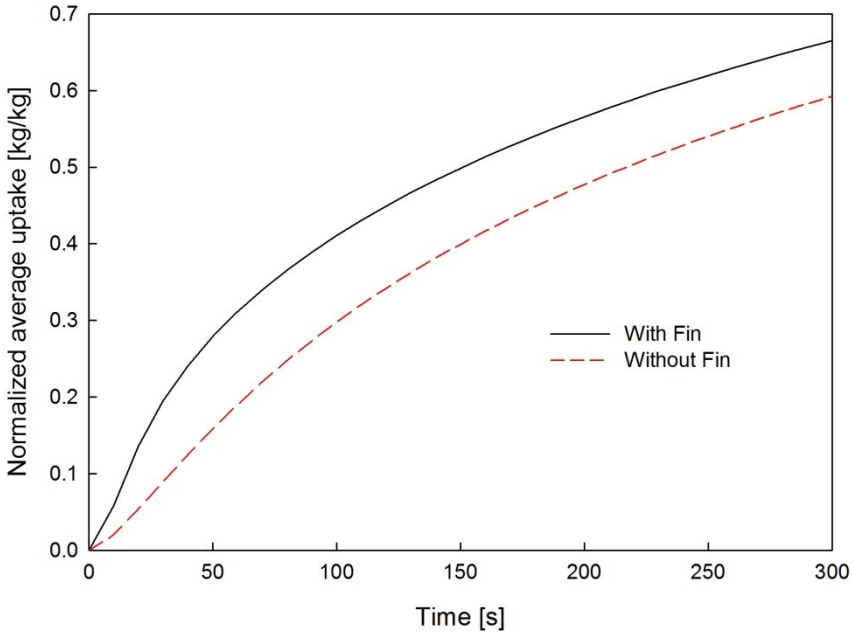

c) Arrangement 3.

Fig. 2.13 Comparison of normalized average uptake curves with and without fin.

2.5. Conclusions

In this chapter, N_2 adsorption isotherms on three different sizes of silica gel RD 2060 and thermophysical properties are also defined using some analysis methods for surface area and pore size analysis. The main findings can be summarized as:

In the adsorption uptake, granular silica gel shows the highest performance of 0.2845 g/g among three different sizes of silica gels followed power 2 and powder 1 at relative pressure of 0.99. In the thermophysical properties, it is found to be that all sizes of silica gels possess large amount of micro pores, however granular silica gel shows the largest micropore surface of 597.97 m^2/g and the largest surface area of 618.36 m^2/g. Pore sizes of all studied silica gels are distributed within 0.5 - 2 nm. Furthermore, large amount of pores were found on the surface of grain type of silica gel and smaller particle has less pores as shown in SEM photos. From above results, it can be concluded that granular silica gel RD 2060 is most suitable adsorbent to apply to adsorption cooling system using the compact fin-tube heat exchanger.

Additionally, a coupled heat and mass transfer model for cylindrical shaped silica gel particles with realistic domain and boundary condition has been evaluated in three possible arrangements. The results obtained in current study show that the orientation of particles has insignificant effect on uptake for a monolayer of cylindrical silica gel particles, however only a marginal decrease in uptake was found for tri-layer arrangement. Further, cylindrical particles were found to have similar normalized average uptake as spherical particles of same radius. However, the packing density of cylindrical particles is significantly higher than spherical particles thus potentially reducing the size of adsorber. Furthermore, the study analyzed the effect of absence of fins on monolayer and tri-layer arrangements. It was found that the absence of fins do not have any significant effect on monolayer arrangements, however absence of fins significantly reduce the average uptake for tri-layer arrangement.

Nomenclature

a	Micropore radius [nm]
c	Vapor concentration [kg/m^3]
C	*BET* Constant
C_p	Specific heat capacity [J/kg·K]
d_p	Particle diameter [mm]
dV	Elementary volume [m^3]
D_p	Pore diffusivity [m^2/s]
D_s	Surface diffusivity [m^2/s]
h	Heat transfer coefficient [W/m^2·K]
K_0	Constant in Tóth's equation
l_p	Length of particle [mm]
P	Pressure [Pa]
q_m	Maximum silica gel uptake [kg/kg]
R_m	Gas constant [J/mol·K]
T	Thickness (mm), time [s]
T	Temperature [K]
V	Volume [m^3]
V_m	Monolayer coverage volume [m^3]

Greek symbols

α	Thermal diffusivity [m^2/s]
ρ	Density [kg/m^3]
ε	Porosity
ϕ	Uptake
λ	Thermal conductivity [J/m·K]
ΔH_{st}	Isosteric heat of adsorption [kJ/kg]
τ	Characteristic time
∇	Symbol for gradient in space

Subscripts

0	Initial
∞	Final
Al	Aluminum
a	Adsorbed phase
ads	Adsorption
b	Boundary
c	Coolant
Cu	Copper
e	Equilibrium
eff	Effective
norm	Normalized
v	Vapor
sat	Saturation
w	Water

References

[1] A. Chakraborty, B. B. Saha and S. Koyama, Adsorption thermodynamics of silica gel-water systems, Journal of Chemical Engineering 54, (2009) 448-452.

[2] H. Demir, M. Mobedi and S. Ülkü, A review on adsorption heat pump: Problems and solutions, Renewable and Sustainable Energy Reviews 12, (2008) 2381-2403.

[3] D. C. Wang, Y. H. Li, D. Li, Y. Z. Xia and J. P. Zhang, A review on adsorption refrigerant technology and adsorption deterioration in physical adsorption systems, Renewable and Sustainable Energy Reviews 14, (2010) 344-353.

[4] R. L. Yeh, T. K. Ghosh and A. L. Hines, Effects of regeneration condition on the characteristics of water vapor adsorption on silica gel, Journal of Chemical Engineering 37, (1997) 259-261.

[5] K. C. Ng, H. T. Chua, C. Y. Chung, C. H. Loke, T. Kashiwagi, A. Akisawa and B. B. Saha, Experimental investigation of the silica gel-water adsorption isotherm characteristics, Applied Thermal Engineering 21, (2001) 1631-1642.

[6] H. T. Chua, K. C. Ng, A. Chakraborty, N. M. Oo and M. A. Othman, Adsorption characteristics of silica gel + water systems, Journal of Chemical Engineering 47, (2002) 1177-1181.

[7] X. Wang, W. Zimmermann, K. C. Ng, A. Chakraborty and J. U. Keller, Investigation of the isotherm of silica gel + water systems : TG and volumetric methods, Journal of Thermal Analysis and Calorimetry 76, (2004) 659-669.

[8] K. Thu, A. Chakraborty, B. B. Saha and K. C. Ng, Thermophysical properties of silica gel for adsorption desalination cycle, Applied Thermal Engineering 50, (2013) 1596-1602.

[9] B. B. Saha, A. Chakraborty, S. Koyama, J. B. Lee, J. He and K. C. Ng, Adsorption characteristics of parent and copper-sputtered RD silica gels, Philosophical Magazine 87 (7), (2007) 1113-1121.

[10] I. Glaznev, I. Ponomarenko, S. Kirik and Y. Aristov, Composites $CaCl_2$/SBA-15 for adsorptive transformation of low temperature heat: Pore size effect, International Journal of Refrigeration 34, (2011) 1244-1250.

[11] I. Glaznev and Yu. I. Aristov, The effect of cycle boundary conditions and adsorbent grain size on the water sorption dynamic in adsorption chiller, International Journal of Heat and Mass Transfer 53, (2010) 1893-1898.

[12] L. X. Gong, R. Z. Wang, Z. Z. Xia and C. J. Chen, Adsorption equilibrium of water on a composite adsorbent employing lithium chloride in silica gel, Journal of Chemical Engineering 55, (2010) 2920-2923.

[13] A. Freni, F. Russo, S. Vasta, M. Tokarev, Yu. I. Aristov and G. Restuccia, An advanced solid sorption chiller using SWS-1L, Applied Thermal Engineering 27, (2007) 2200-2204.

[14] A. Freni, G. Maggio, F. Cipiti and Yu. I. Aristov, Simulation of water sorption dynamics in adsorption chiller: One, two and four layers of loose silica grains, Applied Thermal Engineering 44, (2012) 69-77.

[15] K. S. Chang, M. T. Chen and T. W. Chung, Effects of thickness and particle size of silica gel on the heat and mass transfer performance of a silica gel-coated bed for air-conditioning adsorption systems, Applied Thermal Engineering 25, (2005) 2330-2340.

[16] J. Li, M. Kubota, F. Watanabe, N. Kobayashi and M. Hasatani, Optimal design of fin-type silica gel tube module in the silica gel/water adsorption heat pump, Journal of Chemical Engineering of Japan 37 (4), (2004) 551-557.

[17] K. Nakai, J. Sonoda, H. Iegami and H. Naono, High precision volumetric gas adsorption apparatus, Adsorption 11, (2005) 227-230.

[18] N.C. Srivastava, and I.W. Eames, A review of adsorbents and adsorbates in solid-vapour adsorption heat pump systems, Applied Thermal Engineering 18 (9-10), (1998) 707-714.

[19] I.I. El-Sharkawy, K. Kuwahara, B.B. Saha, S. Koyama, K.C. Ng, Experimental investigation of activated carbon fibers/ethanol pairs for adsorption cooling system application, Applied Thermal Engineering 26, (2006) 859-865.

[20] J. H. de Boer, B. C. Lippens, B. G. Lippens, J. C. P. Broekhoff, A. van den Heuvel and Th. V. Osinga, The t-curve of multimolecular N_2-adsorption, Journal of Colloid and Interface Science 21, (1966) 405-414.

[21] R. SH. Mikhail, S. Brunauer and E. E. Bodor, Investigation of a complete pore structure analysis: I. Analysis of micropores, Journal of Colloid and Interface Science 26, (1968) 45-53.

[22] User's manual, Belsorp mini, Bel Japan Inc.

[23] A.A. Pesaran and A.F. Mills, Moisture transport in silica gel packed beds - I. Theoretical study, International journal of heat and mass transfer 30 (6), (1987) 1037-1049.

[24] Yu. I. Aristov , M. M. Tokarev, A. Freni, I. S. Glaznev and G. Restuccia, Kinetics of water adsorption on silica Fuji Davison RD, Microporous and Mesoporous Materials 96, (2006) 65-71.

[25] C. Tien, Adsorption calculations and modeling, Butter-worth Heinmann Series in Chemical Engineering, (1994)

Chapter 3

Chapter 3

Equilibrium Adsorption Isotherm Characteristics of Water onto Silica Gel RD using Compact Fin-Tube Heat Exchanger

3.1. Introduction

At present, adsorption cooling system is being considered as one of the potential alternative cooling systems of vapor compression cycle. However, adsorption cooling system suffers from demerits of relatively lower COP (coefficient of performance) and large footprint, although it possesses sufficient merits in case of energy conservation and environmental friendliness. Accordingly, many studies have been carried out to solve these problems focusing mainly on the following techniques.

1. Development of new adsorbent materials or improvement in existing adsorbent materials
2. Enhancement in heat transfer between adsorbent and the metallic parts of adsorber/desorber heat exchanger
3. Development and/or modification of adsorption system and cycle operation mode

Followings are some representative examples related to the above mentioned techniques;

3.1.1. Development/modification of adsorbent materials

Gong et al. [1] measured equilibrium uptake of water on composited adsorbent (silica gel + lithium chloride) by the sorption isosteric method and compared the results with those of parent silica gel. Ng et al. [2] conducted adsorption equilibrium uptake of water on type A, 3A and RD silica gels using control volume variable pressure (CVVP) apparatus and isothermal characteristics of these three types of adsorbents are presented by Henry-type isotherm model. Chua et al. [3] investigated equilibrium uptake of water on type A and type RD silica gels using the same apparatus. They also determined the thermophysical properties of the studied adsorbents. Rezk et al. [4] investigated water adsorption characteristics of metal organic frameworks experimentally by a commercially available dynamic vapor sorption (DVS) analyzer and compared the results with water adsorption of RD 2060 silica gel. Aristov et al. [5] investigated kinetics for water adsorption on three different sizes of Fuji Davison RD silica gel experimentally by thermo gravimetry (TG) differential step method. Saha et al. [6] investigated performances of two-bed adsorption chiller employing $CaCl_2$ + KSK silica gel/water as adsorbent/refrigerant pair. They found 20 % and 25 % improvement in cooling capacity and COP, respectively when compared with the performances of two-bed adsorption chiller employing parent silica gel/water as the adsorbent/refrigerant pair.

3.1.2. Enhancement in heat transfer

Freni et al. [7] conducted experiments on water adsorption employing finned tubes heat exchanger coated with SWS-1L ($CaCl_2$ mesoporous silica gel) compact layer and compared the performances with those of a typical SWS-1L pelletized bed. Chang et al. [8] studied the heat transfer performance between adsorbent and metal substrate for a

silica gel-coated adsorber. Furthermore, the effect of the thickness of silica gel layer and the particle size on the heat transfer was investigated. Li et al. [9] developed a fin-type silica gel tube (FST) module, and analyzed numerically the heat and mass transfer characteristics. Saha et al. [10] conducted experiments of equilibrium adsorption uptake of ethanol on activated carbon fibers (ACFs), namely, A-10, A-15 and A-20 using a plate-fin heat exchanger, in which adsorption capacity of the studied adsorbents were compared. Furthermore, they developed an intermittent adsorption refrigeration system using ACF (A-20)/ethanol pair and determined the effects of various operating conditions on the system performance. The effect of the heat exchanger design parameter was analyzed on a two-bed silica gel water adsorption cooling system. The effect of the switching speed was also considered to provide guidelines regarding the design of heat exchanger of adsorbent bed by Alam et al. [11].

3.1.3. Development and/or modification of adsorption system

Saha et al. [12] designed and developed a prototype of a two-stage adsorption chiller. The same authors [13] proposed a three-bed non-regenerative silica gel-water adsorption chiller design. Thu et al. [14] proposed an innovative adsorption system which simultaneously provides desalination and cooling effects.

From the above perspectives, adsorption performance of RD type silica gel and water pair has been investigated experimentally, employing a compact fin-tube heat exchanger. Here, we have presented the temperature profiles of the adsorbent inside the compact heat exchanger, adsorption uptake rate and adsorption isotherms. The experimentally measured adsorption isotherm data were fitted with S-B-K equation.

3.2. Experiment

Water equilibrium adsorption uptake onto granular RD 2060 type silica gel (1 - 1.8 mm of diameter) has been conducted experimentally. The experimental setup comprises an adsorption chamber, an evaporator and connecting pipes and refrigerant valves. The schematic diagram and pictorial view of experimental setup are shown in Fig. 3.1 and Fig. 3.2. The present experiment is mainly focused on the improvement of adsorption performance using a compact fin-tube heat exchanger. This compact fin-tube heat exchanger is made of stainless steel tubes and aluminum fins. This compact fin-tube heat exchanger was placed inside the metallic adsorption chamber and connected to the water circulator through distributor to distribute water uniformly into each pipes of heat exchanger as shown in Fig.3.3. 2.69 kg of adsorbents (silica gel) were fully charged between the fins of the adsorber/desorber heat exchanger and packed with 300 mesh size net. Temperatures of both sides of the heat exchanger were measured by K-type thermocouples. The configuration and pictorial view of the heat exchanger are shown in Fig. 3.4 and Fig. 3.5. A metallic evaporator as shown in Fig. 3.6 was placed inside the water bath to maintain desired temperature. The evaporator is connected to the adsorption chamber through plumbing tubes, three refrigerant valves and two T's. K type thermocouples were used to detect the temperature difference between the outlet of the evaporator and the inlet of the adsorption chamber. Piping components are heated with a wire type silicon heater to avoid condensation of water vapor inside the connecting tubes and all components were thermally insulated. Two water circulators were used to control the temperatures of cooling/hot and chilled water. Temperatures of the inlet and outlet of cooling water and chilled water in the water bath are also

measured by the K type thermocouples. Measured temperatures were calibrated at 0˚C of ice water. Pressures of the adsorption chamber and evaporator are measured by absolute pressure transducers. The specifications of measuring devices are furnished at Table 3.1. At the beginning of the experiment, the adsorption chamber was degased for 24h at 85˚C with pressure at 10^{-4} Pa. The pressures of the test rig were kept near vacuum condition using a vacuum pump, which also eliminates residual water from the adsorbent samples through valves 2 and 3. After degassing, valves 2 and 3 were closed and the temperatures and pressures of adsorption chamber and evaporator were kept at constant temperatures by water circulators until the test rig reached a steady state condition. These temperatures correspond to the desired adsorption and evaporation temperatures. Adsorption equilibrium uptake experiments were conducted by opening valve 1, which allows the vapor flows from the evaporator to the adsorber. Furthermore, after completion of the measurement of the equilibrium uptake at each set temperature, degassing process was conducted for the duration of 8h at 85˚C. In this experiment, dead volume of water vapor was neglected in order to calculate the adsorbed amount of water vapor on the adsorbent. Chilled water temperatures were set at 15, 20 and 25˚C for air-conditioning application and the flow rate of cooling water was set at 3 L/min, which is required for water to flow inside of the heat exchanger tubes under turbulent condition

Table 3.1 Specifications of measuring devices.

	Model	Range	Accuracy
Thermocouple	K type	-40 - 375 [˚C]	±1.5 ˚C
Pressure sensor	Nagano Keiki - KL 79	0 - 20 [kPa]	±0.3 %
Mass flow meter	Oval - FLM20	1 - 15 [L/min]	±3 %

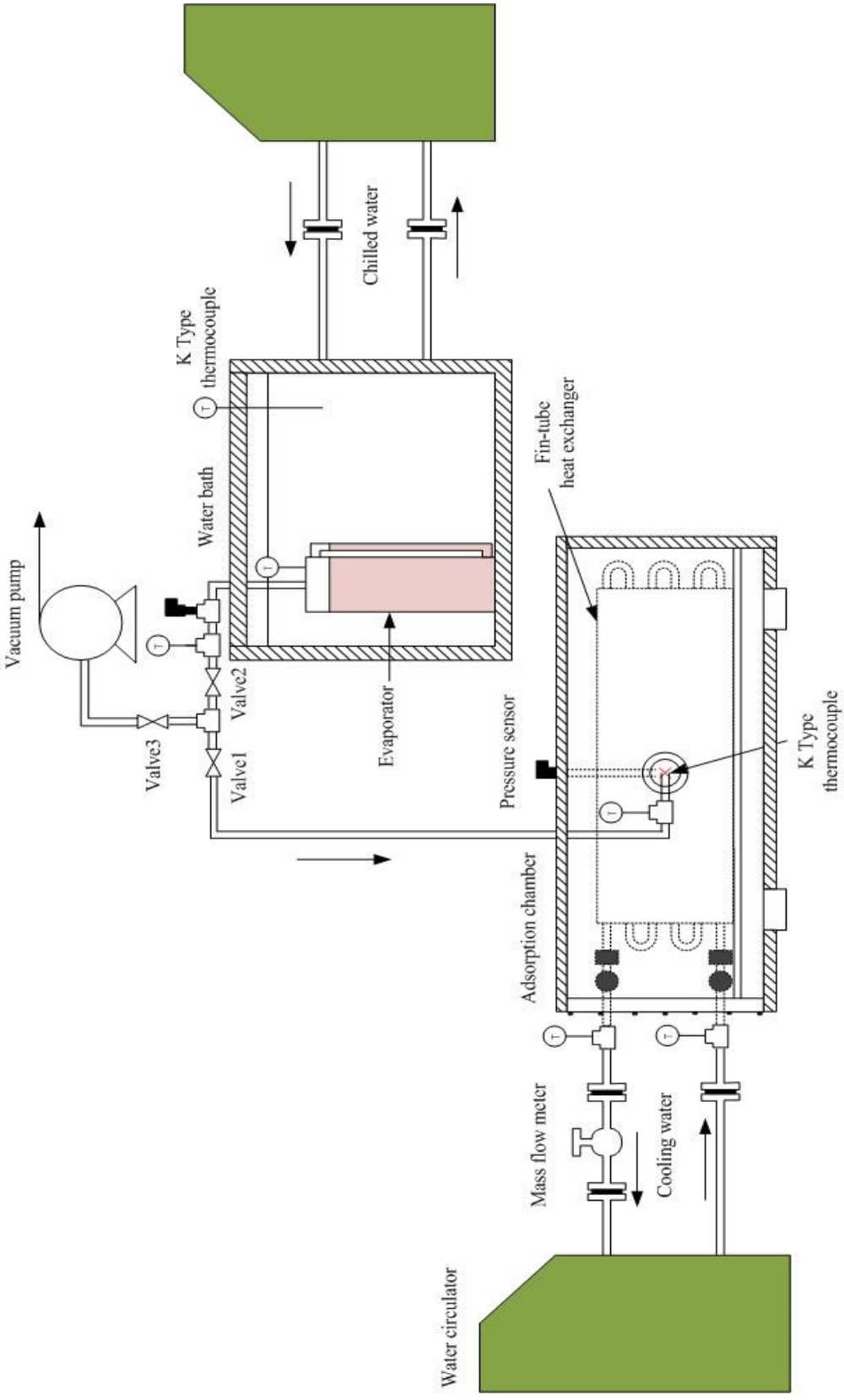

Fig. 3.1 Schematic diagram of the experimental apparatus.

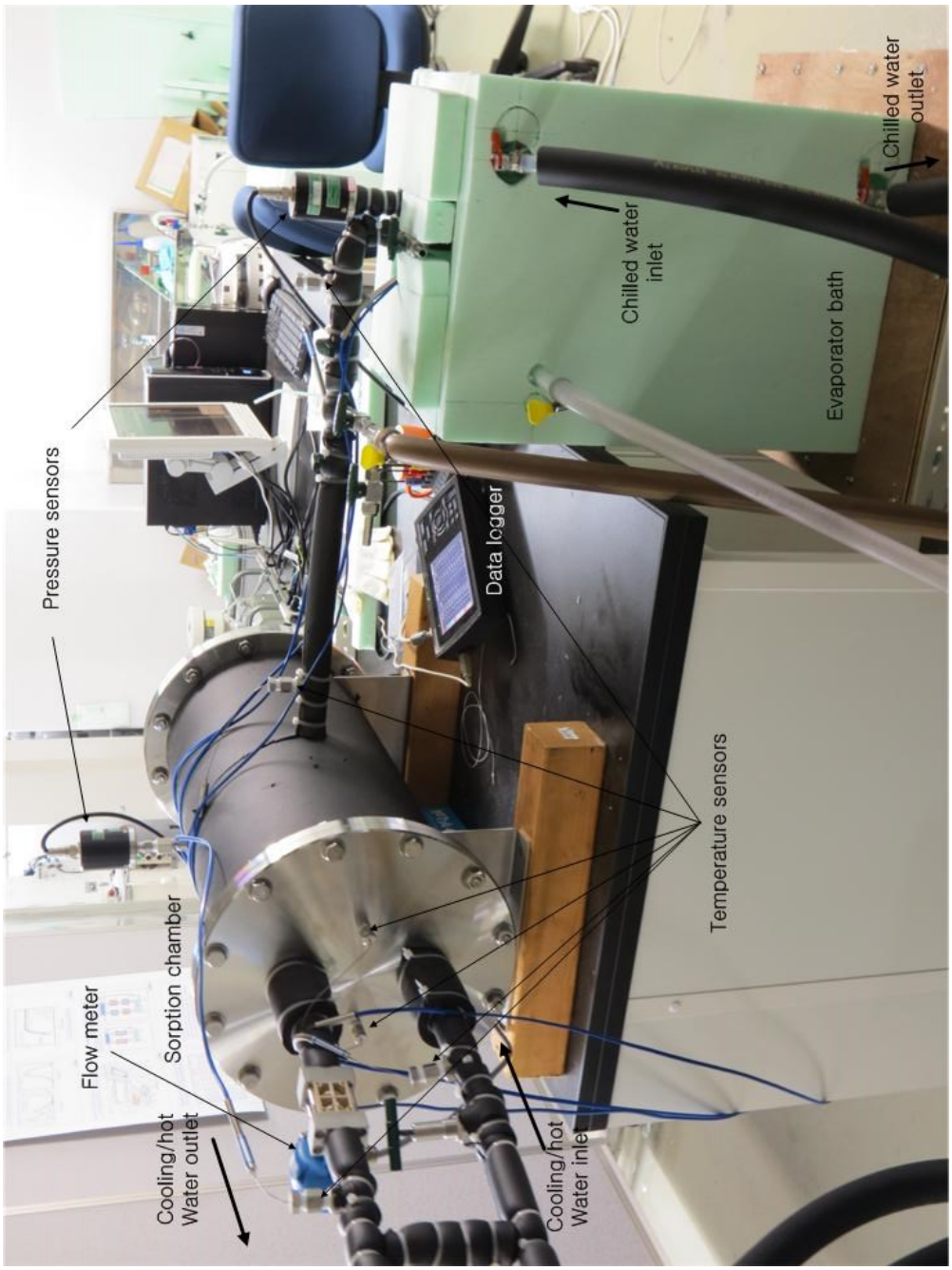

Fig. 3.2 Pictorial view of the experimental setup.

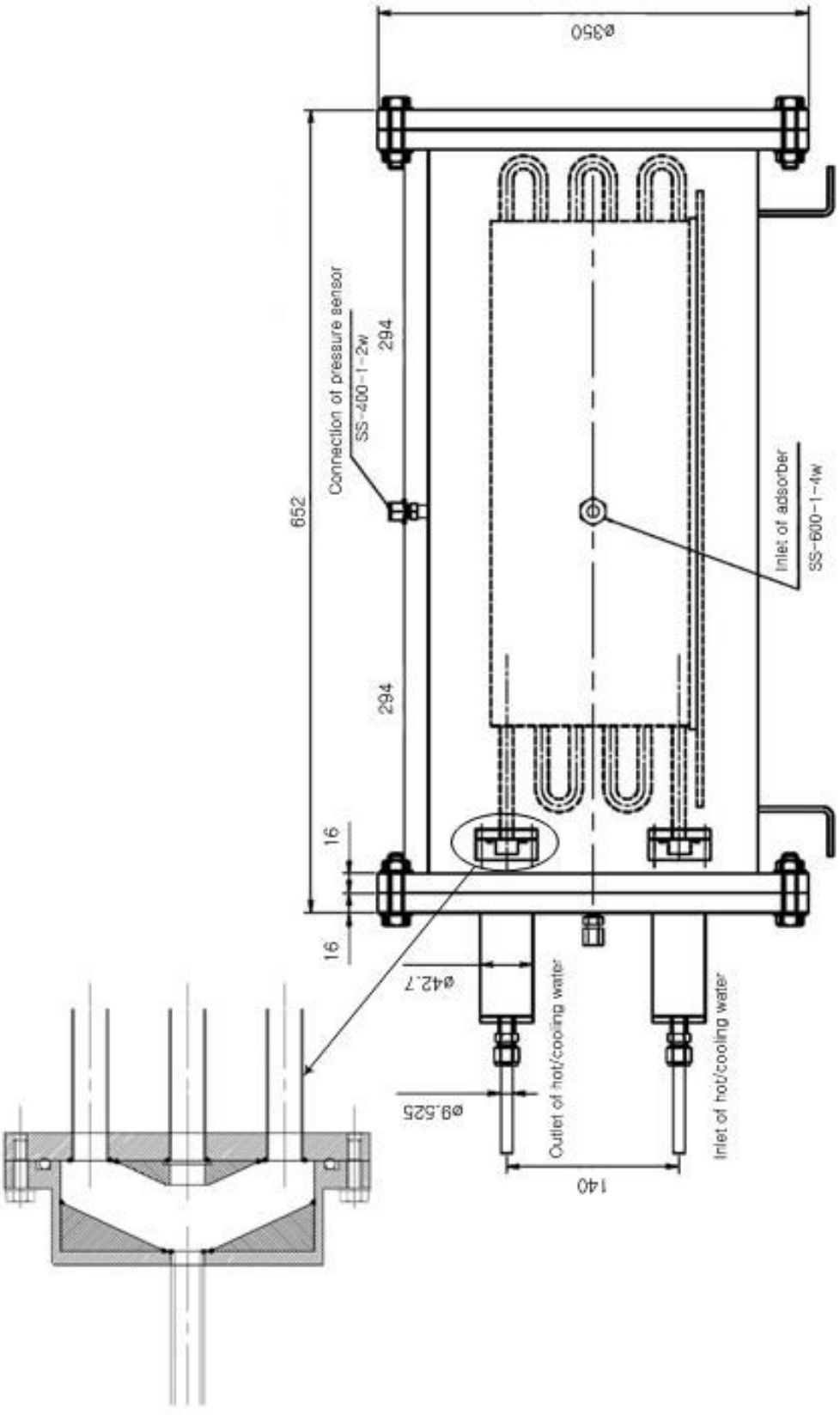

Fig. 3.3 Side view of the adsorption chamber.

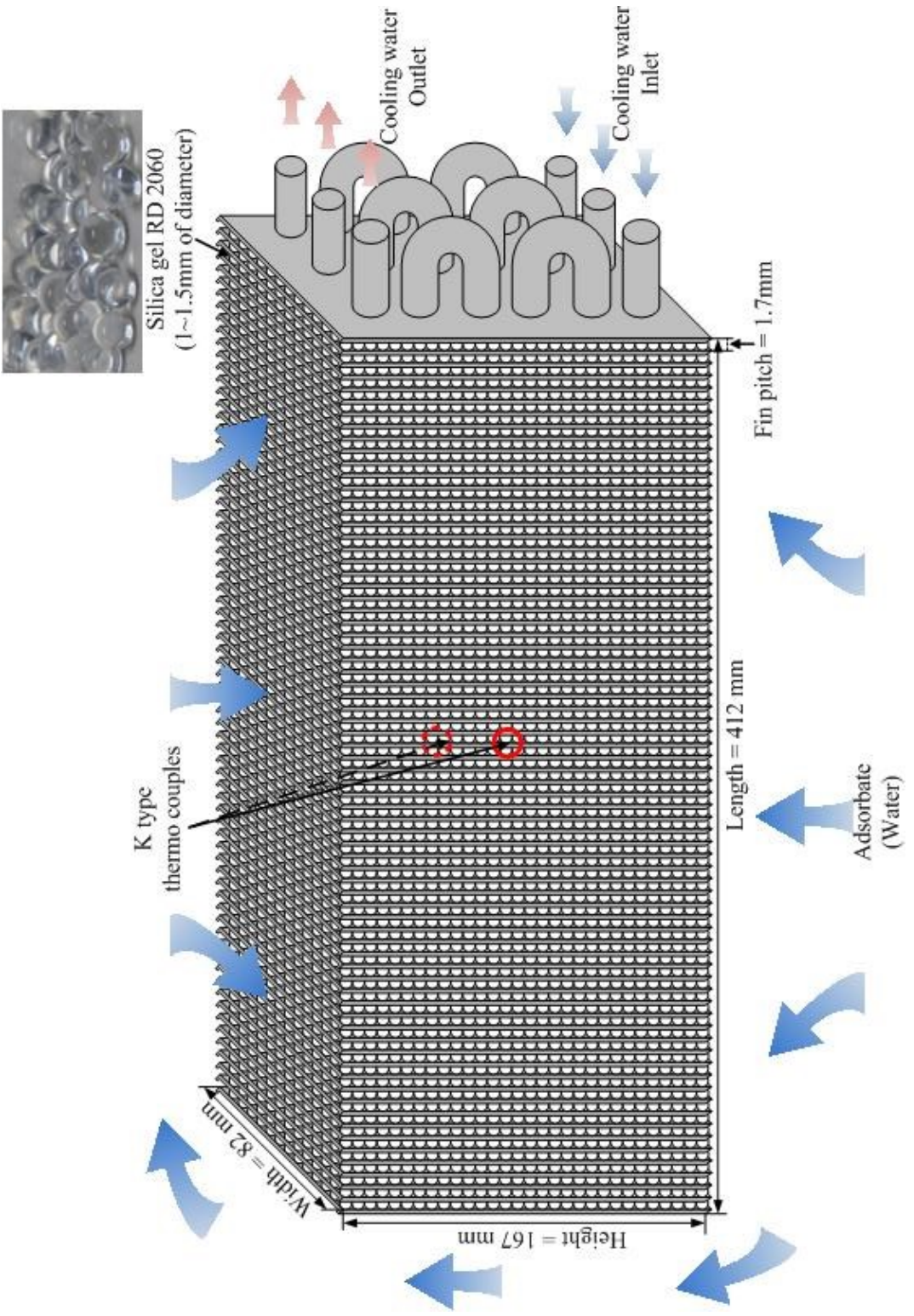

Fig. 3.4 Configuration of the fin-tube heat exchanger.

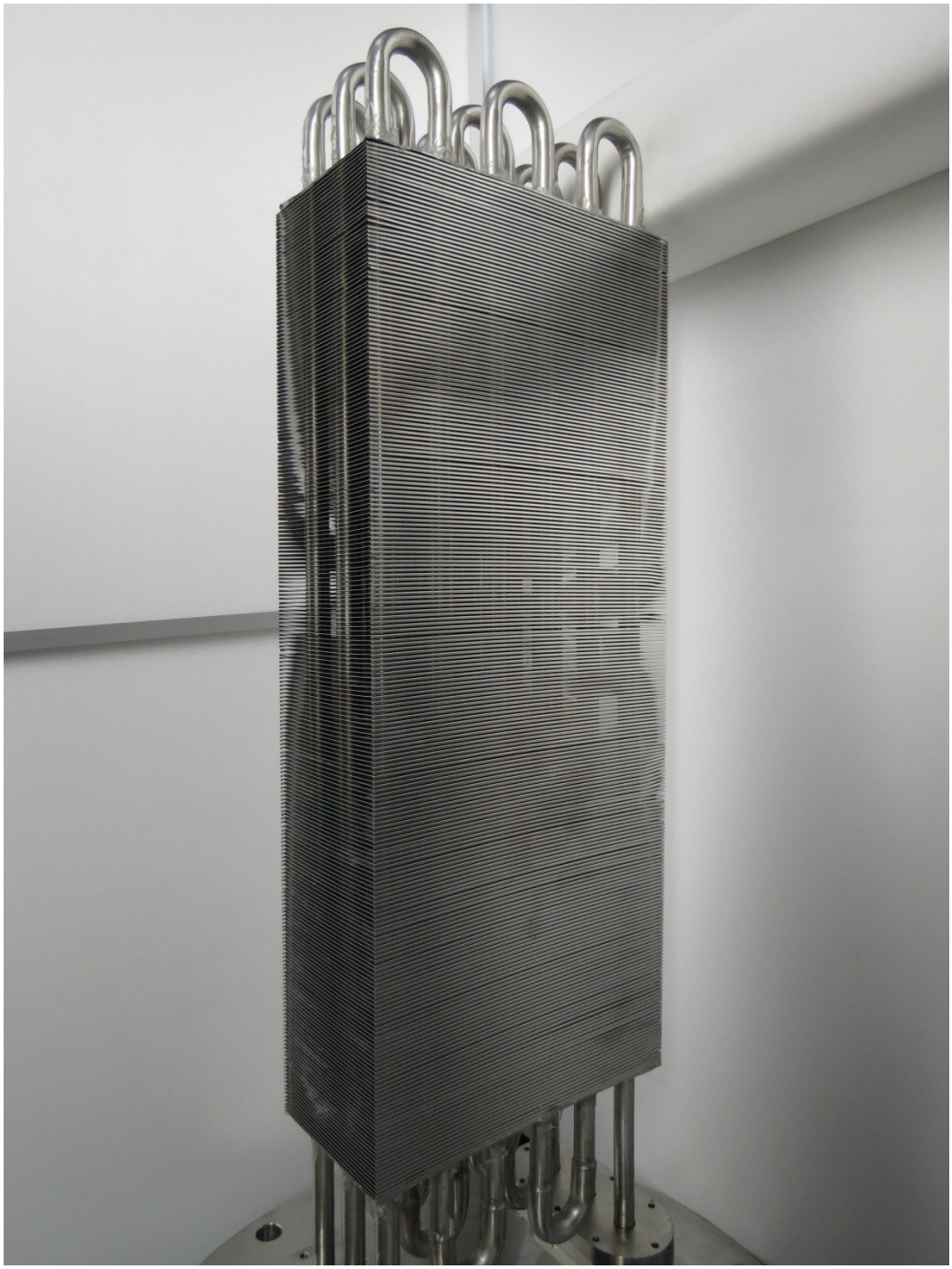

Fig. 3.5 Pictorial view of the compact fin-tube heat exchanger.

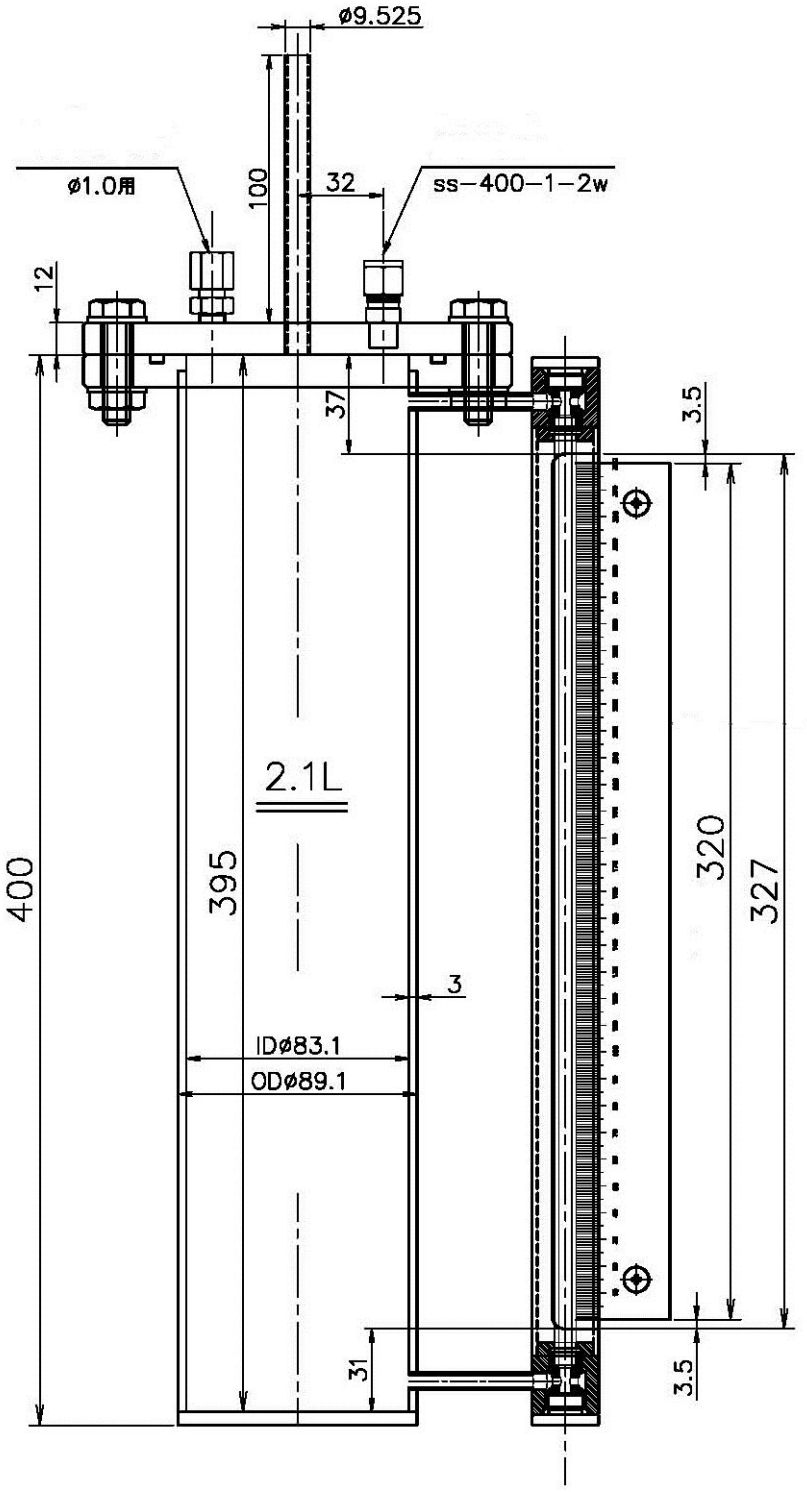

Fig. 3.6 Side view of the evaporator.

3.3. Adsorption equilibrium uptake equation

3.3.1. Freundlich equation

The Freundlich adsorption isotherm equation is widely used to estimate adsorption equilibrium uptake during physical adsorption. *The Fruendlich* equation is expressed by Eq. (3-1), below:

$$W = W_0 \left[\frac{P_s(T_s)}{P_s(T_w)} \right]^{1/n} \tag{3-1}$$

where, W and W_0 denote instantaneous adsorbed amount in equilibrium with pressure $P_s(T_s)$ and maximum uptake, respectively. Here n is taken as constant. The values of W_0 and n for silica gel/water pair were evaluated experimentally and were found to be 0.346 kg/kg and 1.6, respectively by Chihara and Suzuki [15]. $P_s(T_w)$ is the saturation pressure at saturation temperature of the refrigerant (water) and $P_s(T_s)$ is the saturation pressure, corresponding to the adsorbent temperature.

3.3.2. S-B-K equation

The S-B-K equation which was proposed by Saha et al. [16] is used to fit the adsorption uptake of silica gel/water pair and is given by Eq. (3-2)

$$W = A(T_s) \left[\frac{P_s(T_w)}{P_s(T_s)} \right]^{B(T_s)} \tag{3-2}$$

where, W denotes the adsorption uptake at the equilibrium pressure, $P_s(T_s)$. Here $A(T_s)$ and $B(T_s)$ are expressed as functions of adsorbent temperature, T_s;

$$A(T_s) = A_0 + A_1 T_s + A_2 T_s^2 + A_3 T_s^3 \quad (3\text{-}3)$$

$$B(T_s) = B_0 + B_1 T_s + B_2 T_s^2 + B_3 T_s^3 \quad (3\text{-}4)$$

The present authors have simplified *the S-B-K* adsorption isotherm equation by eliminating the constants and 3rd order temperature terms to fit the current experimental data where $A(T_s)$ and $B(T_s)$ can be written as:

$$A(T_s) = A_0 T_s + A_1 T_s^2 \quad (3\text{-}5)$$

$$B(T_s) = B_0 T_s + B_1 T_s^2, \quad 0 < T_s < 100 \quad (3\text{-}6)$$

The numerical values of A_0, A_1 and B_0, B_1 are furnished in Table 3.2.

Table 3.2 Values of parameters used in Eq. (3.5) and (3.6).

Parameter	Value
A_0	0.366×10^{-2}
A_1	-0.697×10^{-5}
B_0	0.941×10^{-2}
B_1	-0.203×10^{-4}

3.4. Results and discussion

In this experiment, equilibrium uptakes of water vapor onto granular RD 2060 type silica gel were measured for adsorption temperature ranges from 16 to 85˚C, at chilled water temperatures of 15, 20 and 25˚C. The experimental isotherm data were compared with the computed data using both *Freundlich* and *modified Freundlich* (*S-B-K*) equations.

3.4.1. Temperature profiles and uptake rate

Figure 3.7 shows the temperature profiles of adsorbents packed inside the compact fin-tube heat exchanger with chilled water temperature of 15˚C and cooling water temperature of 30˚C. As shown in Fig. 3.7, temperature of the adsorbent increases sharply up to about 46˚C during the first 100 seconds of the adsorption isotherm experiment and then gradually decreases. The adsorbent temperature is only about 2˚C higher than the cooling water temperature after an hour and it reaches near the cooling water temperature after 2 hours as adsorption approaches pseudo equilibrium state. Adsorption kinetic behavior is shown in Fig. 3.8. Uptake rate increases rapidly up to about an hour after that the uptake rate is only marginal. Accordingly, the allocated adsorption cycle time for an adsorption cooling system should be smaller than an hour, preferable several minutes.

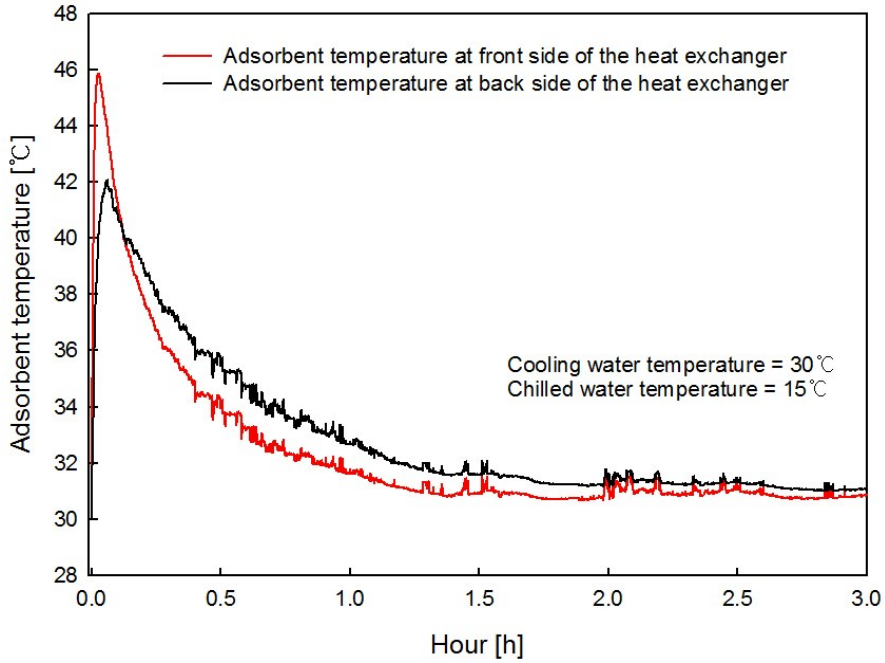

Fig. 3.7 Temperature profiles of adsorbents.

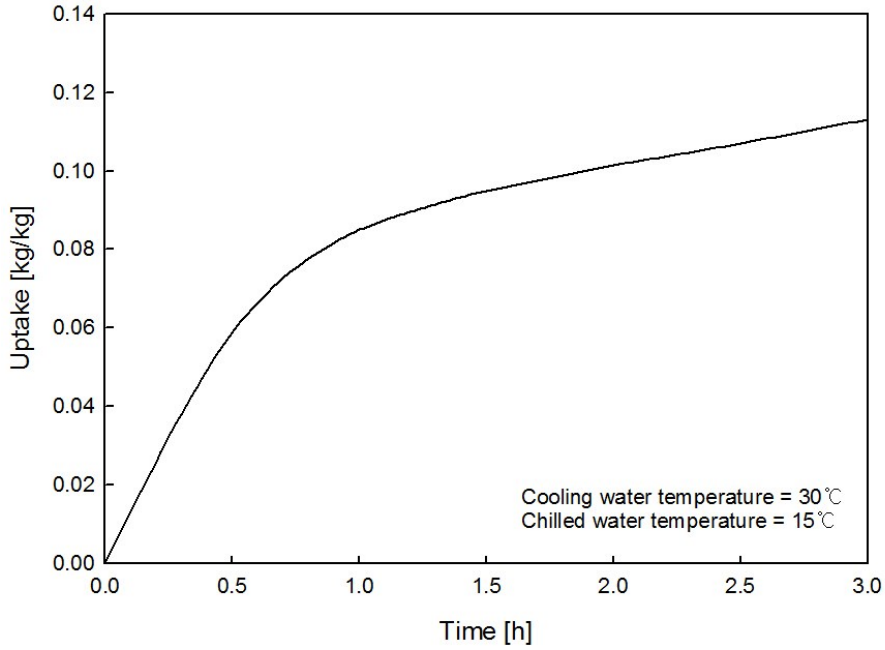

Fig. 3.8 Adsorption uptake rate.

3.4.2. Equilibrium isotherms

In Fig. 3.9, experimental isotherm data are compared with the predicted isotherm data by *Freundlich* and *S-B-K* equations at chilled water temperature of 15˚C. From this figure, it can be observed that there are notable deviations between experimental and predicted data by *Freundlich* equation during low relative pressures. On the other hand, predicted isotherm data by the *S-B-K* model fit well the present experimental data in the whole relative pressure ranges. Thereby Fig. 3.10 shows the uptake balance of experimental isotherms data with *S-B-K* model. As can be seen from Fig. 3.10, the present experimental data fit with the *S-B-K* model within ±5 % of deviation.

Equilibrium adsorption isotherm and variation of equilibrium uptakes are shown in Figs. 3.11 and 3.12, respectively. It is evident from Fig. 3.11 that the equilibrium isotherms for three different chilled water temperatures fall in the same linear line and increase in the whole relative pressure ranges. Equilibrium uptake at 25˚C of chilled water temperature shows the highest value among those of the three different chilled water temperatures. Figure 3.12 shows the equilibrium uptakes versus the adsorption temperatures at three different evaporation temperatures. Water vapor uptake is decreased exponentially with the increase in adsorption temperature.

In addition, equilibrium uptakes in terms of adsorption temperatures in the range of 10 - 70˚C have determined numerically by *S-B-K* equation and are shown in Fig. 3.13. Equilibrium uptake value is 0.26 kg/kg when adsorption temperature is 30˚C at equilibrium pressure of 2.34 kPa. On the other hand, equilibrium uptake value is 0.05 kg/kg at adsorption temperature of 70˚C. This means that an adsorption cooling system employing the studied compact fin-tube heat exchanger can attain 0.21 kg/kg

concentration difference when it works at 30˚C heat sink and 70˚C heat source temperatures.

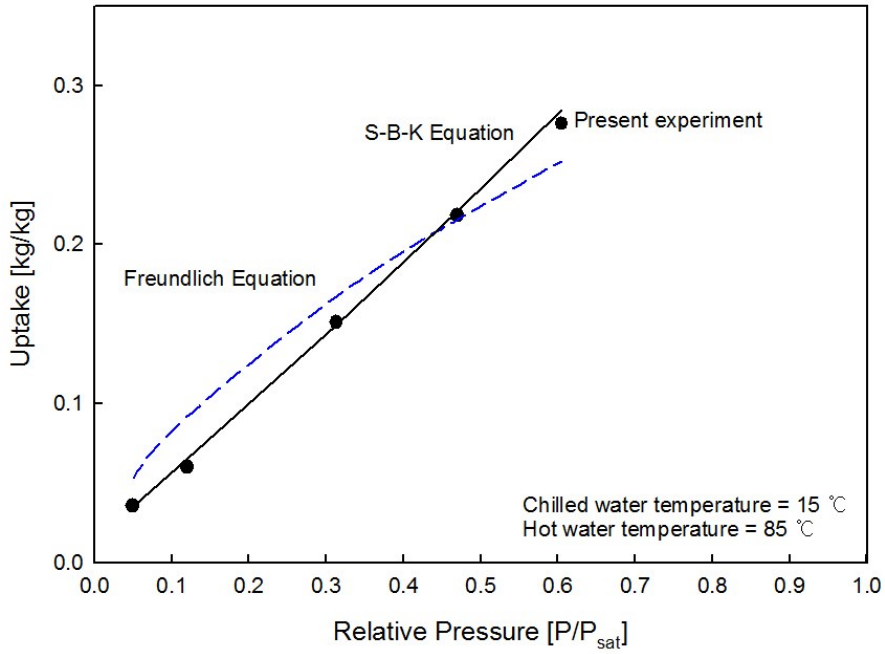

Fig. 3.9 Comparison of equilibrium uptakes with *Freundlich* and *S-B-K* equations. (Plots = present experiment, dotted lines = *Freundlich* equation and solid line = modified *S-B-K* equation)

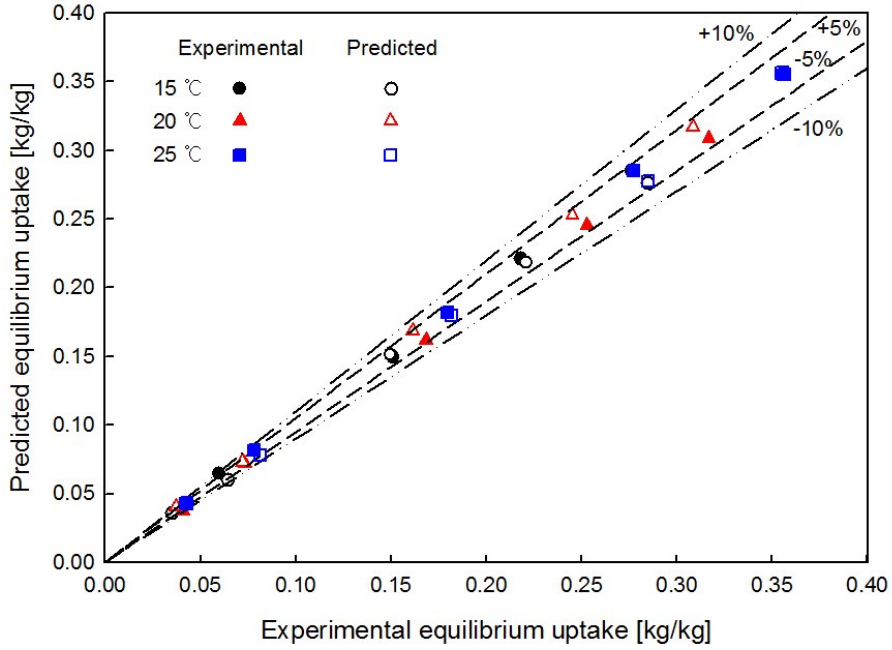

Fig. 3.10 Uptake balance between present experimental results and computed results.

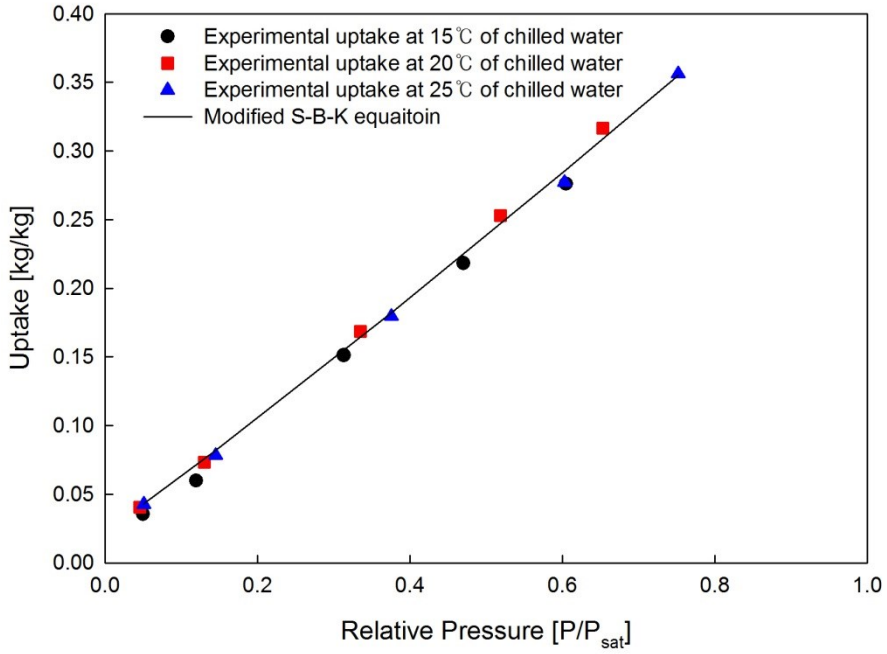

Fig. 3.11 Isotherm data for water vapor adsorption onto silica gel.

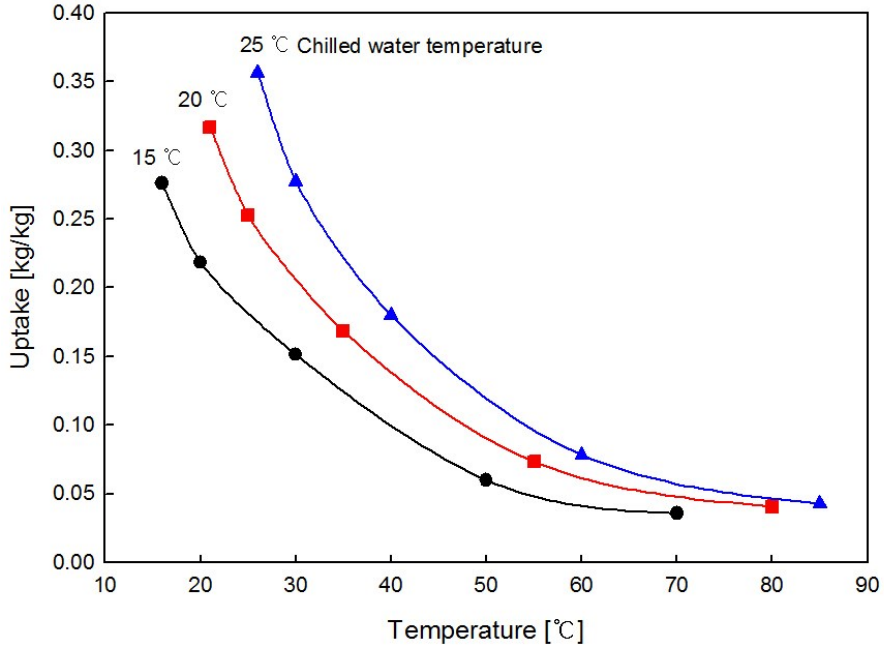

Fig. 3.12 Variations of equilibrium uptakes for water vapor adsorption onto silica gel.

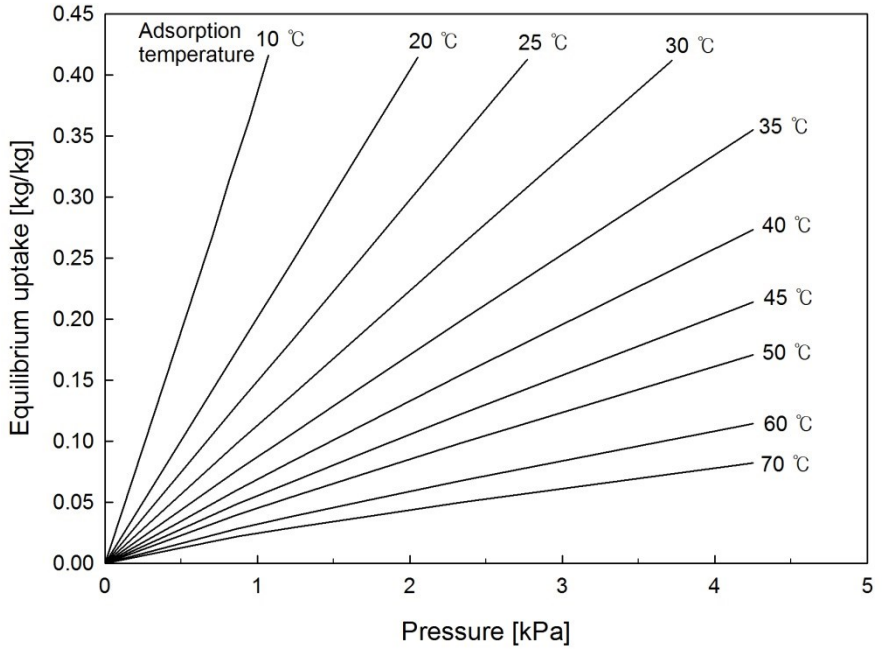

Fig. 3.13 Computed adsorption isotherms versus equilibrium pressure.

3.4.3. Ideal cycles on Dühring diagram

In Fig. 3.14, thermodynamic ideal cycles which were predicted by S-B-K equation using present experimental isotherm data were compared for three different evaporation temperatures on the Dühring (pressure-temperature-concentration) plots. Here, adsorption/condensation and desorption temperatures were fixed at 30˚C and 85˚C, respectively. In this figure, adsrotption/desorption processes are occurred isobaric during a - b (evaporation - adsorption) and c - d (desorption - condensation) processes. In contrast, positive thermal swing (b - c) is occurred at constant isosteres (constant concentration) which is known as the pre-heating process and negative thermal swing (d - a) is occurred at constant isosteres which is known as the pre-cooling process. As can be seen from Fig. 3.14, concentration difference (concentration of adsorption/evaporation - concentration of desorption/condensation) of 0.14 is found for evaporation temperature of 15˚C. However, for 25˚C of evaporation temperature, the concentration difference is found to be as high as 0.31. It is observed that 2 times higher concentration difference for evaporation temperature of 25˚C than concentration difference for evaporation temperature of 15˚C.

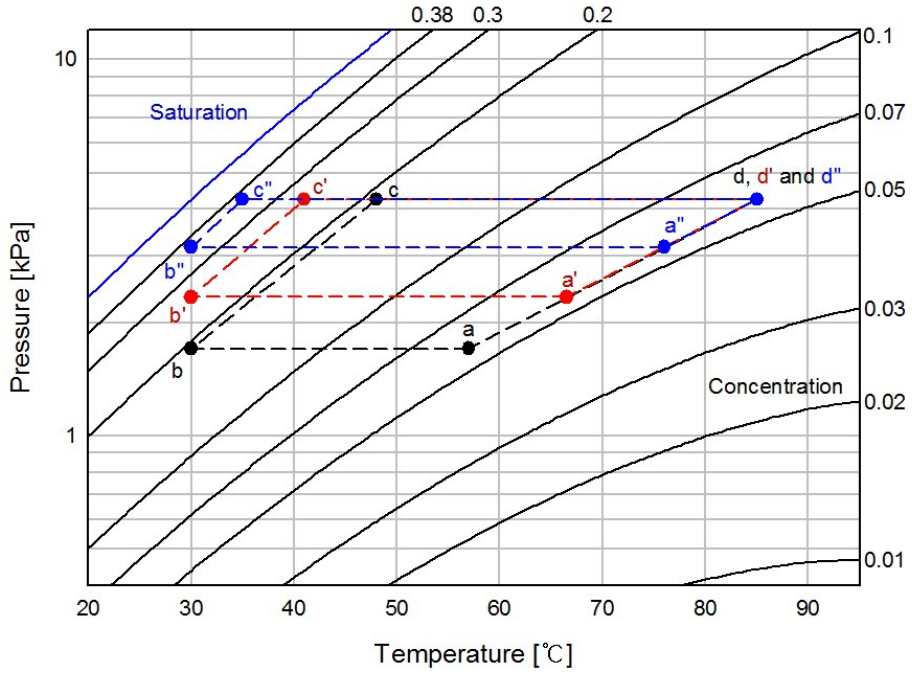

Fig. 3.14 Ideal cycles on Dühring diagram.

(Black solid line = Concentration, Blue solid line = Saturation of refrigerant, Black dotted line = Ideal cycle at evaporation temperature of 15˚C, Red dotted line = Ideal cycle at evaporation temperature of 20˚C and Blue dotted line = Ideal cycle at evaporation temperature of 25˚C)

3.5. Conclusions

In this chapter, equilibrium uptake of water onto granular type RD 2060 of silica gel using a compact fin-tube heat exchanger were investigated experimentally at three different evaporation temperatures suitable for typical air-conditioning application. The main findings can be summarized as:

Adsorption isotherms increase with the increase of relative pressure for all three studied evaporation temperatures. Equilibrium uptake at 25˚C of chilled water shows maximum value of 0.34 kg/kg for a relative pressure of 0.75. The S-B-K equation was found to be able to fit the experimental equilibrium adsorption uptake of water onto RD type silica gel packed inside the compact fin-tube within ±5 % of deviation. The present results may contribute greatly in the design of compact adsorption cooling system.

Nomenclature

A_0	Constant of Eq. (4-3) and (4-5)	W	Equilibrium uptake [kg/kg]
A_1	Constant of Eq. (4-3) and (4-5)	W_0	Maximum uptake [kg/kg]
A_2	Constant of Eq. (4-3)		
A_3	Constant of Eq. (4-3)	*Superscript*	
B_0	Constant of Eq. (4-4) and (4-6)	n	Constant in Fruendlich equation
B_1	Constant of Eq. (4-4) and (4-6)		
B_2	Constant of Eq. (4-4)	*Subscript*	
B_3	Constant of Eq. (4-4)	s	Saturation
P	Pressure [kPa]	w	Saturation of refrigerant
T	Temperature [˚C]		

References

[1] L. X. Gong, R. Z. Wang, Z. Z. Xia and C. J. Chen, Adsorption equilibrium of water on a composite adsorbent employing lithium chloride in silica gel, Journal of Chemical Engineering 55, (2010) 2920-2923.

[2] K. C. Ng, H. T. Chua, C. Y. Chung, C. H. Loke, T. Kashiwagi, A. Akisawa and B. B. Saha, Experimental investigation of the silica gel-water adsorption isotherm characteristics, Applied Thermal Engineering 21, (2001) 1631-1642.

[3] H. T. Chua, K. C. Ng, A. Chakraborty, N. M. Oo and M. A. Othman, Adsorption characteristics of silica gel + water systems, Journal of Chemical Engineering 47, (2002) 1177-1181.

[4] A. Rezk, R. Al-Dadah, S. Mahmoud and A. Elsayed, Experimental investigation of metal organic frameworks characteristics for water adsorption chiller, Journal of Mechanical Engineering Science, (2012) 1-14.

[5] Y. I. Aristov, M. M. Tokarev, A. Freni, I. S. Glaznev and G. Restuccia, Kinetics of water adsorption on silica gel Fuji Davison RD, Microporous and Mesoporous Meterials 96, (2006) 65-71.

[6] B. B. Saha, A. Chakraborty, S. Koyama and Y. I. Aristov, A new generation cooling device employing CaCl2-in-silica gel-water system, Int. Journal of Heat and Mass Transfer 52 (1-2), (2009) 516-524.

[7] A. Freni, F. Russo, S. Vasta, M. Tokarev, Yu. I. Aristov and G. Restuccia, An advanced solid sorption chiller using SWS-1L, Applied Thermal Engineering 27, (2007) 2200-2204.

[8] K. S. Chang, M. T. Chen and T. W. Chung, Effects of thickness and particle size of silica gel on the heat and mass transfer performance of a silica gel-coated bed for air-conditioning adsorption systems, Applied Thermal Engineering 25, (2005) 2330-2340.

[9] J. Li, M. Kubota, F. Watanabe, N. Kobayashi and M. Hasatani, Optimal design of fin-type silica gel tube module in the silica gel/water adsorption heat pump, Journal of Chemical Engineering of Japan 37 (4), (2004) 551-557.

[10] B. B. Saha, S. Koytama, I. I. El-Sharkawy, K. Kuwahara, K. Kariya and K. C. Ng, Experiments for meassuring adsorption characteristics of an Activated carbon fiber/ethabnol pair using a plate-fin heat exchanger, HVAC&R Research Special Issue 12 (3b), (2006) 767-782.

[11] K. C. A. Alam, B. B. Saha, Y. T. Kang, A. Akisawa and T. Kashiwagi, Heat exchanger design effect on the system performance of silica gel adsorption refrigeration systems, Int. Journal of Heat and Mass Transfer 43, 2000, 4419-4431.

[12] B. B. Saha, A. Akisawa and T. Kashiwagi, Solar/waste heat driven two-stage adsorption chiller: the prototype, Renewable energy 23, (2001) 93-101.

[13] B. B. Saha, S. Koyama, J. B. Lee, K. Kuwahara, K. C. A. Alam, Y. Hamamoto, A, Akisawa and T. Kashiwagi, Performance evaluation of a low-temperature waste heat driven multi-bed adsorption chiller, Int. Journal of Multiphase Flow 29, (2003) 1249-1263.

[14] K. Thu, K. C. Ng, B. B. Saha, A. Chakraborty and S. Koyama, Operational strategy of adsorption desalination systems, Int. Journal of Heat and Mass Transfer 52, 2009, 1811-1816.

[15] K. Chihara, M. Suzuki, Air drying by pressure swing adsorption, Journal of Chemical Engineering Japan 16 (4), 293-298.

[16] B. B. Saha, E. C. Boelman and T. Kashiwagi, Computer simulation of a silica gel-water adsorption refrigeration cycle-the influence of operating conditions on cooling output and COP, ASHRAE Trans 101, 1995, 348-357.

Chapter 4

Chapter 4

Dynamic Behavior and Performance Evaluation of a Two-Bed Silica gel/Water Based Adsorption Cooling System Employing Compact Fin-Tube Heat Exchanger

4.1. Introduction

Over the past decades, all over the world suffers energy and electric power shortage, thus adsorption cooling system became most considerable technology alternate to the vapor compression cooling system. Adsorption cooling systems have advantages on environmental friendliness by using natural refrigerants and adsorbents which have non-harmful, non-toxicity, non-flammability and etc. Moreover, these systems can save energy using lower temperature waste heat as the driving heat source. Several studies on adsorption characteristics and adsorption cooling cycles have been performed by various authors. Followings are some representative examples.

Saha et al. [1] investigated silica gel/water based three-stage adsorption chiller using 50˚C of waste heat and determined effect of thermal conductance of sorption bed on the performance. Chua et al. [2] presented transient modeling of two-bed silica gel/water adsorption chiller and compared performances with previous lumped modeled two-bed silica gel/water adsorption system. Ng et al. [3] experimentally investigated water adsorption isotherms on to three types of silica gel namely, A, 3A and RD. Saha et al. [4] found 20 % and 25 % improvement in cooling capacity and COP, respectively, over

parent silica gel/water system employing $CaCl_2$ + KSK silica gel/water as adsorbent/refrigerant pair in a two-bed adsorption chiller. Cooling capacity of both silica gel/water and $CaCl_2$-in-silica gel/water based adsorption chillers were enhanced by 6 % with a new cycle time allocation which was studied by Miyazaki et al. [5]. Modeling of activated carbon/ethanol based adsorption chiller was proposed and performance of the cycle was evaluated by Saha et al. [6, 7]. Demir et al. [8] had compared the performance of adsorption heat pumps with that of the vapor compression and absorption heat pumps. Alam et al. [9] investigated heat exchanger design effect on the performance of two-bed adsorption cooling system with silica gel/water as adsorbent/adsorbate pair. Khan et al. [10] investigate silica gel/water based two-stage adsorption chiller using waste heat between 50 and 70˚C numerically and determined effect of overall thermal conductance of sorption element on the performance. Tso et al. [11] suggested some possible solutions regarding to the problems related to the design of adsorbent bed. The performance of a waste heat driven adsorption chiller based on $CaCl_2$ inside the composite of silica + activated carbon was compared with that of silica gel/water and ACF/water based adsorption chillers. Rezk et al. [12] investigated influences of operating temperature and cycle time on the performance of silica gel/water based adsorption chiller.

From the above mentioned perspectives, the present study deals with the performance investigation of silica gel/water based two-bed type adsorption cooling system employing compact heat exchanger. Effects of the operating conditions on the system performance in terms of cooling capacity and COP are also examined to offer the data required to develop a adsorption cooling system driven by waste heat extracted from fuel cells.

4.2. System description and working principle

The schematic diagram of adsorption cooling system using compact type fin-tube heat exchanger is shown in the Fig. 4.1. As can be seen from Fig. 4.1, the silica gel/water based adsorption cooling system comprises pair of sorption elements, namely SE1 and SE2, condenser and an evaporator. The adsorbents (silica gel RD 2060) are packed between the fins of heat exchanger inside of two identical sorption beds (SE1 and SE2). The operation schedules of valves and sorption elements are furnished in Table 4.1. The cycle has four modes namely, mode A, B, C, and D. In mode A, that is shown in Fig. 4.1(a). SE1 and SE2 act as desorber and adsorber, respectively. Hot water flows into SE1 and cooling water flows into SE2. Refrigerant valves V1 and V3 are opened, while valves V2 and V4 are closed. The evaporated refrigerant (water) from the evaporator flows into SE2 via valve V1 and then, adsorbed into the adsorbent of SE2. The desorbed refrigerant from adsorbent packed inside the SE1 flows into the condenser via valve V3 and then, condensed and refluxed back to the evaporator via the U-bend tube. The condensation heat is removed by cooling water which is being flow inside the condenser. In mode B, all four refrigerant valves are closed and then, flows of cooling water and hot water are switched as shown in Fig. 4.1(b). During a short cycle time of duration 10 - 30 s, the SE1 works in pre-cooling mode while SE2 works in pre-heating mode. In mode C, valves V2 and V4 are opened and SE1 works in adsorption mode while SE2 works in desorption mode as shown in Fig. 4.1(c). After the completion of Mode C, pre-heating of SE 2 an pre-cooling of SE 1 starts, which is opposite of Mode B and known as Mode D.

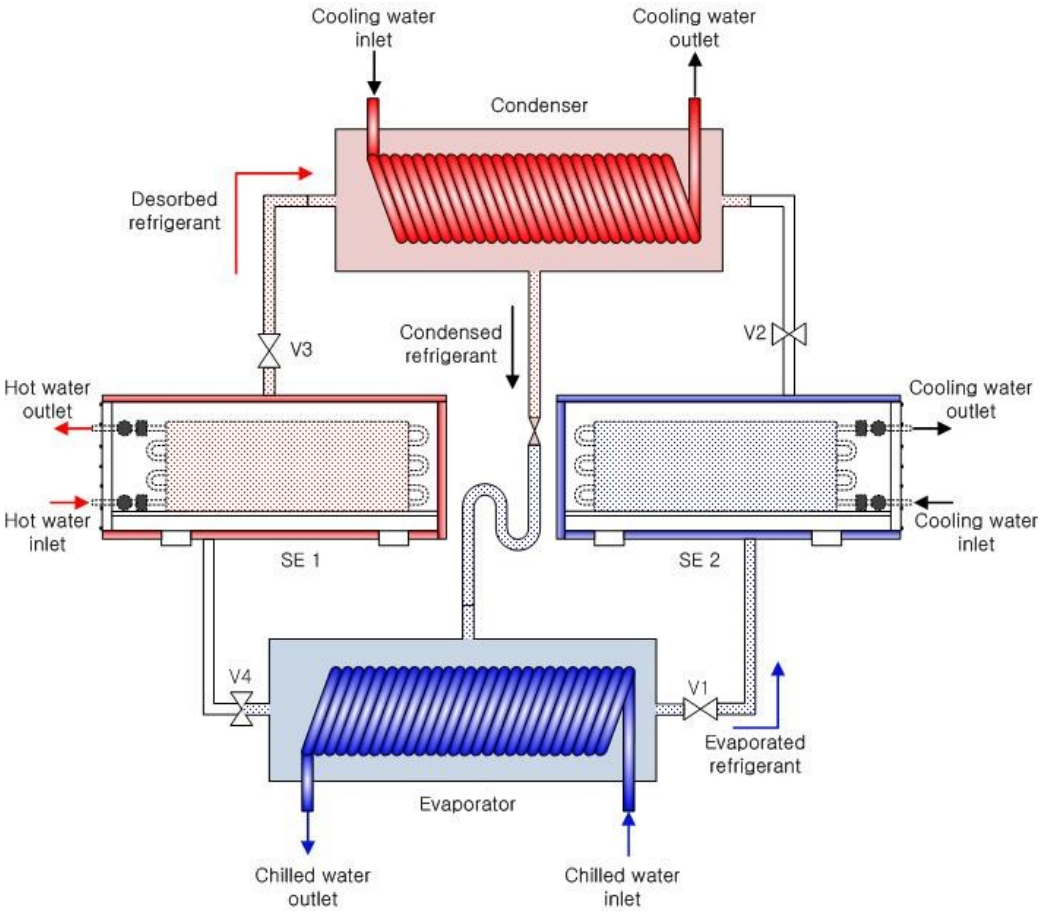

(a) Operation mode A.

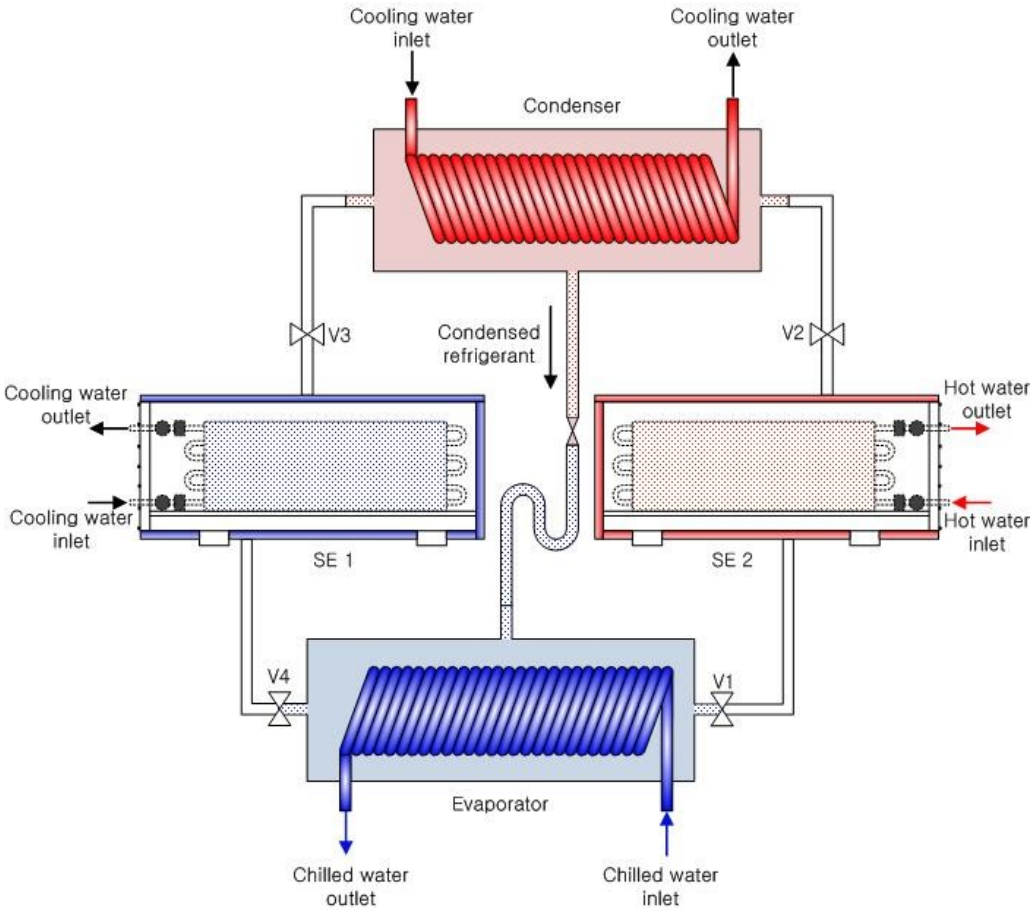

(b) Operation mode B.

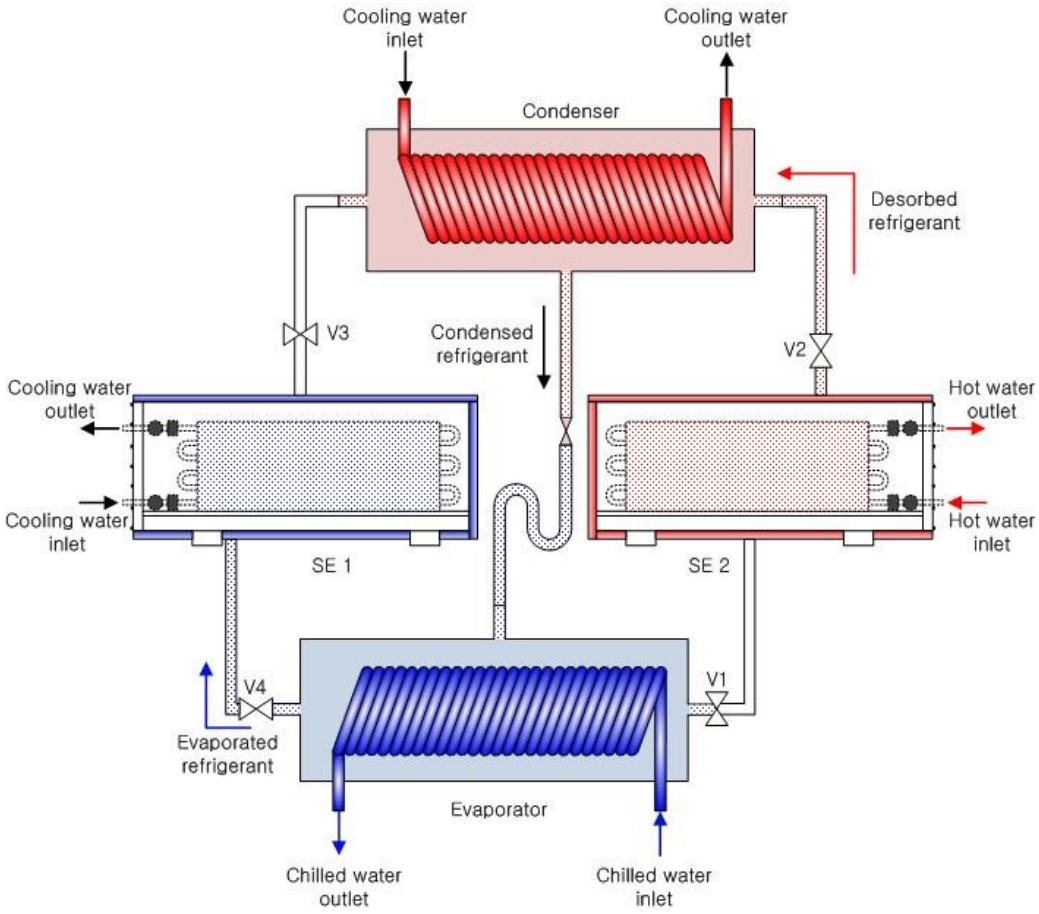

(c) Operation mode C.

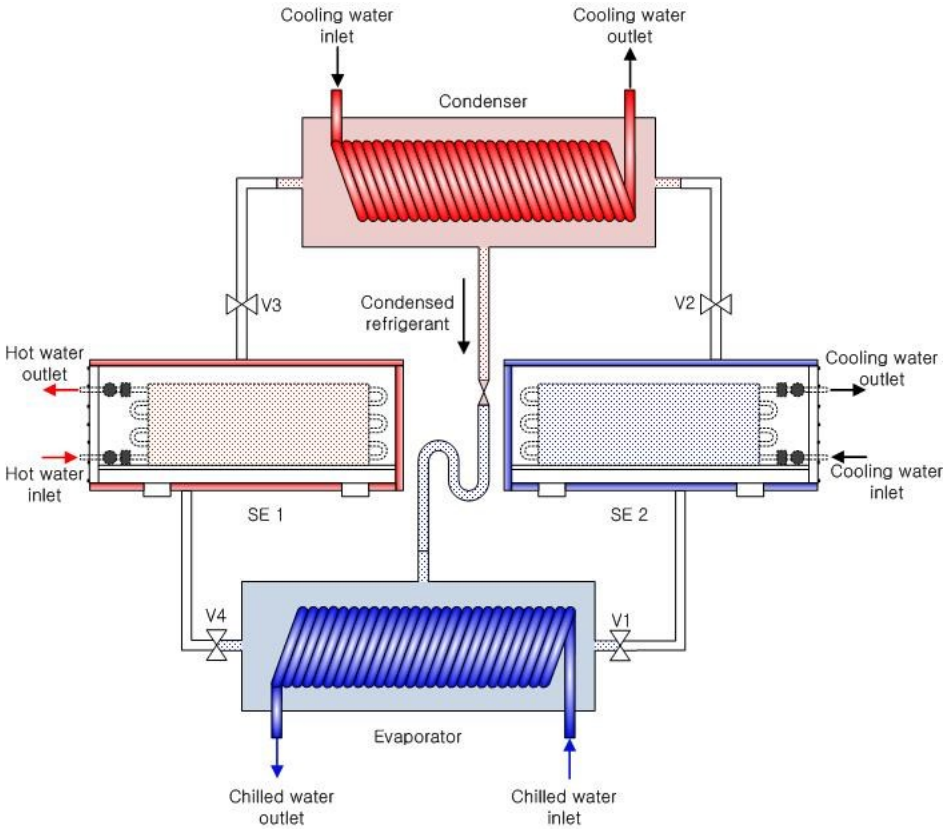

(d) Operation mode D.

Fig. 4.1 Schematic diagrams of silica gel RD/water based adsorption cooling system using compact fin-tube heat exchanger.

Table 4.1 Operation schedules of refrigerant valves and sorption elements

Mode	a	b	c	d
Valve 1	Opened	Closed	Closed	Closed
Valve 2	Closed	Closed	Opened	Closed
Valve 3	Opened	Closed	Closed	Closed
Valve 4	Closed	Closed	Opened	Closed
SE1	Desorption	Pre-cooling	Adsorption	Pre-heating
SE2	Adsorption	Pre-heating	Desorption	Pre-cooling

4.3. Mathematical modeling

4.3.1 Adsorption isotherm

The *modified Freundlich* equation, *S-B-K* equation [13], is used for RD type silica gel/water pair to estimate the equilibrium uptake as given in Eq. (4-1)

$$W = A(T_s)\left[\frac{P_s(T_w)}{P_s(T_s)}\right]^{B(T_s)} \tag{4-1}$$

where, W denotes the adsorption uptake at the equilibrium pressure, $P_s(T_s)$. Here $A(T_s)$ and $B(T_s)$ are expressed as functions of adsorbent temperature, T_s;

where,

$$A(T_s) = A_0 + A_1 T_s + A_2 T_s^2 + A_3 T_s^3 \tag{4-2}$$

$$B(T_s) = B_0 + B_1 T_s + B_2 T_s^2 + B_3 T_s^3 \tag{4-3}$$

The present authors have simplified *the S-B-K* adsorption isotherm equation by eliminating the constant and 3_{rd} order temperature term to fit the current experimental data where $A(T_s)$ and $B(T_s)$ can be found in the previous chapter [See Eqs. (3-5) and (3-6)].

4.3.2 Adsorption kinetics

The adsorption kinetics of adsorption cooling cycles is estimated by LDF equation as given in Eq. (4-4), below.

$$\frac{\partial w}{\partial t} = k_s a_v (W - w) \tag{4-4}$$

where, $k_s a_v$ is overall mass transfer coefficient of the adsorbent/refrigerant pair and W gives equilibrium uptake and w is instantaneous uptake. The $k_s a_v$ can be written as,

$$k_s a_v = F_0 \frac{D_s}{R_p^2} \tag{4-5}$$

where,

$$D_s = D_{so} \exp\left(-\frac{E_a}{R_m T}\right) \tag{4-6}$$

here, F_0 is shape constant [-], D_s is surface diffusion coefficient [m^2/s], R_p stands for particle radius [m], D_{so} is pre-exponential constant [m^2/s] while E_a presents activation energy [kJ/kg] and R is gas constant [kJ/kg·K].

4.3.3 Energy balance of adsorber/desorber heat exchanger

Using the lumped approach for the adsorption bed, which comprises the silica gel, the heat exchanger fins and tubes, the energy balance equation, is given by

$$\begin{aligned}&\left(MC_p\right)_{eff}^{bed}\frac{dT_i^{bed}}{dt}+\left(mC_p\right)_{adsorbate}\frac{dT_i^{bed}}{dt}\\&=\phi M_{adsorben}\left(\frac{dw_i^{bed}}{dt}\right)\Delta H_{st}-\left(\dot{m}C_p\right)_j\left(T_{j,o}-T_{j,in}\right)\end{aligned}\tag{4-7}$$

where, the flag ϕ is equal to 0 and 1 during the switching and adsorption/desorption process, respectively. The subscript *i* indicates the adsorption/desorption bed and *j* denotes the cooling/heating source. The left hand side of Eq. (4-7) presents the internal energy change of heat exchanger including the adsorbent and adsorbate (refrigerant) during the adsorption/desorption process. The first term of the right hand side presents the released heat or absorbed heat during the adsorption and desorption process. The second term of right hand side presents released heat to cooling water for adsorption process or absorbed heat from hot water for desorption process. Isosteric heat of adsorption is estimated experimentally using Henry's law [14]. Numerical value of isosteric heat of adsorption (ΔH_{st}) is found to be 2559 kJ/kg. Henry's law's equation is written as;

$$W=K_0\exp\left[\Delta H_{st}/\left(R_mT\right)\right]P\tag{4-8}$$

where, K_0 is pre-exponential constant and the numerical values of K_0 is found to be 1.25×10^{-9} kPa^{-1}.

The log-mean temperature difference (LMTD) method is employed to estimate the outlet temperature of cooling or heating water, which can be written as;

$$T_{j,o} = T_i^{bed} + \left(T_{j,in} - T_i^{bed}\right) exp\left[\frac{-\left(UA\right)_i^{bed}}{\left(\dot{m}C_p\right)_j}\right] \tag{4-9}$$

Overall heat transfer coefficient, UA^{bed} is considered incrementally at each element where rectangular aluminum fin, bared stainless steel tube, cooling and heating water flowing and silica gel + surrounded refrigerant (water) vapor as shown in Fig. 4.2(a). There are five thermal resistances namely, radial convection thermal resistance from heat transfer fluid (water), radial conduction thermal resistance between tube wall, radial conduction thermal resistance between tube and fin, axial conduction thermal resistance from fin to silica gel + surrounded refrigerant (water) vapor and radial thermal resistance between tube and silica gel + surrounded refrigerant (water) vapor, respectively. Furthermore, thermal resistances of rectangular aluminum fin were analyzed with modification to circular fin which has same surface area of rectangular fin as shown in Fig. 4.2(b). Referring to Fig. 4.2 (a), (b) and (c), the total resistance per unit length can be estimated as follows as;

$$\begin{aligned} R_{j,conv} &= \frac{1}{h_j A_{tb,i}} \\ R_{tb,cond} &= \frac{\ln\left(D_{tb,o} / D_{tb,i}\right)}{2\pi k_{tb}} \\ R_{fin,cond} &= \frac{\ln\left(D_{fin,o} / D_{tb,o}\right)}{2\pi k_{fin}} \end{aligned} \tag{4-10a}$$

$$R_{eff,cond,a} = \frac{\delta_{eff}}{A_{fin} k_{eff}}$$

$$R_{eff,cond,r} = \frac{\ln\left(D_{fin,o} / D_{tb,o}\right)}{2\pi k_{eff}}$$

$$R_{eq,A} = R_{fin,cond} + R_{eff,cond,a} \tag{4-10b}$$

$$R_{eq,B} = \frac{R_{eqA} \cdot R_{eff,cond,r}}{R_{eqA} + R_{eff,cond,r}} \tag{4-10c}$$

therefore,

$$R_{total} = R_{j,conv} + R_{tb,cond} + R_{eq,B} \tag{4-10d}$$

The overall heat transfer coefficient UA^{bed} can be calculated using the following relation;

$$UA^{bed} = \frac{1}{R_{j,conv} + R_{tb,cond} + R_{eq,B}} \tag{4-11}$$

where,

$$h_j = \frac{Nu_D k_j}{D} \tag{4-12}$$

$$Nu_{D,j} = \frac{(f/8)(Re_D - 1000)P_r}{1 + 12.7(f/\varepsilon)^{1/2}(P_r^{2/3} - 1)}\left[1 + \left(\frac{D}{L}\right)^{2/3}\right], (Re_D > 2300, 2000 > P_r > 0.6) \quad (4\text{-}13)$$

$$f = \frac{0.25}{\left[log\left(\frac{1}{3.7(D/\varepsilon)} + \frac{5.74}{Re_D^{0.9}}\right)\right]^2} \quad (4\text{-}14)$$

where, effective thermal conductivity of silica gel + water vapor, k_{eff}, is addapted from Feri et al. [15], surface roughness of stainless steel tube, ε, is 0.0015 mm.

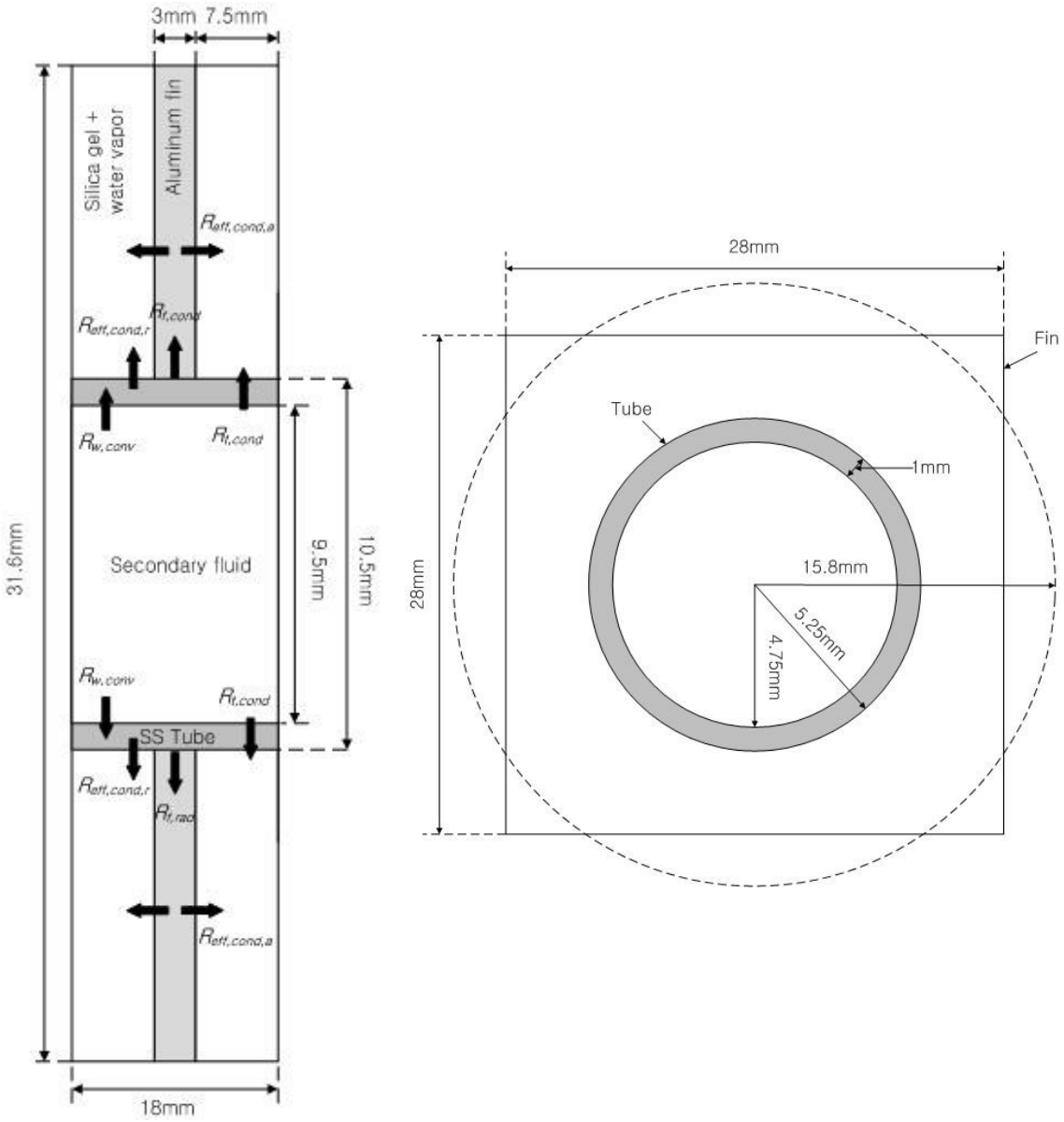

(a) Side view (b) Front view

(c) Analog of thermal resistances

Fig. 4.2 Configuration of incremental thermal analysis.

4.3.4 Condenser energy balance

Condenser is connected with the desorber where desorbed vapor refrigerant can be condensed and delivered to the evaporator through the U bended tube during the desorption process. Energy balance of the condenser can be expressed as;

$$\left(MC_p\right)_{eff}^{cond}\frac{dT^{cond}}{dt}=\phi h_{fg}\left(M_{adsorbent}\frac{dw_{des}^{bed}}{dt}\right)-\left(\dot{m}C_p\right)_{cw}\left(T_{cw,o}-T_{cw,in}\right) \tag{4-15}$$

The left hand side of Eq. (4-15) presents internal energy of metallic parts of shell and tube type heat exchanger. The first term of right hand side provides generated latent heat due to condensation of the desorbed refrigerant from bed in desorption mode. The second term provides released heat to cooling water. The outlet temperature of cooling water can be written as;

$$T_{cw,o}=T^{cond}+\left(T_{cw,in}-T^{cond}\right)\exp\left[\frac{-\left(UA\right)^{cond}}{\left(\dot{m}C_p\right)_{cw}}\right] \tag{4-16}$$

Overall heat transfer coefficient of condenser, UA^{cond}, is presented in terms of convection thermal resistance of water inside of tube, conduction thermal resistance between tube wall and conductive thermal resistance of refrigerant (water) condensation over the tube outside. UA^{cond}, is expressed by Eq. (4-17).

$$UA^{cond}=\frac{1}{R_{cw,conv}+R_{tb,cond}+R_{ref,conv}} \tag{4-17}$$

rewritten as;

$$UA^{cond} = \frac{1}{\frac{1}{h_{cw}A_{tb,i}} + \frac{\ln\left(D_{tb,o}/D_{tb,i}\right)}{2\pi k_{tb}L} + \frac{1}{h_{ref}A_{tb,o}}} \tag{4-18}$$

In this model, condensation is defined as laminar film condensation on the outer surface of a horizontal tube, and convection heat transfer coefficient is given as;

$$h_{ref} = C\left[\frac{g\rho_f\left(\rho_f - \rho_g\right)k^3 h_{fg}}{\mu_f\left(T_{sat} - T_{wall}\right)D}\right]^{1/4} \tag{4-19}$$

where, C constant is 0.729 for the tube, acceleration of gravity, g is 9.81 m/s and h_{fg} is latent heat of water.

4.3.5 Evaporator energy balance

The overall energy balance of evaporator is governed mainly by the heat and mass interaction between the evaporator and the adsorber bed. The energy balance of the evaporator can be given as;

$$\left(MC_p\right)_{eff}^{eva}\frac{dT^{eva}}{dt} = \phi h_{fg}\left(M_{adsorbent}\frac{dw_{ads}^{bed}}{dt}\right) - \left(\dot{m}C_p\right)_{chill}\left(T_{chill,o} - T_{chill,in}\right) \tag{4-20}$$

The left hand side presents internal energy change of metallic parts of heat exchanger and sensible heat of liquid refrigerant. The first term of right hand side presents latent heat of evaporation for the amount of refrigerant adsorbed and the second term shows

the quantity of delivered cooling energy from the evaporator. The outlet temperature of chilled water can be written as;

$$T_{chill,o} = T^{eva} + \left(T_{chill,in} - T^{eva}\right) exp\left[\frac{-\left(UA\right)^{eva}}{\left(\dot{m}C_p\right)_{chill}}\right] \tag{4-21}$$

In the shell and tube heat exchanger, evaporation can be considered as nucleate pool boiling, so heat transfer coefficient is calculated by Rohsenhow equation as given by Eq. (4-24). Overall heat transfer coefficient of evaporator is written as;

$$UA^{eva} = \frac{1}{R_{w,conv} + R_{tb,cond} + R_{ref,conv}} \tag{4-22}$$

$$UA^{eva} = \frac{1}{\frac{1}{h_w A_{tb,i}} + \frac{\ln\left(D_{tb,o} / D_{tb,i}\right)}{2\pi k_{tb} L} + \frac{1}{h_{ref} A_{tb,o}}} \tag{4-23}$$

$$h_{ref} = \frac{\mu_f h_{fg}}{T_{sat} - T_{wall}} \sqrt{\frac{g\left(\rho_f - \rho_g\right)}{\sigma}\left(\frac{C_{p,f}\left(T_{sat} - T_{wall}\right)}{C_{s,f} h_{fg} Pr^n}\right)^3} \tag{4-24}$$

where, numerical values of $C_{s,f}$ and n are 0.0128 and 1 for water/copper combination and σ is surface tension.

4.3.6 Mass balance

The mass change of refrigerant is equal to the amount of adsorbed refrigerant during adsorption process and the quantity of refrigerant that is desorbed during desorption operation. The Mass balance of the refrigerant can be written as;

$$\frac{dM_{ref}}{dt} = -M_{adsorben}\left[\frac{dw_{ads}^{bed}}{dt} + \frac{dw_{des}^{bed}}{dt}\right] \tag{4-25}$$

4.3.7 System performances

In the present study, the performances of adsorption cooling systems are estimated with cooling capacity and COP of the cycles. Cooling capacity and COP can be written, respectively as;

$$Q_{chill}^{cycle} = \frac{\int_0^{t_{cycle}} \left\{\left(\dot{m}C_p\right)_{chill}\left(T_{chill,in} - T_{chill,o}\right)\right\}dt}{t_{cycle}} \tag{4-26}$$

$$COP = \frac{Q_{chill}^{cycle}}{Q_{des}^{cycle}} \tag{4-27}$$

where,

$$Q_{des}^{cycle} = \frac{\int_0^{t_{cycle}} \left\{\left(\dot{m}C_p\right)_{des}\left(T_{hw,in} - T_{hw,o}\right)\right\}dt}{t_{cycle}} \tag{4-28}$$

4.4. Results and discussion

4.4.1. Effects of cycle and switching times

In this study, mathematical modeling for silica gel RD 2060/water based adsorption cooling system using compact fin-tube heat exchanger is optimized and proposed. Flow rates of each heat transfer fluids are proposed to get temperature differences of 2.5˚C for hot water and cooling water and 3˚C for chilled water between inlet and outlet temperatures, and physical parameters are furnished in Table 4.2. Figure 4.3 shows the effect of cycle time on the cooling capacity and COP. As can be seen Fig. 4.3, time is not enough for adsorption or desorption to occur satisfactorily when cycle time is shorter than 600 s, thereby cooling capacity decreases drastically. However, cooling capacity shows maximum value at the cycle time between 900 and 1200 s. the cooling capacity decreases gradually when cycle time is longer than 1200 s. Figure 4. 4 shows switching time effect on the cooling capacity and COP. As shown in Fig. 4.4, the cooling capacity varies slightly with variation of switching time, and it shows optimum values at switching time between 25 and 30 s. COP shows same variation tendency with the cooling capacity.

Transient responses of optimized adsorption cycle are shown in Fig. 4.5 and 4.6. Inlet temperatures of hot water, cooling water and chilled water are fixed at 85, 30 and 15˚C, respectively. In terms of internal temperature profiles of each component, it can be observed that optimized adsorption cycle can be reach to steady state operation over 2400 s of cycle time as shown in Fig. 4.5. Outlet temperature profiles of heat transfer fluids are depicted in Fig. 4.6 for one adsorption/desorption cycle. It can be seen that, outlet temperature of hot water is about 2.5˚C lower than that of hot water while the

outlet temperature of cooling water is 2.5˚C higher than inlet temperature of cooling water for both adsorber and condenser. The outlet temperature of chilled water is 3˚C lower than inlet temperature of chilled water. It is worthy to mention that the chiller working at the above mentioned conditions provides chilled water with an average temperature of about 12˚C.

Thermodynamic process of optimized adsorption system is depicted on the Dühring diagram (pressure-temperature-concentration) and compared with ideal cycle as shown in Fig. 4.7. Total cycle time which includes all four processes namely, adsorption (a - b), pre-heating (switching time of 30 s, b - c), desorption (c - d) and pre-cooling (switching time of 30 s, d - a) was set to be 1200 s for optimized cycle. Solid black line is optimized cycle from our current simulation and dashed red line is ideal cycle. In these figure, positive thermal swing (b - c) in the bed is occurred at constant isosteres (constant concentration) which is known as the pre-heating process and negative thermal swing (d - a) in the bed is occurred at constant isosteres which is known as the pre-cooling process. In contrast, adsorption/desorption processes are occurred isobaric during a - b (evaporation - adsorption) and c - d (desorption - condensation) processes. In the studied adsorption cycle, sudden pressure drop is observed at the beginning of positive thermal swing (pre-heating mode). Since adsorption still occurs during closing whole refrigerant valves even heat is already supplied. Subsequently, thermal swing is occurred at the constant isosteres. There are also unexpected pressure rise and pressure drop at the end of thermal swing phases. This is why pre-cooling/heating during the switching time are stopped before sorption beds is cooled and heated sufficiently, thereby the pressures in the sorption beds cannot reach to the pressures of condensation and evaporation. Consequently, at the end of positive thermal swing, condensate on the

tubes in the condenser is evaporated and adsorbed to the heated adsorbent momentarily. Similarly, at the end of negative thermal swing, adsorbate inside of cooled bed is condensed into the evaporator.

Table 4.2 Values of physical parameters.

Parameter	Unit	Value
F_o	[-]	15
D_{so}	[m^2/s]	2.54×10^{-4}
E_a	[kJ/mol]	4.2
R_p	[m]	4×10^{-4}
$M_{adsorbent}$	[kg]	2.69
$(\dot{m}C_p)_j$	[kW/K]	0.15
$(\dot{m}C_p)_{cond}$	[kW/K]	0.21
$(\dot{m}C_p)_{chill}$	[kW/K]	0.17
$(MC_p)_{bed}$	[kJ/K]	5.35
$(MC_p)_{cond}$	[kJ/K]	0.213×0.385+0.18×4.186
$(MC_p)_{eva}$	[kJ/K]	0.3×0.385+1.1×4.186
$(UA)_{bed}$	[kW/K]	0.48
$(UA)_{cond}$	[kW/K]	0.6
$(UA)_{eva}$	[kW/K]	0.4

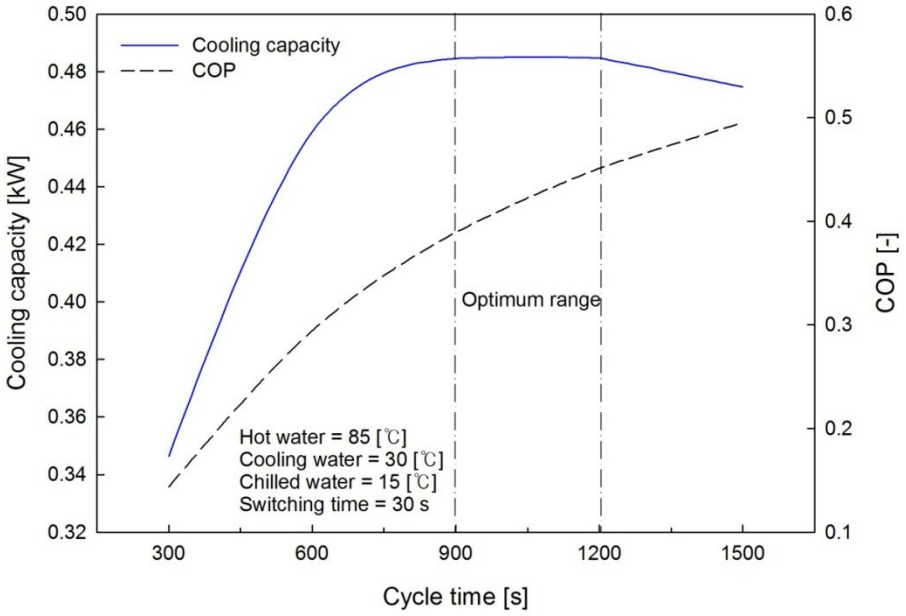

Fig. 4.3 Cycle time effect on cooling capacity and COP.

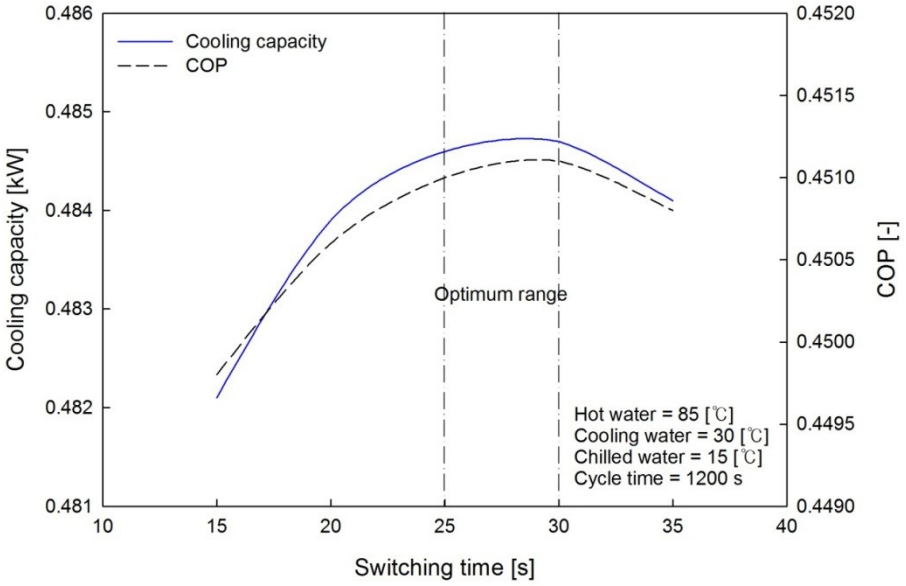

Fig. 4.4 Switching time effect on cooling capacity and COP.

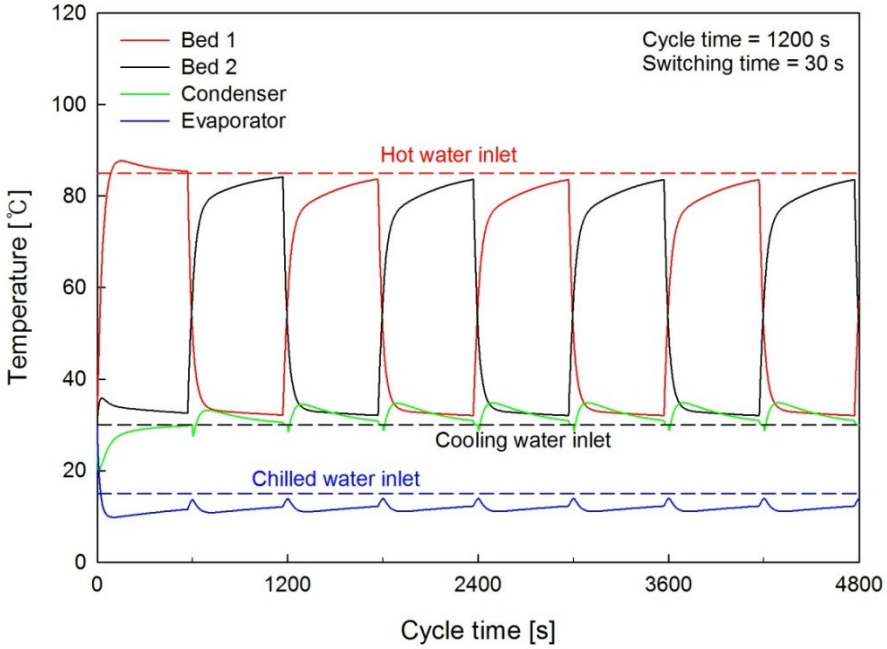

Fig. 4.5 Temperature profiles of each component for optimized cycle time.

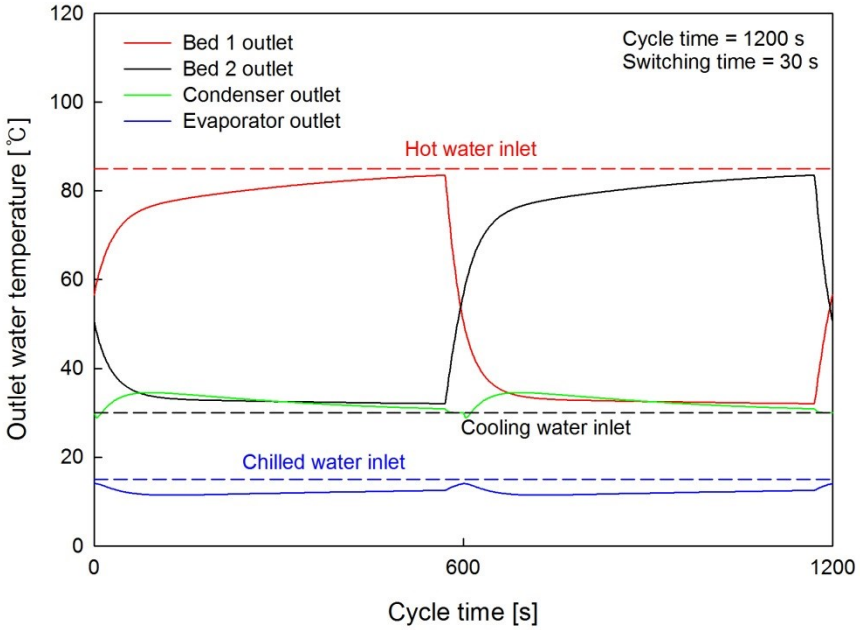

Fig. 4.6 Outlet water temperature profiles of heat transfer fluids for optimized cycle time.

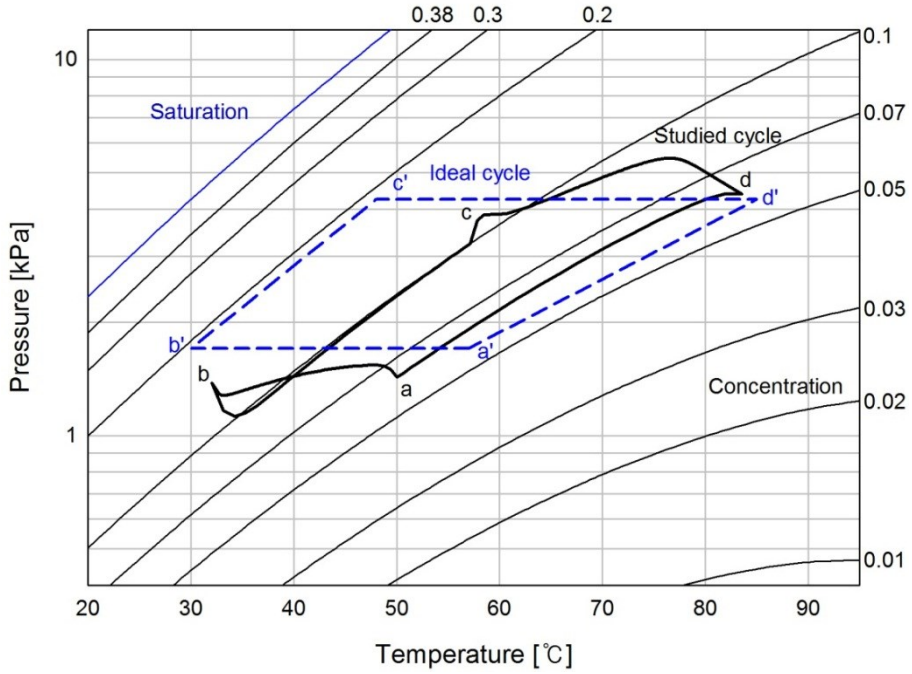

Fig. 4.7 Comparison of optimized cycle with ideal cycle on Dühring diagram.

4.4.2 Effects of operating temperatures

The motivation of this work is to develop adsorption cooling system that can be driven by lower heat source from fuel cell. Accordingly, the effects of heat transfer fluids temperatures variation on the performances are shown in Figs. 4.8 - 4.10. Related temperature conditions of heat transfer fluids are furnished in Table 4.3. Cooling capacity shows increasing tendency linearly from 0.28 to 0.52 kW with higher inlet temperature of hot water. Increment of temperature is highly effective on the COP in the range below 80˚C. COP starts to decrease beyond this temperature as shown in Fig. 4.8. This can be inferred that most amount of adsorbate is desorbed up to 80˚C, subsequently, amount of desorbed adsorbate decreases gradually. In other words, this causes increment of heat loss by larger sensible heat of desorbed adsorbate vapor in the desorption bed.

Figure 4.9 shows effect of cooling water inlet temperature variation to adsorber/condenser. Both cooling capacity and COP decrease gradually with higher cooling water temperature, while COP decreases drastically over 35˚C. These are due to increment of adsorbed adsorbate amount in the lower temperature of cooling water. Cooling capacity and COP show maximum value with 0.84 kW and 0.53 at cooling water temperature of 15˚C.

Figure 4.10 shows effect of chilled water inlet temperature variations. Both cooling capacity and COP increase with higher inlet temperature of chilled water. Cooling capacity and COP show highest performances with 1.12 kW and 0.65. However, Outlet temperature of chilled water also increases along with increasing of chilled water inlet temperature. In other words, the performances of studied adsorption cooling system can be improved regarding to required temperature by user.

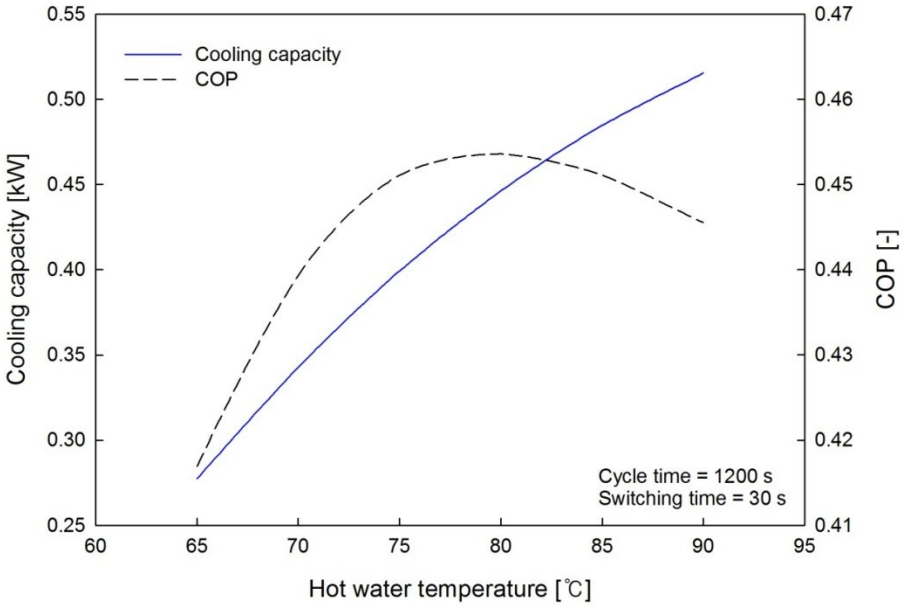

Fig. 4.8 Hot water temperature effect on cooling capacity and COP.

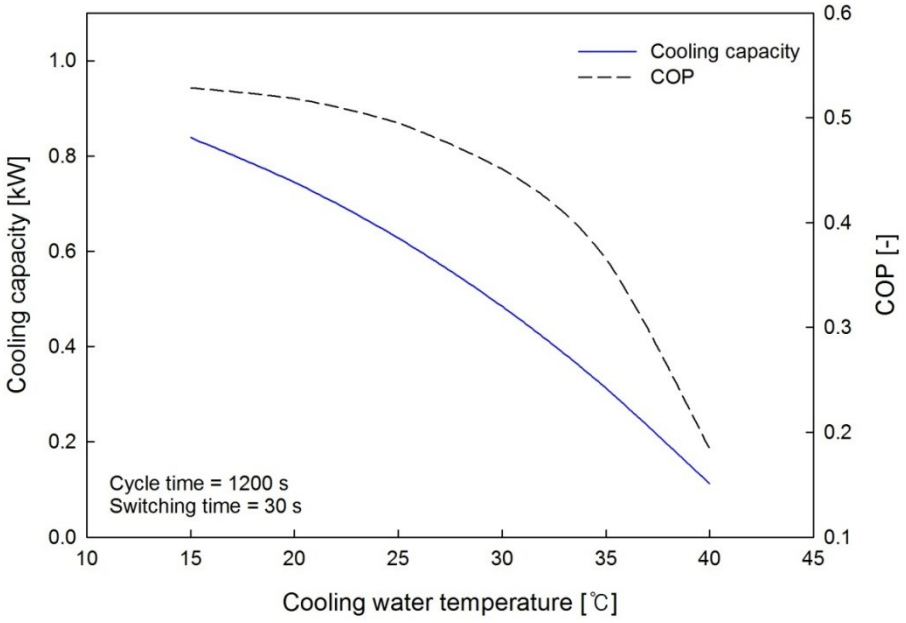

Fig. 4.9 Cooling water temperature effect on cooling capacity and COP.

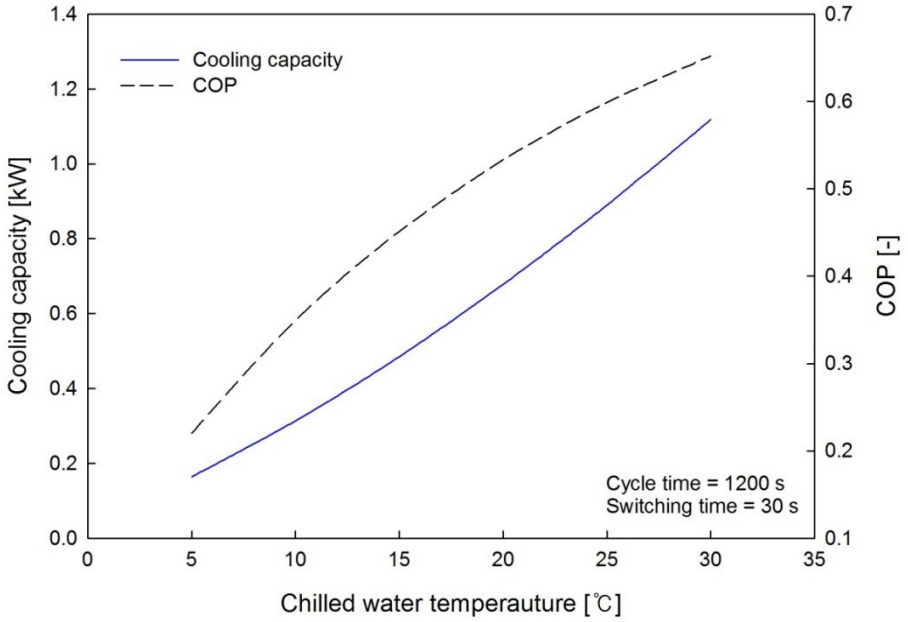

Fig. 4.10 Chilled water temperature effect on cooling capacity and COP.

Table 4.3 Related temperature conditions of heat transfer fluids

Hot water inlet Temperature [˚C]	Cooling water inlet temperature [˚C]	Chilled water inlet Temperature [˚C]
65 - 90	30	15
85	15 - 40	15
85	30	5 - 30

4.4.3 Effects of heat transfer fluids flow rate

Effects of different heat transfer fluids flow rate on the system performance are shown in Figs. 4.11 - 4.13 and related flow rate conditions of heat transfer fluids are furnished in Table 4.4. The effect of hot water flow rate on performances is shown in Fig. 4.11, both cooling capacity and COP increase with higher hot water flow rate. Increasing hot water flow rate is highly effective up to 0.06 kg/s of flow rate, however the increment of both cooling capacity and COP are marginal above this value. The effect of cooling water flow rate on the performances is shown in Fig. 4.12. Both cooling capacity and COP show increasing tendency with higher cooling water flow rate in range between 0.05 - 0.1 kg/s.

The effect of chilled water flow rate on the cooling capacity and COP is shown in Fig. 4.13. Cooling capacity and COP shows increasing tendency with higher chilled water flow rate in the rage of 0.04 - 0.09.

Table 4.4 Related flow rates of heat transfer fluids

Hot water Flow rate [kg/s]	Cooling water Flow rate [kg/s]	Chilled water Flow rate [kg/s]
0.035 - 0.09	0.05	0.04
0.035	0.05 - 0.1	0.04
0.035	0.05	0.04 - 0.09

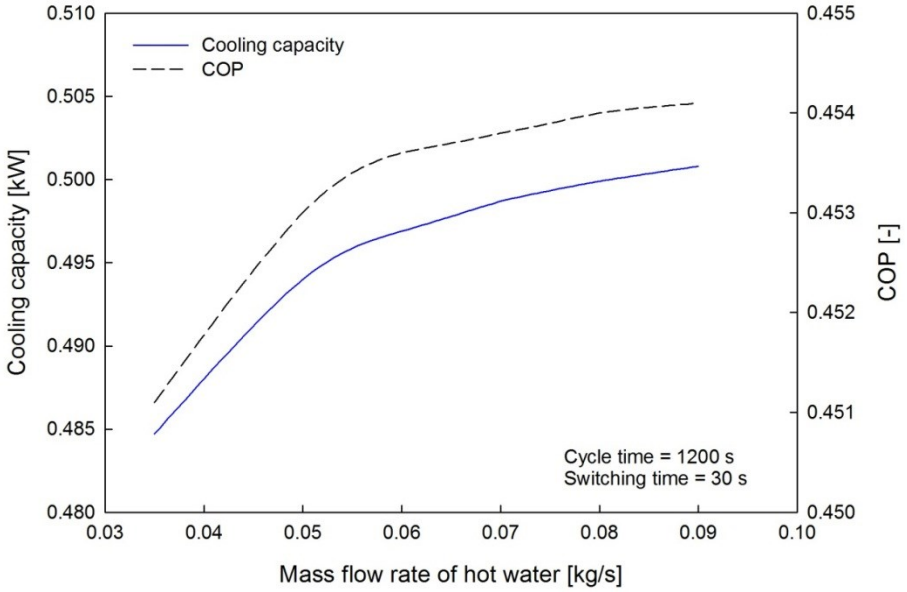

Fig. 4.11 Hot water flow rate effect on cooling capacity and COP.

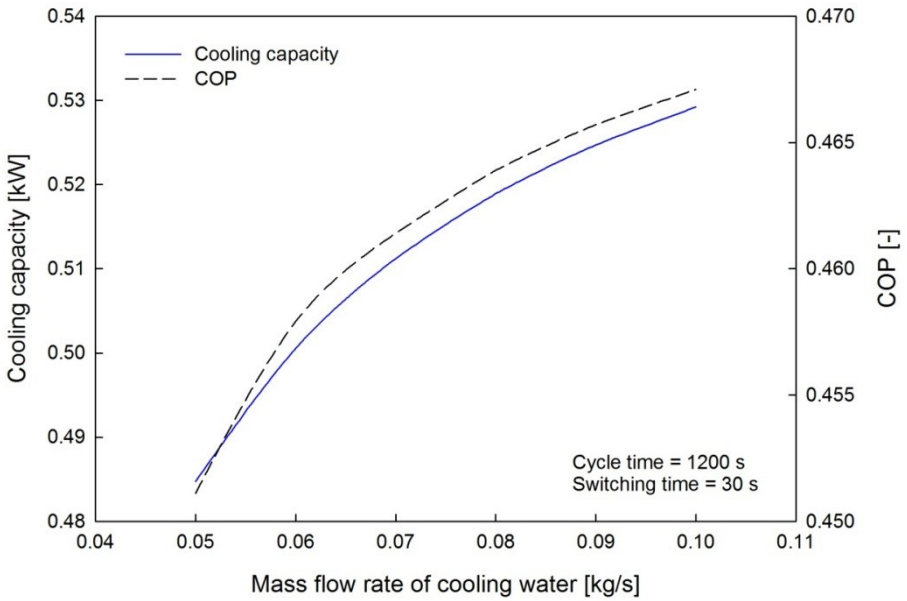

Fig. 4.12 Cooling water flow rate effect on cooling capacity and COP.

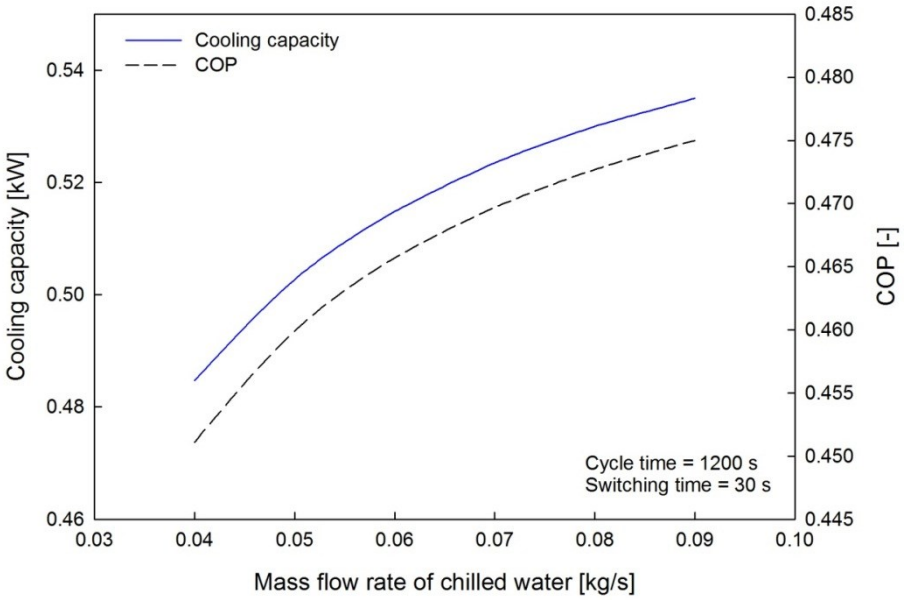

Fig. 4.13 Chilled water flow rate effect on cooling capacity and COP.

4.5. Conclusions

The main remarkable points of this chapter can be summarized as follows;

Theoretical results show that the adsorption chiller employing the compact fin-tube heat exchanger is able to achieve the same cyclic-steady state with two cycles.

The proposed system is able to utilize effectively low temperature waste heat between 60 and 90°C as the driving heat source with cooling water at 30°C. The chiller can be operated with temperature difference between the heat source and heat sink as small as 30°C.

Longer adsorption/desorption cycle time effects on increment of COP and decrement of cooling capacity. Optimum cooling capacity value of 0.485 kW is obtained for adsorption/desorption cycle time at 600 s along with switching time at 30 s.

Cooling capacity increases with higher driving heat source temperature along with a fixed cooling water temperature at 30°C. The optimum COP values are obtained with driving source temperatures between 75 and 80°C.

The performance of the cooling system is improved with increment of hot, cooling and chilled water flow rates. However, the improvement is marginal when flow rate of hot water is above 0.5 kg/s.

Nomenclature

A_0	Constant of Eq. (5-2) and (5-4)	w	Instantaneous uptake [kg/kg]
A_1	Constant of Eq. (5-2) and (5-4)	W	Equilibrium uptake [kg/kg]
A_2	Constant of Eq. (5-2)	W_0	Maximum uptake [kg/kg]
A_3	Constant of Eq. (5-2)		
B_0	Constant of Eq. (5-3) and (5-5)	*Greek symbols*	
B_1	Constant of Eq. (5-3) and (5-5)	ΔH_{st}	Isosteric heat of adsorption [kJ/kg]
B_2	Constant of Eq. (5-3)	δ	Thickness [m]
B_3	Constant of Eq. (5-3)	ε	Surface roughness
C_p	Specific heat [kJ/kg·K]	μ	Friction factor
COP	Coefficient of performance	ρ	Density [kg/m^3]
D	Diameter [m]		
D_s	Surface diffusion coefficient [m^2/s]	*Superscript*	
D_{so}	Pre-exponential constant [m^2/s]	*bed*	Sorption bed
E_a	Activation Energy [kJ/kg]	*cond*	Condenser
F_0	Shape constant [-]	*eva*	Evaporator
g	Acceleration of gravity [9.81m/s]		
h	Heat transfer coefficient [kW/m^2·K]	*Subscript*	
h_{fg}	Latent heat of refrigerant [kJ/kg]	*a*	axial
h	Enthaly [kJ/kg]	*ads*	Adsorption
k	Thermal conductivity [kJ/m·K]	*chill*	Chilled water
$k_s a_v$	Overall mass transfer coefficient [1/s]	*cond*	Conduction
K_0	Constant in Henry's law	*conv*	Convection

L	Length [m]	*cw*	Cooling water
m	Mass [kg]	*des*	Desorption
$\dot{m}$	Mass flow rate [kg/s]	*eff*	Effective
M	Mass [kg]	*f*	Liquid phase
Nu_D	Nusselt number	*g*	Gaseous phase
P	Pressure [kPa]	*hw*	Hot water
P_r	Prantl number	*i*	Adsorption/desorption
Q	Power [kW]	*in*	In
R	Thermal resistance [$m^2 \cdot K/kW$]	*j*	Cooling water/hot water
Re_D	Reynold's number	*o*	Out
R_m	Gas constant [kJ/mol·K]	*r*	Radial
R_p	Particle radius [m]	*Ref*	Refrigerant
t	Time [s]	*s*	Saturation
T	Temperature [˚C]	*tb*	Tube
UA	Overall heat transfer coefficient [kW/K]	*w*	Saturation of refrigerant

References

[1] B. B. Saha, A. Akisawa and T. Kashiwagi, Silica gel water advanced adsorption refrigeration cycle, Energy 22 (4), (1997) 437-447.

[2] H. T. Chua, K. C. Ng, W. Wang, C. Yap and X. L. Wang, Transient modeling of a two-bed silica gel-water adsorption chiller, International Journal of Heat and Mass Transfer 47, (2004) 659-669.

[3] K. C. Ng, H. T. Chua, C. Y. Chung, C. H. Loke, T. Kashiwagi, A. Akisawa and B. B. Saha, Experimental investigation of the silica gel-water adsorption isotherm characteristics, Applied Thermal Engineering 21, (2001) 1631-1642.

[4] B. B. Saha, A. Chakraborty, S. Koyama and Yu I. Aristov, A new generation cooling device employing CaCl2-silica gel-water system, International Journal of Heat and Mass Transfer 52, (2009) 516-524.

[5] T. Miyazaki, A. Akisawa, B. B. Saha, I. I. El-Sharkawy and A. Chakraborty, A new cycle time allocation for enhancing the performance of two-bed adsorption chiller, International Journal of Refrigeration 32, (2009) 846-853.

[6] B. B. Saha, I. I. El-Sharkawy, A. Chakraborty and S. Koyama, Study on activated carbon fiber-ethanol adsorption chiller: Part Ⅰ - system description and modeling, International Journal of Refrigeration 30, (2007) 86-95.

[7] B. B. Saha, I. I. El-Sharkawy, A. Chakraborty and S. Koyama, Study on activated carbon fiber-ethanol adsorption chiller: Part Ⅱ - performance evaluation, International Journal of Refrigeration 30, (2007) 96-102.

[8] H. Demir, M. Mobedi and S. Ülkü, A review on adsorption heat pump: Problems and solutions, Renewable and Sustainable Energy reviews 12, (2008) 2381-2403.

[9] K. C. Alam, B. B. Saha, Y. T. Kang, A. Akisawa and T. Kashiwagi, Heat exchanger design effect on the system performance of silica gel adsorption refrigeration systems, International Journal of Heat and Mass Transfer 43, (2000) 4419-4431.

[10] M. Z. I. Khan, K. C. A. Alam, B. B. Saha, Y. Hamamoto, A. Akisawa and T. Kashiwagi, Parametric study of a two-stage adsorption chiller using re-heat-The effect of overall thermal conductance and adsorbent mass on system performance, International Journal of Thermal Sciences 45, (2006) 511-519.

[11] C. Y. Tso, C. Y. H. Chao and S. C. Fu, Performance analysis of a waste heat driven activated carbon based composite adsorbent-water adsorption chiller using simulation model, International Journal of Heat and Mass Transfer 55, (2012) 7596-7610.

[12] A. R. M. Rezk and R. K. Al-Dadah, Physical and operation effects on silica gel/water adsorption chiller performance, Applied Energy 89, (2012) 142-149.

[13] B. B. Saha, E. C. Boelman and T. Kashiwagi, Computer simulation of a silica gel-water adsorption refrigeration cycle - the influence of operating condition on cooling output and COP, ASHRAE Trans 101, (1995) 348-357.

[14] H. T. Chua, K. C. Ng, A. Malek, T. Kashiwagi, A. Akisawa and B. B. Saha, Milti-bed regenerative adsorption chiller - improving the utilization of waste heat and reducing the chilled water outlet temperature fluctuation, International Journal of Refrigeration 24, (2001) 124-136.

[15] A. Feri, G. Maggio, F. Cipiti and Y. I. Aristov, Simulation of water sorption dynamics in adsorption chiller: One, two and four layers of loose silica grains, Applied Thermal Engineering 44, (2012) 69-77.

Chapter 5

Chapter 5

Fuel Cell Waste Heat Powered Two-Bed Adsorption Cooling System

5.1. Introduction

Currently, adsorption cooling/heat pump systems have been gained considerable attention due to their environmental friendliness and energy conservation potential. Adsorption cooling systems have advantages as their ozone depletion potential (ODP) and global warming potential (GWP) are zero. Furthermore, these systems can save energy using low temperature waste heat as the driving heat source. Several studies on adsorption characteristics and adsorption cooling cycles have been performed by various authors. Followings are some representative examples.

Ng et al. [1] experimentally investigated water adsorption isotherms on to three types of silica gel namely, A, 3A and RD. Saha et al. [2] found 20 % and 25 % improvement in cooling capacity and COP, respectively, over conventional silica gel/water system employing $CaCl_2$ + KSK silica gel/water as adsorbent/refrigerant pair in a two-bed adsorption chiller. Cooling capacity of both silica gel/water and $CaCl_2$-in-silica gel/water based adsorption chillers were enhanced by 6 % with a new cycle time allocation which was studied by Miyazaki et al. [3]. Saha et al. [4] compared the adsorption capacity of ACF (A-20), ACF (A-15) and ACF (A-10) with ethanol as adsorbate. Modeling of activated carbon/ethanol based adsorption chiller was proposed

and performance of the cycle was evaluated by Saha et al. [5, 6]. Demir et al. [7] had compared the performance of adsorption heat pumps with that of the vapor compression and absorption heat pumps. Furthermore, the same authors suggested some possible solutions regarding to the problems related to the design of adsorbent bed. Okunev et al. [8] investigated mathematical modeling for coupled heat and mass transfer in single adsorbent grain (SWS-1L) which thermal contacted with a metal plate. The performance of a waste heat driven adsorption chiller based on $CaCl_2$ inside the composite of silica + activated carbon was compared with that of silica gel/water and ACF/water based adsorption chillers by Tso et al. [9]. Rezk et al. [10] investigated influences of operating temperature and cycle time on the performance of silica gel/water based adsorption chiller. Recently, Zhang et al. [11] investigated power output of a PEMFC (Polymer Electrolyte Membrane Fuel Cell)/absorption hybrid refrigeration system. Clausse et al. [12] compared the performances of adsorption air conditioning systems powered by PEMFC waste heat for activated carbon/methanol, silica gel/water and zeolite/water pairs. Fadar et al. [13] proposed numerical modeling of continuous two-bed type adsorption refrigeration system powered by parabolic trough solar collector and determined the performances. Mahesh et al. [14] reviewed various types of adsorption cooling systems powered by solar energy and compared the performances of those systems. Hassan et al. [15] reviewed previous studies on solar driven closed type physisorption refrigeration systems and discussed various refrigeration technologies and advancements to improve the performance of adsorption systems. Alghoul et al. [16] proposed a dual purpose continuous solar adsorption system employing activated carbon/methanol pair and estimated the performance theoretically.

In this study, silica gel RD 2060/water based two-bed type adsorption cooling system powered by fuel cell waste heat using a compact fin-tube heat exchanger was proposed and performances were compared within various temperatures for heat transfer fluids by mathematical modeling.

5.2. System description and working principle

In this chapter, outlet water from the fuel cell heat recovery cycles are used as the driving heat source of adsorption cooling systems. It is assumed that fuel cells run all day long (24 hours a day) and adsorption cooling systems run only 8 hours per day. Cooling capacity and COP of silica gel/water cycle are compared with various cycle times. The cycle time includes adsorption and desorption times along with 30 s of two switching times required to switch between adsorption and desorption processes. The schematic diagram of adsorption cooling system using a compact fin-tube heat exchanger is shown in the Fig. 5.1. As can be seen from Fig. 5.1, this system consists of CV1 (Control volume 1) which contains fuel cell unit, heat recovery cycle, mixing chamber and heat storage tank, and CV2 (Control volume 2) which comprises of one pair of sorption elements, namely SE1 and SE2, one condenser and an evaporator. The adsorbent (silica gel RD 2060) was packed between the fins of heat exchanger inside of two identical sorption beds (SE1 and SE2). Hot water is supplied to either SE1 or SE2 (as shown in CV2) from heat recovery cycle of CV1. The operation modes and operation schedules were explained in detail in the previous chapter. (See Fig. 4.1 and Table 4.1)

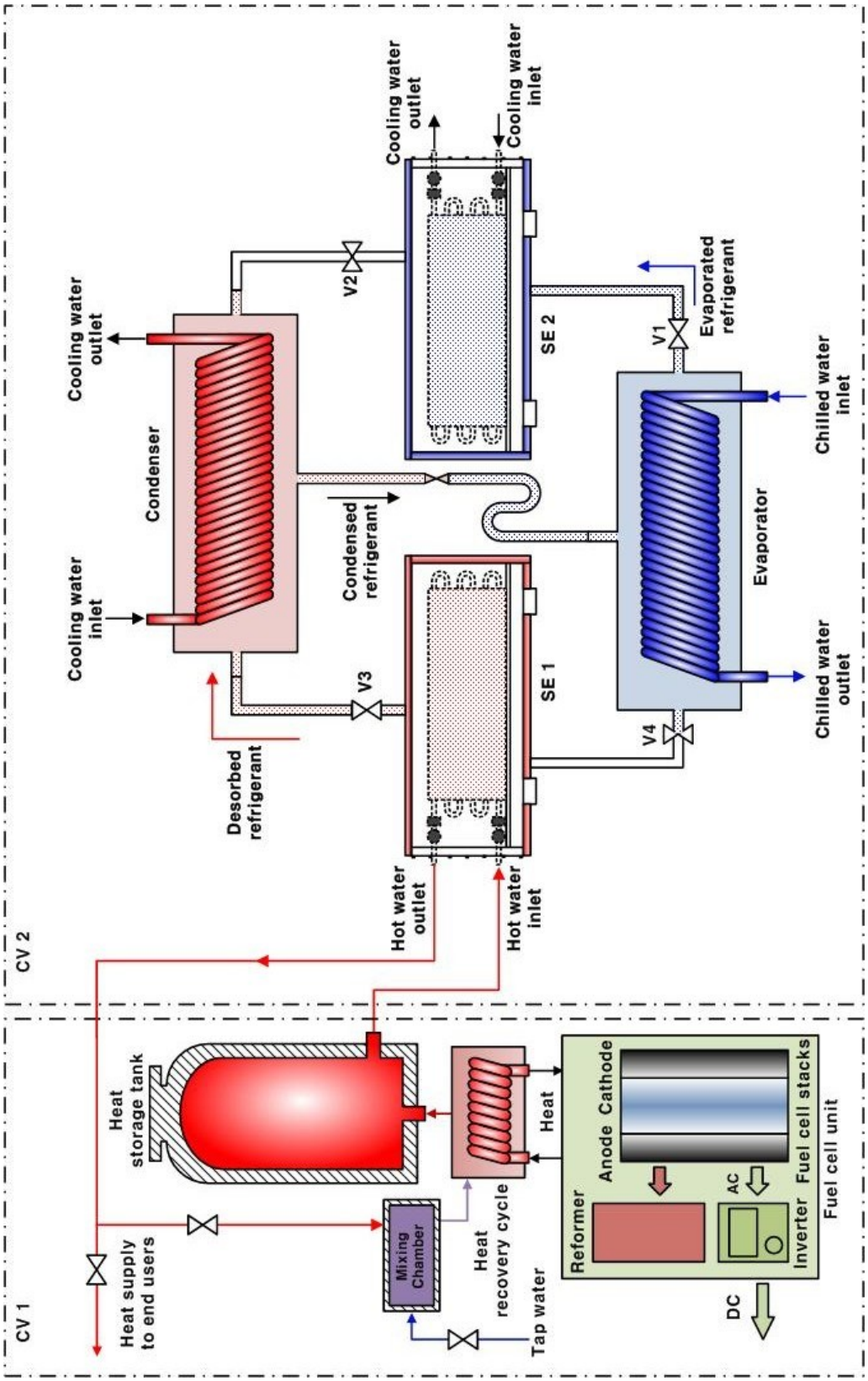

Fig. 5.1 Silica gel/water based adsorption cooling system powered by fuel cell waste heat

5.3. Mathematical modeling

5.3.1. Adsorption isotherm

The modified S-B-K equations are considered as the adsorption isotherm equations which are described in detail in chapter 3 [see Eqs. (3-2) - (3-6)].

5.3.2. Adsorption kinetics

The LDF equation is considered as the adsorption kinetics equation which is described in detail in the previous chapter [see Eqs. (4-4) - (4-6)].

5.4. Heat recovery from fuel cells

Currently, many researches are involved in conducting research, development and demonstration (RD&D) activities on the fuel cell co-generation system as an energy saving technology for industry and building applications. Hamada et al. [17] evaluated the performance of PEFC prototype which includes heat recovery cycle and heat storage tank for residential energy system. It generates 1 kW of electricity and 1.7 kW of heat using waste heat from PEFC. Farhad et al. [18] evaluated three biogas-fueled SOFC micro combined heat and power (micro-CHP) systems for application in residential dwellings through computer simulation. It generates 1 kW of electricity and 2.09 kW of heating energy using waste heat from SOFC. In this paper, the performances of adsorption cooling systems has been evaluated based on the fuel cell waste heat data of Hamada et al. [17] and Farhad et al. [18], and the specifications of the fuel cells are furnished in Table 5.1.

Table 5.1 Specifications of fuel cells. [17, 18]

Parameter	Unit	Values	
		PEFC	SOFC
Electricity production	[kW]	1	1
Recovered heat	[kW]	1.7	2.09
Inlet water temperature to heat recovery cycle	[˚C]	22	40
Outlet water temperature from heat recovery cycle of fuel cell	[˚C]	61.2	90

5.5. Results and discussion

In this chapter, mathematical modeling and performance evaluation of fuel cell waste heat powered silica gel RD 2060/water based adsorption cooling systems using a compact fin-tube heat exchanger are presented. For the adsorption chillers, inlet temperatures are set to 30˚C for cooling water and 15˚C for chilled water, respectively, and the values of physical parameters are furnished in Table 5.2.

5.5.1. Adsorption cooling system powered by PEFC waste heat

Figure 5.2 shows the effect of cycle time on the performances of adsorption cycle powered by waste heat from PEFC. Both cooling capacity and COP show increasing tendency with the increase in cycle time. However, improvement of cooling capacity is only marginal when the cycle time exceeds 1200 s. Effect of switching time effect on

cooling capacity and COP at fixed cycle time of 1800s is shown in Fig. 5.3. Both cooling capacity and COP increases up to 50 s of switching time and then start to decrease. Adsorption cooling system powered by PEFC waste heat shows highest cooling capacity of 0.2 kW and COP of 0.487 at 50 s switching time.

Transient responses of adsorber/desorber heat exchangers, condenser and evaporator at optimized cycle time are shown in Fig. 5.4. It can be observed from Fig. 5.4 that the adsorption cycle powered by PEFC waste heat can reach to steady state operation after 3600 s of cycle time. Figure 5.5 shows outlet temperature profiles of heat transfer fluids. Outlet temperature of cooling water is 1.1˚C higher than cooling water inlet temperature for both adsorber and condenser. On the other hand outlet temperature of chilled water is 1.4˚C lower than the inlet temperature of chilled water. On an average the studied system offers 13.6˚C of delivered chilled water temperature.

Table 5.2 Values of physical parameters.

Parameter	Unit	Value	
		Using PEFC	Using SOFC
F_o	[-]	15	
D_{so}	[m^2/s]	2.54×10^{-4}	
E_a	[kJ/mol]	4.2	
R_p	[m]	4×10^{-4}	
$M_{adsorbent}$	[kg]	2.39	2.74
$(\dot{m}C_p)_j$	[kW/K]	0.133	0.152
$(\dot{m}C_p)_{cond}$	[kW/K]	0.186	0.213
$(\dot{m}C_p)_{chill}$	[kW/K]	0.151	0.173
$(MC_p)_{bed}$	[kJ/K]	4.75	5.45
$(MC_p)_{cond}$	[kJ/K]	0.189×0.385+0.18×4.186	0.216×0.385+0.18×4.186
$(MC_p)_{eva}$	[kJ/K]	0.266×0.385+1.1×4.186	0.306×0.385+1.1×4.186
$(UA)_{bed}$	[kW/K]	0.43	0.49
$(UA)_{cond}$	[kW/K]	0.53	0.61
$(UA)_{eva}$	[kW/K]	0.36	0.41

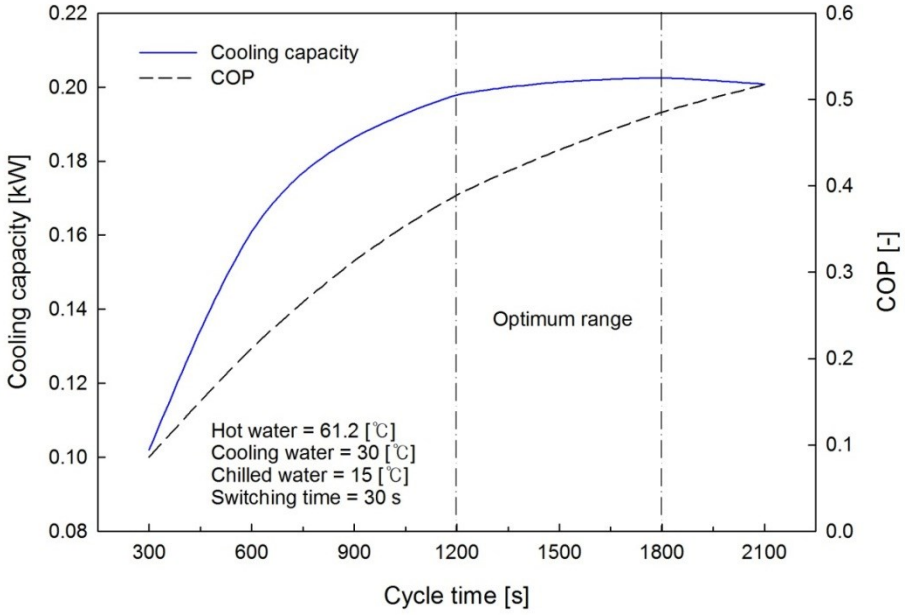

Fig. 5.2 Cycle time effect on performances of cycle powered by PEFC waste heat.

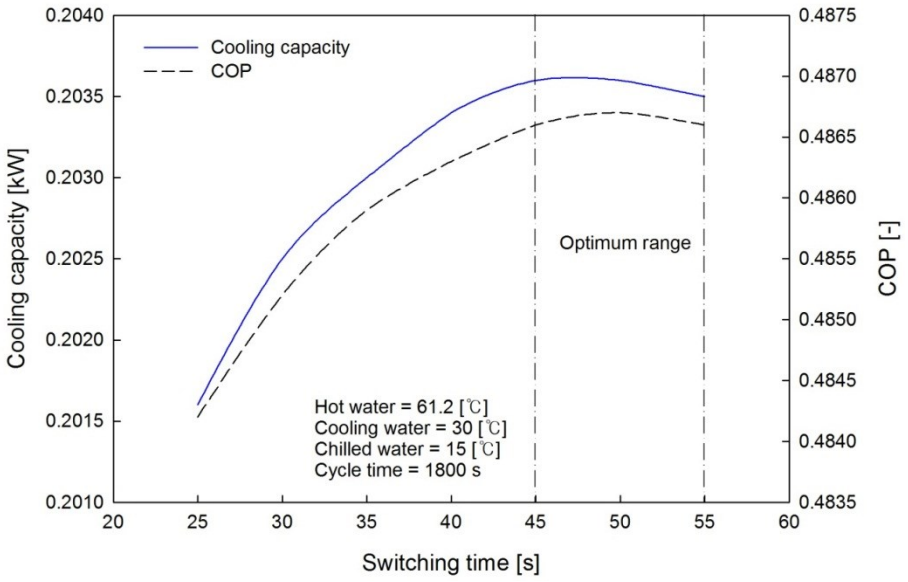

Fig. 5.3 Switching time effect on performances of cycle powered by PEFC waste heat.

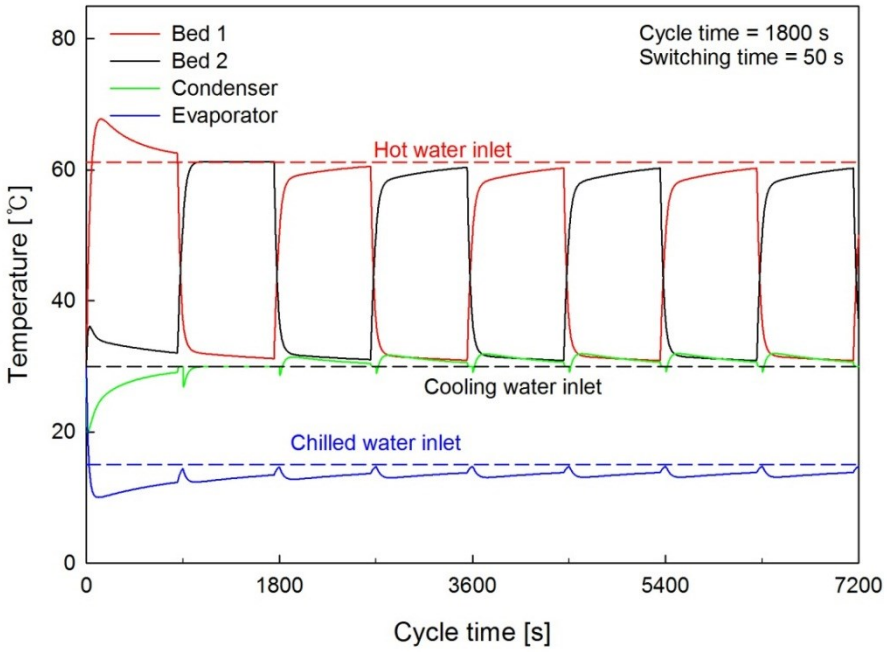

Fig. 5.4 Temperature profiles of each component for cycle powered by PEFC.

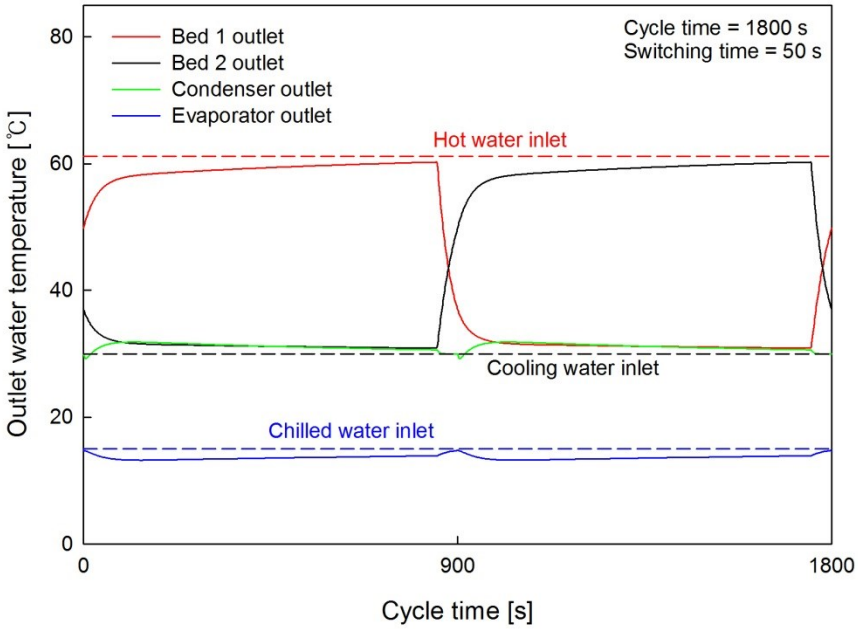

Fig. 5.5 Outlet temperature profiles of heat transfer fluids for cycle powered by PEFC.

5.5.2 Adsorption cooling system powered by SOFC waste heat

Figure 5.6 shows the effect of cycle time on the performances of adsorption cycle powered by waste heat from SOFC. Cooling capacity increases up to 900 s of cycle time, then start to decrease. On the other hand, COP shows increasing tendency with the increase in cycle time. Figure 5.7 shows the effect of switching time on both cooling capacity and COP for a fixed cycle time of 900. Both cooling capacity and COP increases with switching time up to 30 s. Adsorption cooling system powered by SOFC waste heat shows highest performance at 30 s of switching time. In this case the cooling capacity is found to be 0.53 kW and COP as 0.38.

Transient responses of adsorber/desorber heat exchangers, condenser and evaporator at optimized cycle time are shown in Fig. 5.8. It can be observed from Fig. 5.8 that the adsorption cycle powered by SOFC waste heat can reach to steady state operation after 3600 s of cycle time. Figure 5.9 shows outlet temperature profiles of heat transfer fluids. Outlet temperature of cooling water is about 2.6˚C higher than its inlet temperature for both adsorber and condenser. The averaged outlet chilled water temperature is about 3.1˚C lower than chilled water inlet temperature.

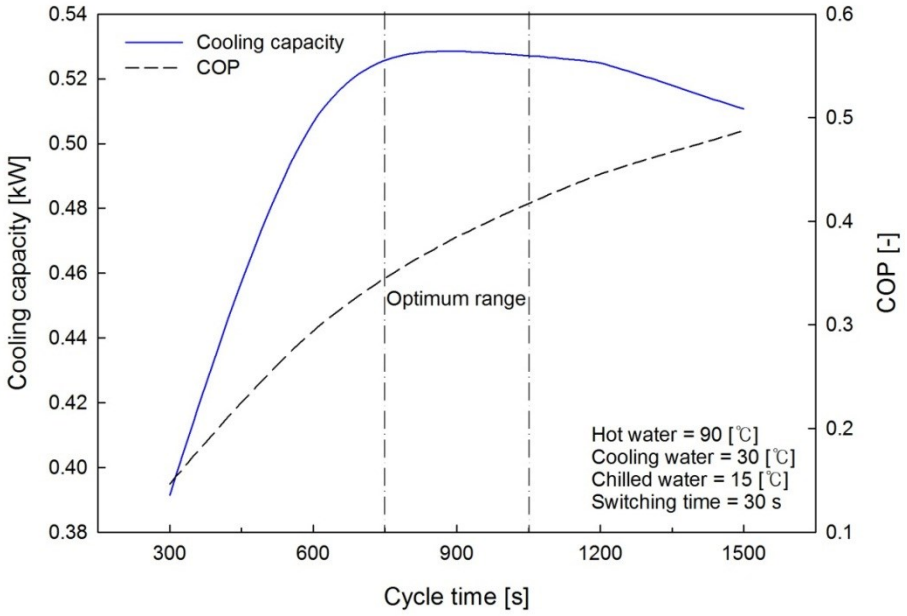

Fig. 5.6 Cycle time effect on performances of cycle powered by SOFC waste heat.

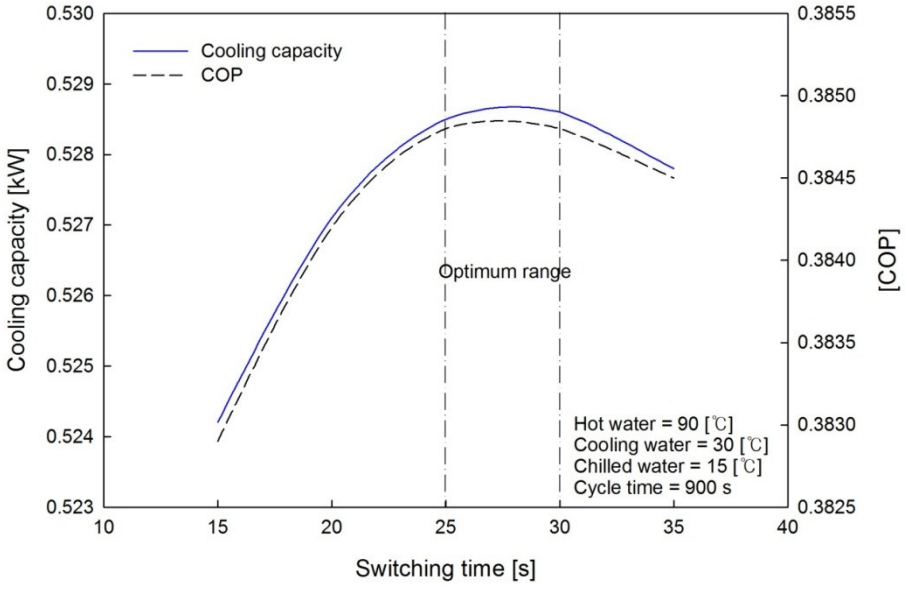

Fig. 5.7 Switching time effect on performances of cycle powered by SOFC waste heat.

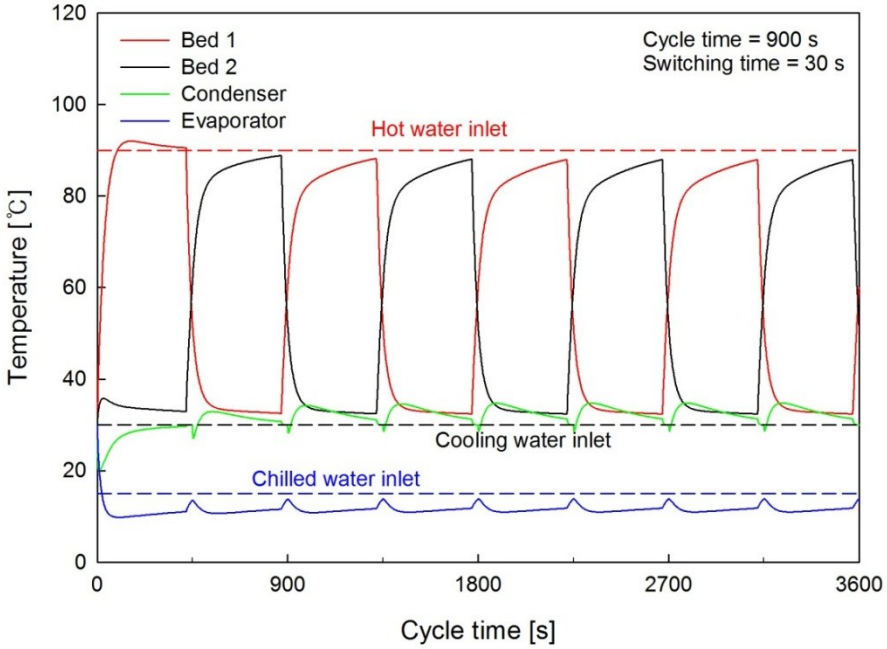

Fig. 5.8 Temperature profiles of each component for cycle powered by SOFC.

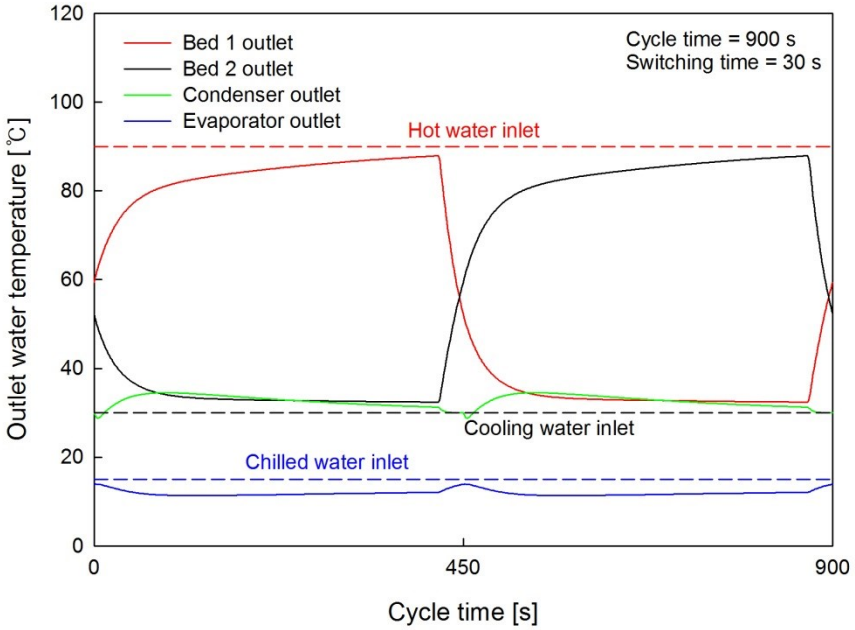

Fig. 5.9 Outlet temperature profiles of heat transfer fluids for cycle powered by SOFC.

5.5.3 Thermodynamic process on the Dühring diagram

Figure 5.10 shows the Dühring (pressure-temperature-concentration) plots of both PEFC and SOFC powered adsorption cooling cycles. Blue dashed line represents the adsorption cycle powered by PEFC waste heat and red dashed line shows adsorption cycle powered by SOFC waste heat. Total cycle time which includes all pre-heating, desorption and pre-cooling and adsorption cycles was set to be 1800 s for the adsorption system powered by PEFC waste heat. For the SOFC waste heat powered adsorption cycle the total cycle time is set at 900 s. In the Dühring plots, the positive thermal swing (b - c) in the bed is occurred at constant isosteres (constant concentration) and is known as the pre-heating process, while the negative thermal swing (d - a) in the bed is occurred at constant isosteres and is known as the pre-cooling process. In contrast, adsorption/desorption processes are occurred isobarically during a - b (evaporation - adsorption) and c - d (desorption - condensation) processes. It can be observed that during the cold-to-hot thermal swing of the bed, momentary adsorption takes place at the beginning of pre-heating phase even though heat source is applied. This momentary adsorption causes a small pressure drop just after closing the refrigerant valve (Valve 1 in Fig. 5.1) connecting the adsorber and the evaporator. As can be seen from Fig. 5.10, the concentration difference for SOFC waste heat powered adsorption system is about 10 % higher than that of the PEFC waste heat powered adsorption system. Higher concentration difference has been obtained for SOFC waste heat powered adsorption cycles due to the utilization of relatively higher temperature of heat source.

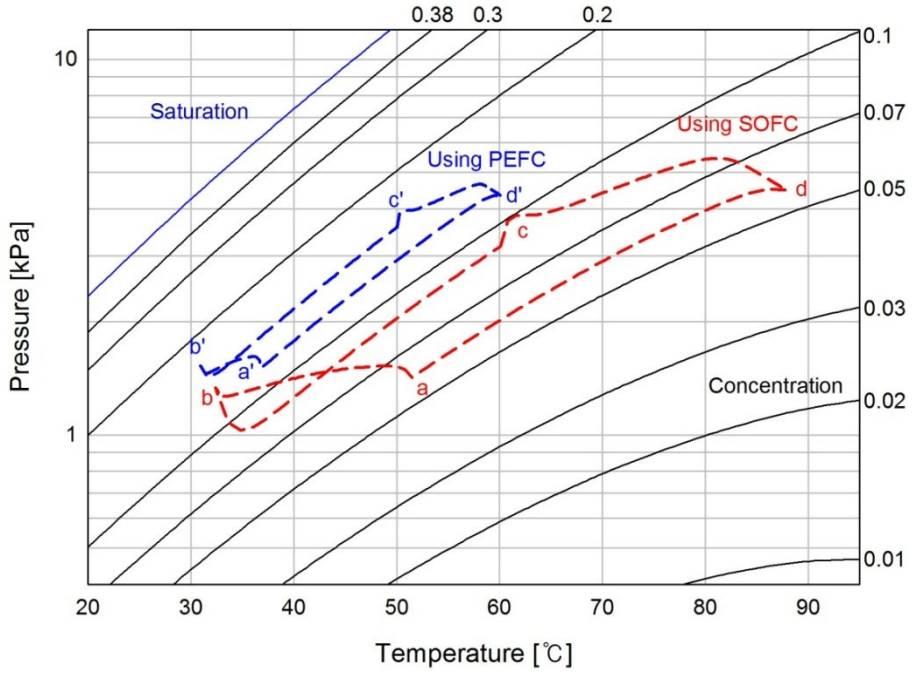

Fig. 5.10 Comparison of thermodynamic processes between PEFC and SOFC systems.

5.5.4 Comparison of performances with conventional adsorption cooling system

Figure 5.11 shows the comparison of specific cooling capacity (SCC) and COP of SOFC waste heat powered adsorption cooling system and two bed silica gel/water based adsorption cooling system at operation conditions of 30˚C of cooling water inlet temperature and 15˚C of chilled water temperature. Both systems show same trends in both SCC and COP. SOFC waste heat powered adsorption cooling system shows 7 - 13 % of SCC improvement over the two-bed adsorption cycle within the whole range of cycle time. However, the COP values for both systems are almost equal. The Dühring (pressure-temperature-concentration) plots of both SOFC powered adsorption cooling cycle and conventional adsorption cycle are shown in Fig. 5.12. Red dashed line shows SOFC powered adsorption cooling system and black solid line represents conventional adsorption cooling system. As can be seen from Fig. 5.12, the concentration difference of SOFC powered adsorption cooling system is slightly larger than that of the conventional adsorption cooling system.

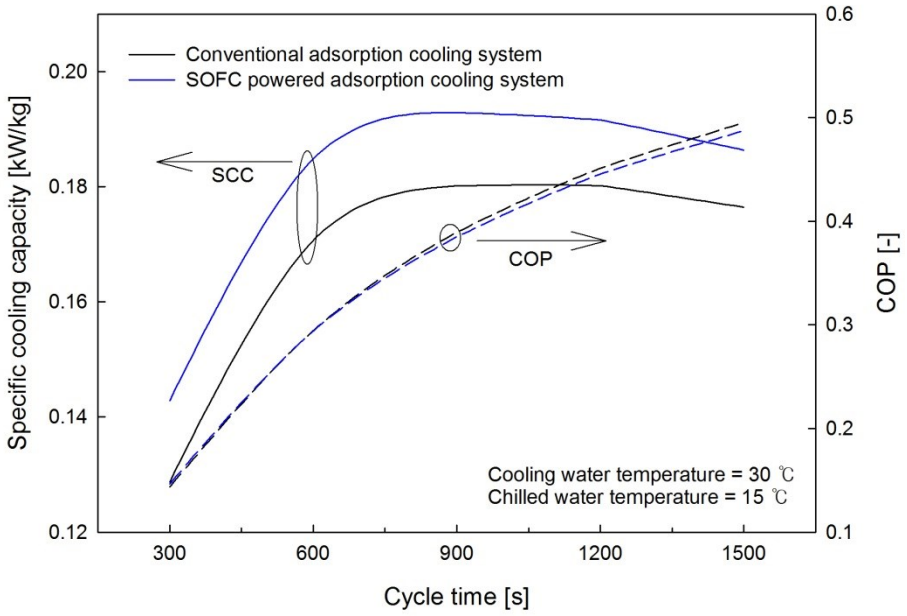

Fig. 5.11 Comparison of SCC and COP with conventional adsorption cooling system.

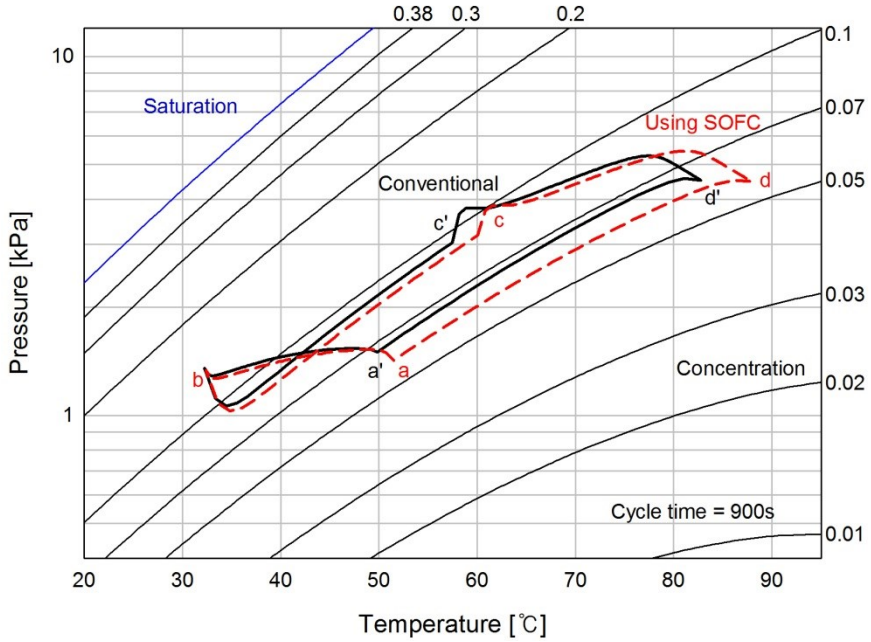

Fig. 5.12 Comparison of thermodynamic process with conventional adsorption cooling system.

5.6. Conclusions

In this study, granular silica gel RD 2060/water based adsorption cycles which are powered by two different fuel cells and utilize a compact fine-tube heat exchanger were analyzed numerically. The main findings can be summarized as:

In case of PEFC waste heat powered adsorption cooling system, both cooling capacity and COP increase with the increase in cycle time. However, the improvement of cooling capacity is only marginal for cycle time above 1200 s. Both cooling capacity and COP increase up to 50 s of switching time. Adsorption cooling system powered by PEFC waste heat performs optimally at 1800 s of total cycle time.

For SOFC waste heat powered adsorption cooling system, cooling capacity increases up to 900 s of total cycle time, then start to decrease. However, COP shows increasing tendency with the increase in cycle time. Adsorption cooling system powered by SOFC waste heat performs optimally at 900 s of total cycle time and the optimum cooling capacity and COP are found to be 0.53 kW and 0.38, respectively.

SOFC waste heat powered adsorption cooling system shows 7 - 13 % of improvement in cooling capacity over the conventional adsorption cooling system at 30˚C of cooling water inlet temperature and 15˚C of chilled water inlet temperature.

Nomenclature

C_p	Specific heat [kJ/kg·K]
COP	Coefficient of performance
D_{so}	Pre-exponential constant [m^2/s]
E_a	Activation Energy [kJ/kg]
F_0	Shape constant [-]
$\dot{m}$	Mass flow meter [kg/s]
M	Mass [kg]
R_p	Particle radius [m]
UA	Overall heat transfer coefficient [kW/K]

Subscript

bed	Sorption bed
chill	Chilled water
cond	Condenser
e	Evaporator
j	Cooling water/hot water

References

[1] K. C. Ng, H. T. Chua, C. Y. Chung, C. H. Loke, T. Kashiwagi, A. Akisawa and B. B. Saha, Experimental investigation of the silica gel-water adsorption isotherm characteristics, Applied Thermal Engineering 21, (2001) 1631-1642.

[2] B. B. Saha, A. Chakraborty, S. Koyama and Yu I. Aristov, A new generation cooling device employing CaCl2-silica gel-water system, International Journal of Heat and Mass Transfer 52, (2009) 516-524.

[3] T. Miyazaki, A. Akisawa, B. B. Saha, I. I. El-Sharkawy and A. Chakraborty, A new cycle time allocation for enhancing the performance of two-bed adsorption chiller, International Journal of Refrigeration 32, (2009) 846-853.

[4] B. B. Saha, K. Shigeru, I. I. El-Sharkawy, A. Kuwahara, K. Kariya and K. C. NG, Experiments for measuring adsorption characteristics of an activated carbon fiber/ethanol pair using a plate-fin heat exchanger, Heating, Ventilating and Air Conditioning Research Special 12, (2006) 767-782.

[5] B. B. Saha, I. I. El-Sharkawy, A. Chakraborty and S. Koyama, Study on activated carbon fiber-ethanol adsorption chiller: Part Ⅰ - system description and modeling, International Journal of Refrigeration 30, (2007) 86-95.

[6] B. B. Saha, I. I. El-Sharkawy, A. Chakraborty and S. Koyama, Study on activated carbon fiber-ethanol adsorption chiller: Part Ⅱ - performance evaluation, International Journal of Refrigeration 30, (2007) 96-102.

[7] H. Demir, M. Mobedi and S. Ülkü, A review on adsorption heat pump: Problems and solutions, Renewable and Sustainable Energy reviews 12, (2008) 2381-2403.

[8] B. N. Okunev, A. P. Gromov, L. I. Heifets and Y. I. Aristov, A new methodology of studying dynamics of water sorption/desorption under real operating conditions of adsorption heat pumps: Modeling of coupled heat and mass transfer in a single adsorbent grain, International Journal of Heat and Mass Transfer 51, (2008) 246-252.

[9] C. Y. Tso, C. Y. H. Chao and S. C. Fu, Performance analysis of a waste heat driven activated carbon based composite adsorbent-water adsorption chiller using simulation model, International Journal of Heat and Mass Transfer 55, (2012) 7596-7610.

[10] A. R. M. Rezk and R. K. Al-Dadah, Physical and operation effects on silica gel/water adsorption chiller performance, Applied Energy 89, (2012) 142-149.

[11] X. Zhang, X. Chen, B. Lin and J. Chen, Maximum equivalent efficiency and power output of a PEM fuel Cell/refrigeration cycle hybrid system, International Journal of Hydrogen Energy 36, (2011) 2190-2196.

[12] M. Clausse, F. Meunier, J. Coulie and E. Herail, Comparison of adsorption system using natural gas fired fuel cell as heat source, for residential air conditioning, International Journal of Refrigeration 32, (2009) 712-719.

[13] A. El Fadar, A, Mimet and M. Pérez-García, Modeling and performance study of a continuous adsorption refrigeration system driven by parabolic trough solar collector, Solar Energy 83, (2009) 850-861.

[14] A. Mahesh and S. C. Kaushik, Solar adsorption cooling system: An overview, Journal of Renewable and Sustainable Energy, 4 (2012) 022701.

[15] H. Z. Hassan and A. A. Mohamad, A review on solar powered closed physisorption cooling systems, Renewable and Sustainable Energy Reviews 16, (2012) 2516-2538.

[16] M. A. Alghoul, M. Y. Sulaiman, K. sopian and B. Z. Azmi, Performance of dual purpose solar continuous adsorption system, Renewable Energy 34, (2009) 920-927.

[17] Y. Hamada, M. Nakamura, H. Kubota, K. Ochifuji, M. Murase and R. Goto, Field performance of a polymer electrolyte fuel cell for a residential energy system, Renewable and Sustainable Energy reviews 9, (2004) 345-362.

[18] S. Farhad, F. Hamdullahpur and Y. Yoo, Performance evaluation of different configurations of biogas-fulled SOFC micro-CHP systems for residential applications, International Journal of Hydrogen Energy 35, (2010) 3758 - 3768.

Chapter 6

Chapter 6

Overall Conclusions

6.1 Main application of adsorption refrigeration system

The present study deals with utilization of waste heat from fuel cell between 60 - 90˚C as driving heat source. There are many advanced adsorption refrigeration system can be used effectively in industries, buildings and etc. where low temperature of waste heat is available. The utilization of waste heat can be applied in following specified areas;

- Solar energy utilization: Solar energy is commercialized and widely used to get heating source about 50 to 90˚C without primary energy sources in the detached house, building, factories and so on. Generated heat form solar energy is sufficient to power adsorption chiller.

- Diesel engine waste heat utilization: Diesel engine of boats, locomotives and automobile exhausts large amount of thermal heat. Mobile air-conditioning or refrigeration can be made possible utilizing diesel engine powered advanced adsorption refrigeration system.

6.2 Chapter summaries

The primary objective of present thesis is to develop fuel cell waste heat powered adsorption cooling system using a compact fin-tube heat exchanger which employs silica gel RD (2060)/water as the adsorbent/refrigerant pair. To achieve this objective, following studies have been conducted:

Chapter 1 presents a comprehensive review of various adsorption cooling systems. Extensive studies are conducted to investigate the performance of adsorption cooling systems using various adsorbent/refrigerant pairs and to enhance the performance of adsorption cooling system by the development and/or improvement of new and/or parent adsorbent materials. Applications of adsorption systems are also reviewed. Further, scopes and objectives of the present thesis are also discussed.

In chapter 2, adsorption characteristics of three different sizes of silica gel RD 2060, namely, powder 1 (75 - 250 μm), powder 2 (250 μm - 1 mm) and grain (1 - 1.81 mm) are determined using N_2 adsorption isotherm data by volumetric adsorption characteristic analyzer, Belsorp Mini II. Analysis of surface area and micropore characteristics are conducted by the *BET* method and *t-plot* method as well as pore size distribution (PSD) is also analyzed by the MP method. It is found that grain type of silica gel possessed the largest surface area of 618.36 m^2/g and micropore surface area of 597.97 m^2/g among studied adsorbent. Pore sizes of all studied silica gels are distributed within the range of 1 - 1.1 nm on the surface. Furthermore, grain type of silica gel performed highest adsorption uptake.

Additionally, adsorption dynamic of cylindrical silica gel was analyzed using finite volume based ANSYS FLUENT environment in three possible arrangements. The results obtained that the arrangement of particles has insignificant effect on uptake for a monolayer of cylindrical silica gel particles. However, only a marginal uptake decrease was found for tri-layer arrangement. Furthermore, the effect of fins has been analyzed on three different arrangements. It was found that the absence of fins do not have any significant effect on monolayer arrangements, however absence of fins significantly reduce the average uptake for tri-layer arrangement.

Chapter 3 aims to improve adsorption performance using a compact fin-tube type heat exchanger. The equilibrium isotherm characteristics of water onto granular RD type silica gel have been experimentally studied at three evaporation temperatures. The adsorbents were packed between the fins of the compact heat exchanger. The experimental adsorption equilibrium isotherms data have been fitted with Freundlich model and modified Fruendlich equation which is known as S-B-K adsorption isotherm model. The S-B-K equation fits satisfactorily the present experimental equilibrium adsorption uptake within ±5 % of deviation.

Chapter 4 deals with the dynamic behavior of silica gel/water based adsorption cooling system employing a compact heat exchanger. The motivation of this study is to investigate theoretically the performance of adsorption cooling system period of the development of integrated adsorption cooling/fuel cell system. Silica gel RD 2060 is used as adsorbent whilst water is used as refrigerant. Overall heat transfer coefficient of the compact heat exchanger is experimentally evaluated and the numerical value is

employed in the mathematical model. Size of evaporator and condenser is optimized to meet the cooling capacity of the system. Parametric study is conducted to estimate effects of heat transfer fluid (hot, cooling and chilled water) inlet temperatures, heat transfer fluid flow rates, adsorption/desorption cycle time and switching time on the system performance in terms of cooling capacity and COP.

From the theoretical analysis, a relatively longer adsorption/desorption cycle time results in COP gains but the cooling capacity of cycle decreases. Thus an optimum cooling capacity exists at a cycle time at 600 s along with switching time at 30s.

The effect of desorption temperature on the performances of adsorption cooling system driven by waste heat from fuel cells has been analyzed. Two different temperature levels of waste heat from polymer electrolyte fuel cell (PEFC) and solid oxide fuel cell (SOFC) are used as the heat source of the adsorption cooling system. The adsorption cycles consist of one pair of adsorber/desorber heat exchangers, a condenser and an evaporator. System performance in terms of specific cooling capacity (SCC) and coefficient of performance (COP) are determined and compared with studied conventional adsorption cooling system in chapter 4.

From above theoretical modeling, it is found that optimum cooling capacity exists at a cycle time at 900 s along with switching time at 50s in case of PEFC waste heat powered system and cooling capacity performed optimal at a cycle time at 600 s along with switching time at 30s in case of SOFC waste heat powered system. SOFC waste heat powered adsorption cooling system shows 7 - 13 % of improvement in the cooling

capacity compared with that of parent adsorption cooling system at 15˚C of chilled water inlet temperature along with 30˚C of cooling water inlet temperature.

In Chapter 6, the contents of previous chapters are summarized. This chapter also discusses overall conclusions of present work and future work needed for the improvement of adsorption performance of studied system.

6.3 Overall conclusions

In conclusion, main purpose of the present study is to reduce the footprint of adsorber/desorber heat exchanger using a compact fin-tube heat exchanger and to utilize fuel cells waste heat as driving heat source of silica gel/water based adsorption cooling system. Theoretical analysis is conducted using parametric values extracted from experiment to evaluate performances of silica gel/water based adsorption cooling system powered by waste heat from PEFC and SOFC. PEFC waste heat powered adsorption system shows 20 % of additional cooling effect while SOFC waste heat powered adsorption system shows 52 % of additional cooling effect over the fuel cell only system. Furthermore, SOFC waste heat powered adsorption cooling system shows 7 - 1 3 % of improvement in the cooling capacity compared with that of conventional adsorption cooling system.

6.4 Future work

Further study is recommended employing CaCl2-in-silica gel/water or powered silica gel/water based adsorption system.

It may contribute towards the enhancement of adsorption cooling system performance

Appendix

Appendix A

Evaporator and Condenser Surface Area

In the current study, evaporator and condenser are considered as shell and tube type heat exchanger as shown in Fig. A.1. The equation for internal heat transfer of evaporator/condenser heat exchanger is given by;

$$Q = UA \cdot LMTD \tag{A-1}$$

rewritten as;

$$UA = \frac{Q}{LMTD} \tag{A-2}$$

where, Q is capacity of evaporator or condenser [kW], A presents surface area [m^2] and U is overall heat transfer coefficient [$kW/m^2 \cdot K$]. Related conditions for capacity of evaporator and LMTD are 1.5 - 2kW and 5˚C, and capacity of condenser is assumed 1.5 times higher than that of evaporator in current study.

The overall heat transfer coefficient U is written as;

$$U = \frac{1}{\frac{1}{h_w} + \frac{A_i \, ln(D_o / D_{in})}{2\pi kL} + \frac{A_i}{A_o}\frac{1}{h_{ref}}} \tag{A-3}$$

Invoking $A_i = \pi D_i L$ and $A_o = \pi D_o L$, the above relation can be reduced as;

$$U = \frac{1}{\frac{1}{h_w} + \frac{D_i \ln(D_o / D_{in})}{2k} + \frac{D_i}{D_o}\frac{1}{h_{ref}}} \tag{A-4}$$

where, D_i presents inner diameter of tube [m], D_o is outer diameter of tube [m], L is length of tube [m], k gives thermal conductivity of tube [kW/m^2·K], h_w is heat transfer coefficient of water side [kW/m^2·K] and h_{ref} is heat transfer coefficient of refrigerant side [kW/m·K]. h_w and h_{ref} are described in detail in chapter 4. [see Eqs. (4-12) - (4-14), (4-19) and (4-24)].

Therefore, surface area can be calculated by;

$$A = \frac{Q}{LMTD \cdot U} \tag{A-5}$$

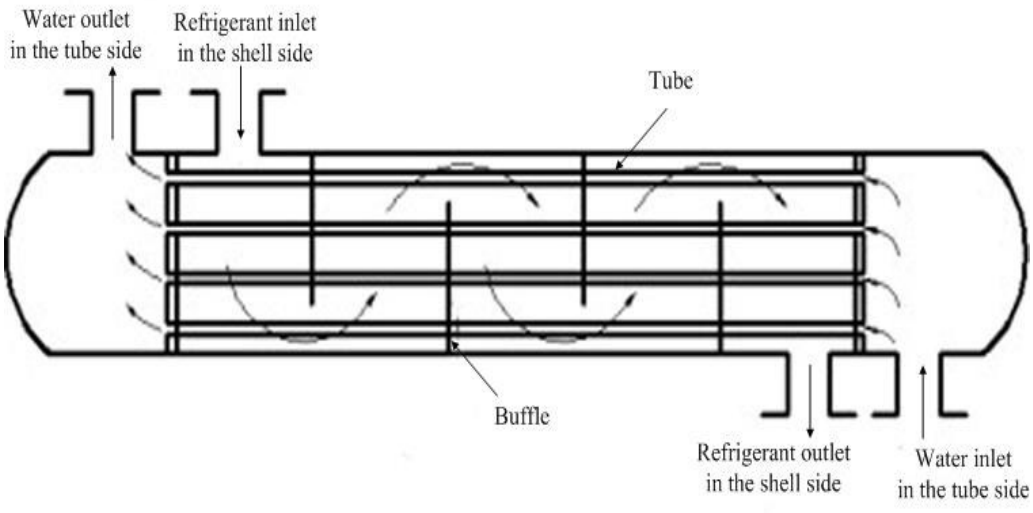

Fig. A.1. Shell and tube type heat exchanger [1].

References

[1] J. Guo, M. Xu and L. Cheng, The application of field synergy number in shell-and-tube heat exchanger optimization design, Applied Energy 86, (2009) 2079-2087.